C.P. No. 1148

C.P. No. 1148

MINISTRY OF AVIATION SUPPLY

AERONAUTICAL RESEARCH COUNCIL

CURRENT PAPERS

Gun Tunnel Force Measurements on some Thin Delta Wings suitable for Hypersonic Cruising Flight

By

T Opatowski

Department of Aeronautics, Imperial College

LONDON: HER MAJESTY'S STATIONERY OFFICE

1971

Price £1·15 net

C.P. No. 1148*

February 1969

Gun Tunnel Force Measurements on Some Thin Delta Wings suitable for Hypersonic Cruising Flight

- By -

T. Opatowski,

Department of Aeronautics, Imperial College

SUMMARY

The forces developed by sharp delta wings with vee roofs at hypersonic speeds have been experimentally investigated and theoretical consideration given to the relationship of these results to full scale conditions.

The theoretical development considered the case of upper surfaces held streamwise and derived the maximum lift/drag ratio and corresponding optimum thickness (θ') which result from applying this restraint. Simple expressions for both these quantities and their variation with Mach number, Reynolds number and surface heat transfer have been obtained using a new formula for pressure versus flow deflection at hypersonic speeds developed for this purpose. When related to practical cruise vehicles operating in the atmosphere, these optimum configurations proved to be unrealistic as they corresponded to vehicles that were only 1° to 2° thick or had very low wing loadings.

Numerical estimates for vehicles having practical wing loadings and thicknesses showed that reasonable lift/drag ratios could only be obtained at the lower altitudes, i.e. up to about 150,000 ft and at these altitudes base drag had a significant effect. It was also shown that for these conditions the maximum lift/drag ratio occurred when the upper surfaces were streamwise for a thickness of about 5°.

A significant result, applicable to wings of thickness around 5° to 10° was that while viscous effects played an important part at the Reynolds numbers usual in tunnel testing, they were relatively unimportant in the conditions appropriate to a cruise vehicle in the atmosphere.

The experimental programme was carried out in the Imperial College gun tunnel at a Mach number of 8·3 and two strain gauge balances were developed for this purpose. The models were sharp deltas with vee roofs and included two thicknesses, two aspect ratios, flat-bottomed, caret and twisted shapes which were tested at Reynolds numbers of $0{\cdot}9 \times 10^6$ to $3{\cdot}5 \times 10^6$.

The/

---

* Replaces A.R.C.30 997

The results agreed with theoretical estimates to within the estimated experimental accuracy. The lift of the flat wings was seen to be closely predicted by the two-dimensional oblique shock equations assuming each surface to be part of an infinite unswept plane, the difference being the order of 3-5% as predicted by Babaev for almost similar conditions. The loss of lift with leading edge shock detachment was seen to be small.

Within the margin of unknowns, the skin friction was adequately predicted by strip theory and the intermediate enthalpy method. There was some evidence of transition on a flat-bottomed wing which was not so evident on a similar wing of lower aspect ratio, an apparent increase of transition Reynolds number with increasing sweep. There was also evidence of viscous effects on the caret wings and on the twisted wing.

At the Reynolds numbers of the tests there was little to choose between the three different cross-sectional shapes in terms of maximum lift/drag ratio. The caret and twisted wings developed their maximum lift/drag ratio at a higher value of lift coefficient which is advantageous for cruise vehicles in the atmosphere, and this benefit would be expected to remain at the appropriate full scale Reynolds numbers, at least in the case of the caret wing. The twisted wing had its centre of pressure 2% further forward - also advantageous - and a more useful cross-sectional area distribution.

The experimental results also substantiated the theoretical estimates of optimum thickness with streamwise upper surfaces (θ') for the conditions of the tests.

List/

List of Contents

Appendix A/

List/

List of Figures

The first digit of each Fig. number indicates the paragraph in which the Fig. is discussed.

3.3/

3.10/

Notation/

Notation

a	speed of sound
b	base pressure ratio, see equation (2.8)
C	constant in Sutherland viscosity law
$\bar{C}$	constant in simplified viscosity law, see equations (B.9) and (B.10)
C_D	drag coefficient, $\dfrac{D}{0{\cdot}5\,\gamma\,M_\infty^2\,p_\infty\,S}$
C_p	pressure coefficient, $\dfrac{p - p_\infty}{0{\cdot}5\,\gamma\,M_\infty^2\,p_\infty}$
C_L	lift coefficient, $\dfrac{L}{0{\cdot}5\,\gamma\,M_\infty^2\,p_\infty\,S}$
D	drag
E_U E_L	ratio of surface areas, see equation (B.13)
H	constant related to surface cooling, see equations (B.15) and (B.17)
$\bar{H}$	$\left[\dfrac{H(\gamma - 1)}{2}\right]^{\frac{1-n}{2}}$, see equation (B.21)
K	skin friction parameter, see equation (B.31)
L	lift
ℓ	overall length of vehicle
M	Mach number
n	power in viscosity law, see equation (B.9)
p	pressure
$Q_{1,2..}$	ratio of dynamic pressures $\dfrac{\rho_{1,2...}\,U_{1,2..}^2}{\rho_\infty\,U_\infty^2}$
R_e	Reynolds number
R_{e_1}	Reynolds number based on unit length

S/

S	wing plan area
s	semi-span
T	temperature
U	velocity
V	volume
$\bar{V}$	volume parameter $\frac{V}{S^{3/2}}$ $\left(\text{sometimes } \frac{V^{2/3}}{S}\right)$
x	distance aft of leading edge
α_o	incidence of wing centre-line, see Appendix A and Fig. 4.1
β	wing semi-thickness angle, see Appendix A
γ	ratio of specific heats, taken as 1.4
δ	flow deflection angle
θ	wing thickness angle
θ'	wing thickness angle for maximum lift/drag ratio with upper surfaces streamwise
μ	viscosity
ρ	density
σ	relative density
τ_o	surface skin friction
χ	leading edge interaction parameter, see equation(2.1)
ω	wing loading, $\frac{W}{S} = \frac{L}{S}$

Suffixes

B	base
D	drag
F	total skin friction
f	local skin friction
L	lower surface
ℓ	based on vehicle length
S	standard
U	upper surface

W/

W	at wall
W_o	adiabatic recovery at wall
x	distance from leading edge
∞	free stream
$_1$	lower surface with upper surface streamwise
$_3$	at deflection equal to half thickness angle
*	based on intermediate temperature defined by equation (B.15)
$'$	optimum values
max	maximum obtainable at any incidence
θ^1	maximum with upper surface streamwise

---

1. Introduction

The work described in this report was carried out at the Imperial College of Science and Technology on an NPL sponsored research programme aimed at measuring the forces on lifting bodies in the gun tunnel. It was thought desirable to restrict the measurements to a small area of what was otherwise a rather large field of possible configurations and so attention was concentrated on two related topics which have recently aroused considerable interest in this country, namely hypersonic cruise vehicles (Refs 1-4) and wave-rider designs (Refs. 5-15). Various estimates for one or the other of these can be found in the literature (Refs. 16-22).

Hypersonic lifting vehicles can be roughly divided into those in which lift is used only transiently as a control, as in lifting re-entry vehicles (e.g. Ref. 23), and those in which a proportion of the weight is borne by aerodynamic means in an equilibrium condition, such as cruise vehicles. The former are characterized by very high Mach numbers, high incidence and high heating rates, low Reynolds numbers and low lift/drag ratios, large amounts of blunting and the possibility of significant variations of aerodynamic characteristics arising from non-equilibrium, dissociation and possibly ionization effects. The provision of volume is not usually a problem.

Among cruise vehicles there is a division between the lower speeds where the majority of the weight is borne by aerodynamic means and air breathing engines are possible and higher, near orbital speeds where only a fraction of the lift is aerodynamic. The test Mach number of 8·3 implied the former of the two above alternatives and the latter has not been explicitly examined, though it is not difficult to read from one to the other in some cases. These lower speed vehicles operate at comparatively high Reynolds numbers, high lift/drag ratios and low incidences and can have effectively sharp leading edges [29]. The main aerodynamic problems are those of providing adequate lift and volume at reasonable lift/drag ratios.

Cruise vehicles can be further sub-divided into interference and non-interference designs, a typical example of the former being the flat delta wing with underslung half-cone (e.g. Ref. 34). These shapes compare favourably with the merged configurations such as wave riders at Mach numbers below about 8 but begin to lose this advantage as Mach number is increased and require increasingly complicated shapes in order to derive the full benefits available (Refs. 24-27). These shapes have not been investigated.

The particular object of the present work therefore, was to study the factors affecting the performance of hypersonic lifting cruise vehicles of the merged wing-body type. These bodies are included in the designation 'wave-riders' which can be applied to any bodies with nominally attached leading edge shocks including interference designs.

2. Lift Drag Performance of Delta Wing Cruise Vehicles

2.1 General

An analysis has been carried out on sharp, flat-bottomed or caret delta wings with vee roofs and attached leading edge shocks. The object has been to find the conditions giving the highest value of lift/drag ratio with reasonable volume and wing loading, to investigate the characteristics of these wings in the atmosphere and to obtain an indication of the relevance of tunnel tests to free flight conditions.

2.2/

2.2. Analysis

2.2.1 Assumptions

Wing shape

The basic shape considered in this section is a flat-bottomed delta with a vee roof. A delta was chosen as being representative of the sort of shape that would be practical as a cruise vehicle since low speed handling and transonic stability are as essential as good hypersonic performance. Since the theory used herein assumes an average pressure over each surface equal to the two-dimensional oblique shock pressure applied to a streamwise section, the basic equations are equally applicable to caret wings and, with an appropriate change of a numerical constant, to wave-rider wings of any planform, provided leading edge shock attachment is maintained.

The assumption of sharp leading edges should not be a severe limitation. Some calculations presented in Ref. 28 show typical leading edge radii of one or two inches in the range of speeds and heights of interest to cruise vehicle design and Capey[29] shows that if provision is made for heat conduction, the leading edge can be made arbitrarily sharp. Additionally, Ref. 31 shows that for highly swept edges, even quite large amounts of blunting have only a small effect on the lift/drag ratio.

Flow conditions

Air is assumed to behave as a perfect gas and the entire boundary layer flow is assumed laminar. For the 200 ft vehicle in the atmosphere for which numerical calculations have been made, the average Reynolds number is of the order of 40×10^6 and the assumption of completely laminar flow is probably optimistic. Information on transition at hypersonic speeds is sparse and there are known variations between different tunnels and between tunnel and free flight. From some recent free flight measurements on a caret wing, Picken and Greenwood[43] obtained a maximum transition Reynolds number of 8×10^6 at a Mach number of 3. With the known tendency of transition Reynolds number to increase with Mach number, the above assumption may not be impossible but the position of transition must remain one of the largest unknowns especially when the possible effects of blunting and sweep are included.

Leading edge interaction has been assumed negligible. Cooke in Ref. 18 gives the following criterion for interaction to affect less than 5% of a delta surface

$$x_\ell = \frac{M^3}{\sqrt{R_{e_\ell}}} < 0{\cdot}22$$

where M = Mach number

R_{e_ℓ} = Reynolds number based on overall length.

For a 200 ft vehicle at Mach 10 and 100,000 ft $x_\ell = 0{\cdot}07$ and hence the above assumption is likely to be adequate.

Theoretical/

Theoretical methods used

The average pressure on each plane surface has been assumed to be given by the two-dimensional oblique shock equations, assuming the surface to be part of an infinite unswept plane. Babaev[37] has solved the problem of flow over such surfaces numerically, and has demonstrated that for the sweep angles considered (0°-50°), the loss of average pressure from the 2 - D value is only 2-4% up to an incidence of 21° on the pressure surface, and less than 2·5% up to -7° incidence on the suction surfaces at a Mach number of 4 to 5.

The present experimental results tend to confirm that the appropriate figure for the higher Mach numbers and sweep angles of these tests, is also less than 5%. The lift/drag ratio is rather insensitive to small variations in the assumed pressure.

Strip theory has been used in calculating the laminar skin friction, assuming that each streamwise strip behaved as a sharp flat plate at zero incidence and with free stream conditions equal to those after the oblique shock. No allowance has been made for boundary layer displacement in the approximate development of this section. (Boundary layer displacement is included in the comparative theoretical results of Section 3).

Other assumptions

Since maximum lift/drag ratio is achieved with a wing of zero thickness, another form of optimum must be sought if one wants a practical vehicle. A maximum in lift/drag ratio versus thickness other than zero thickness, can be obtained by fixing the incidence of the upper surface at some appropriate value. A convenient value is zero, i.e. the upper surfaces are held streamwise and the resulting relationship between the L/D for this condition and the L/D for any thickness and incidence is shown schematically in Figs. 2.1 and 2.2, the appropriate equations being given in Appendix A. If a negative upper surface incidence (i.e. suction) had been chosen, the curve would have started at some positive value of L/D and touched the full curve at a lower thickness with an opposite trend for fixed positive upper surface incidences. Anticipating the results, the upper surface streamwise condition coincides with the maximum lift/drag condition for thicknesses around 5°.

2.2.2 Theory

A full derivation of the theory is given in Appendix B, it being given only in outline here. Pressure versus flow deflection was obtained, as shown in Ref. 42 from the expression

$$\left(\frac{p}{p_\infty} - 1 \right) = \gamma M\delta + 1{\cdot}1\,(M\delta)^{2\cdot15} \qquad \cdots (2.1)$$

For the case of upper surface streamwise, all pressure forces are generated on the lower surface whose incidence is equal to the thickness angle θ. For slender wings the normal force is nearly equal to the lift force and hence with equation (2.1) above,

$$C_L \simeq \frac{2\theta}{M} + 1{\cdot}5M^{0\cdot15}\,\theta^{2\cdot15} \qquad \cdots (2.2)$$

for $\gamma = 1{\cdot}4$

It/

It is shown in Appendix B (equation(B.26a) and equation (2.6) below) that the skin friction on any surface can be expressed by

$$C_{D_F} \sim \left(\frac{p}{p_\infty} \right)^{1/2} \qquad \cdots (2.3)$$

For slender wings the rates of change of pressure with incidence of upper and lower surfaces are nearly equal in magnitude and opposite in sign and therefore so also is the rate of change of skin friction. Hence total skin friction is approximately invariant with wing incidence at fixed thickness.

Using the Blasius solution of the laminar boundary layer on a flat plate with zero pressure gradient, the reference temperature method of Ref. 39 and performing the necessary integration for the triangular planform[19] the total skin friction drag becomes,

$$C_{D_F} = 1{\cdot}77 Q_3 \ (E_L + E_U) \sqrt{\frac{\bar{C}_3}{R_{e_{3_L}}}} \qquad \cdots (2.4)$$

where upper and lower surfaces are taken at $\theta/2$ incidence, and

Q_3 is $\dfrac{\rho_3 U_3^2}{\rho_\infty U_\infty^2}$; E_U and E_L , upper and lower surface area/S respectively,

and $\bar{C}_3 = \left(\dfrac{T^*}{T_3} \right)^{1-n}$ $\qquad \cdots (2.5)$

where n is the exponent in the assumed power relationship between temperature and viscosity and can be found for any temperature range, by using Sutherland's law. T^*, the intermediate temperature can be incorporated in a parameter $\bar{H}$ which only varies over narrow limits (0·7 to 0·8) as the wall temperature varies from static to adiabatic wall temperature, i.e. as the cooling varies from 100% to zero.

After some manipulation, given in Appendix B, the total skin friction drag is,

$$C_{D_F} = \frac{1{\cdot}77 \ (E_L + E_U)}{\bar{H} \ M_\infty^{1-n} \sqrt{R_{e_{\infty_L}}}} \cdot \left(\frac{p_3}{p_\infty} \right)^{1/2} \qquad \cdots (2.6)$$

and from a graphical solution using the exact relation for the pressure rise through an oblique shock

$$\left(\frac{p_3}{p_\infty} \right)^{1/2} = 1 + \frac{1}{4} \gamma M\theta + 0{\cdot}0485 \ (M\theta)^{1{\cdot}77} \qquad \cdots (2.7)$$

where, for the condition given by the suffix 3 the flow deflection angle δ is half the thickness angle θ .

In considering the lift/drag ratio, it is easier to treat the reciprocal, i.e. drag/lift ratio. From Appendix B.

$\dfrac{C_D}{C_L}$ /

$$\frac{C_D}{C_L} = \theta + \frac{1{\cdot}77(E_L + E_U)M^{(1+n)}\left[1 + 0{\cdot}33(M\theta) + 0{\cdot}048(M\theta)^{1{\cdot}77}\right]}{\bar{H}\sqrt{R_{e_{\infty_L}}}\left[2\theta M + 1{\cdot}5(M\theta)^{2{\cdot}15}\right]}$$

$$+ \frac{b\theta}{1{\cdot}4M\theta + 1{\cdot}05(M\theta)^{2{\cdot}15}}$$

where

$$b = \frac{p_\infty - p_b}{p_\infty} \qquad \cdots (2.8)$$

This expression has a minimum with respect to thickness θ which is the optimum thickness θ' as defined in Section 2.1.4 and Fig. 2.2. Putting $b = 0$, i.e. assuming that base drag has only a small effect on the thickness angle for maximum lift/drag ratio (see Section 3) a relationship is obtained,

$$f_1(M\theta') = K(M\theta') \qquad \cdots (2.9)$$

where

$$K = \frac{1{\cdot}77(E_L + E_U)\,M^{(2+n)}}{\bar{H}\sqrt{R_{e_{\infty_L}}}} \qquad \cdots (2.10)$$

The solution to equation (2.9) is,

$$M\theta' = 0{\cdot}688K^{0{\cdot}477} \qquad \cdots (2.11)$$

which enables θ' to be found, given the vehicle geometry and the flight or test conditions. Substituting equation (2.11) into equation (2.8) and solving (graphically) gives

$$M\left(\frac{D}{L}\right)_{\theta'} = 1{\cdot}23K^{0{\cdot}466} + \frac{b}{1{\cdot}38 + 0{\cdot}68K^{0{\cdot}553}} \qquad \cdots (2.12)$$

which is the maximum lift/drag ratio with upper surfaces streamwise.

Combining the Mach number terms to obtain the variation with M gives

$$\theta' \sim \left[M^{n-0{\cdot}8}\right]^{0{\cdot}477}$$

$$\theta' \sim M^{0{\cdot}076} \qquad \text{for } n = 0{\cdot}76 \qquad \cdots (2.13)$$

and/

and $$\left(\frac{D}{L}\right)_{\theta'} \sim \left[M^{n-0.66}\right]^{0.466}$$

$$\left(\frac{L}{D}\right)_{\theta'} \sim M^{-0.047} \quad \text{for } n = 0.76 \qquad \cdots (2.14)$$

2.3 Numerical illustration

The theory of Section 2.2.2 has been illustrated by applying it to a delta wing in the atmosphere. Values have been obtained for the optimum thickness, θ' together with the corresponding lift/drag ratios and wing loadings.

The results cover heights from 75,000 to 200,000 ft and Mach numbers from 5 to 20. A 200 ft long vehicle has been used as was done in Ref. 19. The heat transfer parameter, $\bar{H}$, was taken as 0·75, a value representative of the condition half way between the adiabatic wall condition and 100% cooling ($T_w = T_\infty$). Atmospheric data were obtained from Ref. 41.

Fig. 2.3 gives the results for the optimum thickness angle θ', versus Mach number and altitude and Fig. 2.4 gives the corresponding lift/drag ratios and wing loadings.

Some interesting points emerge. The optimum thickness angles are extremely small, except at very high altitudes. The wing loadings corresponding to θ' are impossibly small except at low altitudes and high Mach numbers. It is evident that the optimum (θ') vehicle is not a practical design and that wing loading is a major factor.

This being so, some calculations were performed to illustrate the performance of non-optimum vehicles (but still with upper surfaces streamwise), having practical wing loadings. Lift/drag ratios corresponding to the range of wing loadings from 20 to 90 lb/sq ft are given versus height for Mach number of 5, 10 and 15 in Figs. 2.5 (a),(b) and (c) respectively. The corresponding thickness angles are plotted in Figs. 2.6 (a),(b) and (c). The lift/drag ratios are given both for the case of zero base drag and for a base drag corresponding to a base pressure equal to half the free stream static pressure.

If a lift/drag ratio of 5 is arbitrarily taken as a minimum, then the usable area of the flight spectrum is reduced to the lower altitudes. The following table shows the position with base drag included

Wing loading	Maximum altitude for L/D ⩽ 5		
	M = 5	M = 10	M = 15
20 lb/sq ft	110,000 ft	150,000 ft	170,000 ft
90 lb/sq ft	80,000 ft	112,000 ft	125,000 ft

Figs. 2.5 clearly show the considerable effect of base drag, especially in the area of interest, i.e. low altitudes, moderate Mach numbers and high lift/drag ratios. Base drag must rank as one of the major uncertainties in estimating lift/drag ratio.

The/

The results also show that the inclusion of base drag produces little change in the thickness angle for maximum lift/drag ratio, thus substantiating an assumption made in Section 2.2 and Appendix B.

Results for constant thickness angles of 6° and 10° have been extracted from the figures and are given in Fig. 2.7. The lift/drag ratios achieved depend mainly on the thickness and secondly on the Mach number. Altitude, and hence Reynolds number, has little effect except on wing loading. This is because the thickness angles are well away from the optimum and hence the skin friction drag is small in comparison with the pressure drag.

2.4 Analytical results and deductions

2.4.1 Relationship of upper surface streamwise condition to general case

The maximum lift/drag ratio is evidently achieved with a wedge of zero thickness at an incidence determined by the skin friction, (see Appendix A and Figs. 2.1 and 2.2). The upper surface is at a negative angle equal to the lower surface flow deflection angle which is usually small (say, 1° to 2°) for practical Reynolds numbers. As thickness, and hence volume, is introduced, the maximum L/D is reduced continuously while the lower surface incidence is increased, and that of the upper surface becomes less negative until, again for practical Reynolds numbers, it becomes streamwise as the lower surface reaches about 5°. For greater thickness angles, the optimum condition corresponds to slightly positive values of the upper surface incidence. Taking the upper surface streamwise condition as constant in this report has introduced an optimum thickness θ' and corresponding maximum lift/drag ratio, with the L/D falling to zero as the thickness and incidence fall to zero. For thicknesses greater than θ', the absolute L/D_{max} has been slightly underestimated with the optimum incidence being slightly greater below about 5° and slightly lower above it.

2.4.2 Significance of θ'

From the Newtonian standpoint, negative upper surface incidence would have no effect on the lift/drag ratio, thus reducing the volume for no gain. In practice, the upper surface is capable of, but less efficient at, producing lift than the lower surface and thus the optimum thickness θ' may be regarded as a point of diminishing returns below which the gain in L/D is not worth the loss of volume. At θ', numerical results show that the viscous drag is approximately equal to the pressure drag.

Simple expressions have been obtained for θ' and the corresponding L/D_{max}, enabling their value to be obtained quickly for any particular conditions. While practical cruise vehicles would be mainly well away from these optimum conditions, this does not apply to tunnel tests or to tests of small models in the atmosphere. The relative importance and effect of several of the variables is different, depending on whether the case being considered is near or far from θ', and a knowledge of θ' is helpful in making any comparisons or extrapolations.

For example, the curves of Figs. 2.3 and 2.4 show the position for a typical vehicle of 200 ft length in the atmosphere. Optimum thicknesses are entirely ruled out in this case, mainly due to insufficient wing loading. In the small area of very high Mach number and low altitude where the wing loading is adequate, θ' is ruled out due to insufficient volume, (thicknesses of 1° to 2°).

The/

The provision of adequate wing loadings has the effect of moving the point of operation well away from θ'. Viscous effects become considerably less important while thickness angles, which are now reasonable, become of primary importance. Thus, comparisons made at or near θ' become entirely different when transposed to the region of practical operation. This change is particularly important since many tunnel tests are performed near θ', (e.g. a 6° thick vehicle in a wind tunnel would be operating at its optimum, θ' condition at a Reynolds number of $2{\cdot}5 \times 10^6$ while at full scale in the atmosphere the relevant value of θ' would be $< 2°$).

2.4.3 Deductions from previous analysis

The spectrum of practical operation is covered by Figs. 2.5 and 2.6. Increasing Mach number at constant wing loading and altitude reduces the thickness and hence increases L/D. Alternatively, the effect of keeping the thickness constant is shown in Fig. 2.7. Increasing the Mach number still tends to increase the lift/drag ratio though not so markedly. Thus it is advantageous to have the highest Mach number possible.

The lift/drag ratio varies little with wing loading. This is due partly to the smallness of the viscous drag compared to the pressure drag and partly to the fact that the change of base drag with altitude tends to cancel the change of viscous drag. Thus the lift/drag ratio is firstly a function of wing thickness, secondly of Mach number and is almost independent of the wing loading which only determines the required altitude.

In practice, the design Mach number could well be limited by heating and the minimum thickness limited by the need for volume. Typical figures could be Mach number of 10, 5° thickness and 50 lb/sq ft wing loading giving an altitude of about 100,000 ft and L/D of about 8·5 for the case of base pressure equal to half static pressure. If 10° thickness were required, the figures would be 112,000 ft and L/D of 5.

It is evident that altitudes greater than about 150,000 ft are unlikely to be usable (for cruise) and even this height will require very high Mach numbers with very high heating rates. One result of this is that base drag has a comparatively large effect, being largest at the lower altitudes and Mach numbers. At present, base drag seems to be a major uncertainty.

In looking for experimental confirmation of the theoretical estimates from tests performed in low Reynolds numbers facilities, the best quantity to compare is the thickness for maximum lift/drag ratio with upper surfaces streamwise (θ'). This is because, as has been shown, θ' is relatively insensitive to the value of base drag while the actual value of L/D_{max} is very sensitive to it. Such a comparison is made in Section 3 where the values of θ' and $(L/D)_{\theta'}$, appropriate to the tunnel conditions of the present tests are also given.

3. Experimental Results and Analysis

3.1 Model and test conditions

3.1.1 Model design

The six delta wing models tested are listed below and shown in Figs. 3.1 (a),(b) and (c) together with their leading particulars. All models had vee roofs and the thickness angles quoted refer to angles in the vertical plane parallel to the centre-line chord. All were 5 in long with sharp leading edges of 0·003 in to 0·007 in diameter.

Model/

Model	Cross-sectional shape	Thickness angle	AR	Sweep
1	Flat bottom	10°	1	76°
2	Caret	10°	1	76°
3	Flat bottom	6°	1	76°
4	Flat bottom	6°	3/2	69·5°
5	Caret	6°	3/2	69·5°
6	Twisted	6° Nominal	3/2	69·5°

The angle between the plane of the leading edge and the lower ridge line of both caret wings was 6°. For inviscid flow at the test Mach number of 8·3, the shock would lie in the leading edge plane at lower ridge line incidences of 4° and 16° and be within 0·7° of this plane between the above angles (e.g. Ref. 36). Thus essentially two-dimensional flow would be expected at close to these incidences, with probably only small departures in the intervening range. Large departures from this state would probably indicate significant viscous effects.

The twisted wing was designed to have the same volume as the 6° wings of equal aspect ratio and to have a linear reduction of lower surface incidence from centre-line to tip such that the centre-line incidence was twice that at the tip. The object of the design, apart from merely testing the effect of twist, was to try to obtain some of the benefits of interference designs by utilizing the effect of the boundary layer in spreading pressures laterally, as has been noted in the case of delta wings with underslung half cones where the leading edges were outside the conical shock from the half cone, e.g. Ref. 32. In these cases, pressures at the leading edges were obtained that were much higher than those to be expected in inviscid flow and this difference was attributed to the presence of the boundary layer and a resulting spreading of the shock induced pressures, outwards to the tips. A similar phenomenon occurring on the twisted wing would produce a high pressure towards the tips than that appropriate to the local incidence and hence a higher lift for a given lift/drag ratio. Appendix C gives the derivation of the expressions by which the ordinates of the twisted wing were obtained.

3.1.2 Test conditions

The relevant conditions for the results obtained on the MK 2 balance and used for comparative purposes here are given in Ref. 38. Details of the MK 3 balance, on which the bulk of the present results were obtained, can be found in Refs. 50 and 51, which also include details of the flow field calibrations. The gun tunnel characteristics are dealt with in Ref. 44.

Fig. 3.2 shows the available tunnel unit Reynolds numbers against driver conditions extracted from Ref. 44 with Mach 8·3 nozzle conditions added and the conditions of the present tests marked. The following conditions were obtained for the 5 in chord models used.

Driver pressure	Barrel pressure	Mach No.	Reynolds No.	q psi	T_T °K	T_∞ °K	Balance
1,000 psi	14·7 psia	8·3	$0{\cdot}9 \times 10^6$	3·05	1030	70	MK 3
1,000 psi	40 psia	8·3	$1{\cdot}5 \times 10^6$	3·05	740	50	MK 2
2,000 psi	95 psia	8·3	$3{\cdot}5 \times 10^6$	6·1	700	47	MK 3

3.1.3 Tests made

Model and test conditions were as follows:

Model	Incidence	M_N	R_e	Balance
Wings 1-6	0-12°	8·3	$0{\cdot}9 \times 10^6$ $3{\cdot}5 \times 10^6$	MK 3
Wings 1 and 2	0-11°	8·3	$1{\cdot}48 \times 10^6$	MK 2
20° half angle cone	0-30°	8·3	$1{\cdot}48 \times 10^6$	MK 2
Hemisphere	0°	8·3	$0{\cdot}9 \times 10^6$ $1{\cdot}48 \times 10^6$ $3{\cdot}5 \times 10^6$	MK 2 and MK 3

(For wing details refer to table of model geometry, page 19 and Fig. 3.1)

In each case the quoted incidence is that of the line joining the tip to the mid-point of the trailing edge in the plane of the centre-line chord except for the twisted wing where a line 3° from the upper ridge line was used as datum. (*)

Measurements were made of lift, drag, and pitching moment (axial force, normal force and pitching moment in the case of the MK 3 balance). In addition schlieren photographs of the flow in side and plan views were obtained for the two 10° models and some 6° models.

3.2 Comparative theory

Details of the theoretical estimates used for comparison with the results obtained on the MK 2 balance are contained together with the results in Ref. 38. For the results obtained on the MK 3 balance, the theoretical estimates shown on Figs. 3.3 to 3.10 were obtained using the methods outlined in Section 2 but applied individually to each plane surface and including a boundary layer displacement correction obtained by the methods of Ref. 40. The correction was applied by calculating the displacement thickness δ^*_ℓ at the trailing edge of the root chord and assuming a uniform angular displacement over the surface of δ^*/ℓ. The value of n in the expression

$\frac{u}{\mu^*} \sim \left(\frac{T}{T^*}\right)^n$ taken as appropriate to the tunnel conditions was $n = 0{\cdot}84$.

Newtonian/

(*) This datum was chosen so that upper surface conditions would be identical between models at the same incidence. Thus differences would be due to the lower surfaces alone.

Newtonian theory was shown to be very inaccurate under the conditions of the present tests [38] and has therefore not been considered again.

Convenient and significant parameters for comparing the theory of Section 2 with the experimental results are the thickness angle required for maximum lift/drag ratio to occur with upper surfaces streamwise and the associated maximum lift/drag ratio. Applying the tunnel conditions to the appropriate equations, i.e.

$$M\theta' = 0{\cdot}688K^{0{\cdot}477} \qquad \cdots (2.11)$$

and

$$M\left(\frac{D}{L}\right)_{\theta'} = 1{\cdot}28K^{0{\cdot}466} \quad \text{for zero base drag} \qquad \cdots (2.12)$$

where

$$K = \frac{1{\cdot}77(E_{\ell} + E_{u})M^{(2+n)}}{\bar{H}\, R_{e_{\infty_L}}^{0{\cdot}5}} \qquad \cdots (2.10)$$

gives,

Reynolds No.	θ'	$\left(\frac{L}{D}\right)_{\theta'}$
$0{\cdot}9 \times 10^6$	$7{\cdot}45°$ $(6{\cdot}4°)$	$4{\cdot}16$ $(4{\cdot}85)$
$1{\cdot}50 \times 10^6$	$6{\cdot}6°$ $(5{\cdot}7°)$	$4{\cdot}66$ $(5{\cdot}42)$
$2{\cdot}65 \times 10^6$	$6{\cdot}0°$ $(5{\cdot}1°)$	$5{\cdot}1$ $(5{\cdot}95)$
$3{\cdot}5 \times 10^6$	$5{\cdot}4°$ $(4{\cdot}7°)$	$5{\cdot}71$ $(6{\cdot}65)$

where $n = 0{\cdot}84$ for the tunnel conditions and the figures in brackets give the corresponding values if n were taken as $0{\cdot}76$, the usual value in the atmosphere.

It can be seen that for the 6° wings a maximum L/D of $5{\cdot}1$ should be achieved when the upper surfaces are streamwise at a Reynolds number of $2{\cdot}65 \times 10^6$. Keeping the upper surfaces streamwise and increasing the Reynolds number will raise the lift/drag ratio. The condition for $(L/D)_{max}$ however will no longer be with upper surfaces streamwise.

3.3 Results obtained with the MK 3 balance
(Those from the MK 2 balance are contained in Ref. 38)

3.3.1 Magnitude of significant variations

For differences in the results to be significant, it is necessary for them to be greater than the differences to be expected from experimental sources and other unknowns. The magnitude of the unknown errors vary according to the particular quantities being compared. Thus, for example, in comparing the experimental results of different models with each other, only the random part of the balance error is important while in a comparison between the experimental results and the theoretical predictions consistent errors are involved.

It/

It is possible to divide the incidence range into three parts in each of which the relationship of pressure to viscous forces is different and from which, in consequence, different deductions can be made. These are: near zero incidence, at maximum lift/drag ratio and at the highest incidences tested. The minimum significant variation for each type of comparison and each incidence range is:-

Parameter	Comparisons between models and incidences			Absolute comparison with theory and data from other balances		
	$\alpha_o = 0°$	$(L/D)_{max}$	$\alpha_o = 12°$	$\alpha_o = 0°$	$(L/D)_{max}$	$\alpha_o = 12°$
Axial force	16%	15%	9%	29%	27%	25%
C_{D_F} + base drag	24%	24%	22%	44%	40%	30%
C_D	16%	12%	8%	29%	21%	10%
C_L	9%	9%	9%	3%	3%	9%
L/D	25%	21%	17%	32%	24%	19%

In the above table the consistent errors include a contribution for base drag equal to half the free stream static pressure (14% of zero lift/drag) and a further contribution for balance induced surface separation which occurred at high incidence (6% lift at $\alpha_o = 12°$) but no contribution from random errors since the figures refer to the mean line in every case. The figures for random error include twice the balance error[51] and an allowance for possible variations of base drag up to a quarter of the free stream static pressure.

In the absence of sting effects, the expected variation of base pressure with Reynolds number is given, for example, by Hama[46]. Base pressure reduces with increasing Reynolds number as transition moves upstream from the far wake to the body. The evidence of Hama[46], King[45] and McLellan et al.[48] would suggest a value of p_b/p_∞ of 0.5 to 0.8 for fully laminar flow reducing to 0.2 to 0.3 for the fully turbulent case.

The schlieren photographs presented as Figs. 3.5, however, clearly show that the presence of the sting and balance has severely modified the base flow and caused upper surface separation which is just visible at $\alpha_o = 5°$ for the 6° wings, and becomes progressively more extensive with increasing incidence. In these circumstances the base pressure would be expected to be higher than that for a free wake and probably close to the free stream static. Thus the allowance for variations of base pressure incorporated in the table of significant magnitudes should be entirely adequate.

The effect of the observed upper surface separation has been estimated on two assumptions; that the separated area lay parallel to the leading edges and that the leading edge of the separated area was at right angles to the centre-line. Both lift and drag were considered and the worst result incorporated in the table. Only the high incidence case was affected as the separation occurred only at incidences higher than those for maximum lift/drag ratio.

3.3.2/

3.3.2 Axial force (Figs. 3.3. and 3.4)

Referring to the figures, the difference in theoretical axial force as between plain wings and caret wings is due to a combination of higher pressure drag from the greater pressure recovery of the caret wing and its greater skin friction drag resulting from greater wetted area. There is also a compensating contribution due to a smaller pressure difference $p - p_\infty$ on the roof surfaces resulting from their greater angling relative to the flow.

The experimental results show a pattern of variation as between different models which is significantly different to the theoretical pattern. The differences are more noticeable at the lower Reynolds number of $0{\cdot}9 \times 10^6$ but many of the differences are also present at $R_e = 3{\cdot}5 \times 10^6$. Near zero incidence, at $R_e = 0{\cdot}9 \times 10^6$ the twisted wing has a higher drag than the plain wings and so, to some extent has the caret wing, but these variations are no longer significant at the incidence for maximum lift/drag ratio. The fact that the discrepancy occurs at low Reynolds numbers and incidence suggests a boundary layer effect, on the concave lower surfaces.

At both Reynolds numbers there is a significant difference of axial force between the results for the two 6° plain wings of different aspect ratio at intermediate and high incidences. At the higher incidences, the axial force contains a substantial contribution from the lower surface pressure and a smaller contribution from the upper surface suction. In order to trace the source of the observed differences in axial force, these contributions have been subtracted from the observed values of axial force, using the measured values of normal force together with a theoretical estimate of the relative contributions from upper and lower surfaces to deduce the average pressures. The resulting values of C_{D_F} + base drag * are shown in Figs. 3.4.

Comparing the results for the two 6° plain wings and recalling that differences greater than 24% are significant, it can be seen that the higher aspect ratio wing has the higher drag in all conditions except at low incidence and high Reynolds number. Low aspect ratio appears to be beneficial, especially at low Reynolds numbers. The amount by which the experimental value of C_{D_F} + base drag exceeds the theoretical for the $AR = 3/2$ wing at $R_e = 3{\cdot}5 \times 10^6$ and $\alpha_o = 12°$ is also significant (> 100%) and this could be due to the onset of transition. If this is the case, the figures suggest that transition is delayed by increased sweep, at least under the test conditions.

Comparing plain and caret wings (Figs. 3.4(d) and (e)) there is little to choose between the two for the higher aspect ratio, 6° thick wings except for the near zero incidence effect previously noted. In the case of the lower aspect ratio, 10° thick wings (Figs. 3.4(a) and (b)) the caret wings show a marked increase in C_{D_F} plus base drag over both the plain wing results and the theoretical estimates at the highest incidences, most probably due to viscous effects in the streamwise corner of the under-surface[35] which was, of course, more acute on the $AR = 1$ wing than on the $AR = 3/2$ wing.

3.3.3/

---

*These values are strictly the axial components of skin friction and base drag but $\Delta C_D = \Delta C_A \cos\alpha$ and $\cos\alpha \simeq 1$ for the range of α of these tests.

3.3.3. Lift (Figs. 3.6 and 3.7)

Referring to the figures, the theoretical differences in C_L between caret and plain wings are very small as they arise only from differences in upper surface geometry. At low incidences, in all cases, the experimental lift coefficients for the plain wings lie close to the 2-D values while, in contrast, the caret wing results are above. This is another indication of the viscous effects on the caret wings at low incidence noted in the axial force results and this is further substantiated by the fact that the effect in question is greater at the lower Reynolds number.

With increasing incidence the caret wing results become equal to the 2-D values while the plain wings fall away, partly as would be expected from the numerical calculations of Babacv already discussed (Section 2), partly due to the upper surface separation mentioned in Section 3.3.1, and partly due to leading edge shock detachment which would occur at about 6·8° pressure surface incidence for wings of AR = 1 and at about 14·7° for wings of AR = 3/2 .

The values of lift coefficient obtained at zero incidence reflect the different geometries of the models with caret wings giving more lift than plain wings due both to the lower losses on the lower surfaces as a result of more 2-D flow (and viscous effects previously mentioned) and to lower losses from the upper surfaces as a result of the greater angling of these surfaces. The above effects are accentuated on thicker wings, resulting in greater zero incidence lift on 10° wings than on 6° wings.

3.3.4 Drag

The drag coefficients are geometric resolutions of the axial and normal forces and are presented in Figs. 3.8.

3.3.5 Centre of pressure position (Fig. 3.9)

The MK 3 balance was extremely sensitive to pitching moment[51] and much of the scatter on Fig. 3.9 may be due to small variations in tunnel conditions. In a number of cases the pitching moment (and, by comparison with the lift trace, therefore, the centre of pressure also) could be seen to vary gradually through a run. The C.P. positions at zero incidence were nearly indeterminate and these points have been disregarded.

There appears to be a tendency for the C.P. to move initially forward with increasing incidence and then to move slightly aft with a total movement of about 1% root chord. This pattern is followed to some extent by all the models.

The moment about the model moment datum is made up of a contribution from the normal force and a contribution from the axial force, for all the models except the caret wings, the axial force moment would be negligible, but the anhedral of the caret wings would have produced a nose down drag moment and hence these wings have a C.P. position slightly aft of that which can be attributed to the normal force alone. The 6° wings have C.P. positions forward of those for the 10° wings due, at least in part, to the trailing edge planes being perpendicular to the centre-line for the 6° wings and perpendicular to the upper surfaces for the 10° wings.

As would be expected, the twisted wing gave C.P. positions further forward (2%) than any other wings as a result of having a larger proportion of its lift in the central area of the wing.

3.3.6/

3.3.6 Lift/drag ratio (Figs. 3.10)

The figures for minimum significant differences in results for the different models, given in Section 3.3.1, for L/D include twice the random errors for both lift and drag. Within the quoted margins, only the differences at zero incidence are significant and these reflect the differences in the lift results. However, the likelihood that all the worst errors will combine is small and this is substantiated by the general consistency of the experimental points.

At maximum lift/drag ratio, the differences primarily reflect the significant variations in 'C_{D_F} plus base drag' discussed in Section 3.3.2. This is also true of the results at high incidence, largely because in terms of pressure forces, the lift/drag ratio is almost entirely a function of the incidence alone for the models under consideration and hence at a given incidence only viscous forces and possibly base drag differ significantly.

The difference between the experimental points and the theoretical estimates is less than that which can be expected from the various sources of possible error. This also applies to the difference between the results obtained on the two balances where the errors appear to have been of opposite sign.

A good curve of L/D versus incidence can be obtained by using smoothed curves of lift and drag, both of which have only gentle variations with incidence. Such curves are shown in Figs. 3.1 (a) and (b). Being derived from smoothed curves, their random error would be expected to be better than the figures given in Section 3.3.1, and this should be especially so for the angle for maximum lift/drag ratio since this quantity would, in addition, be largely unaffected by consistent errors. Thus the angle for maximum lift/drag ratio so obtained is a good parameter with which to compare the theory of Section 2.

The relevant estimates, given in Section 3.2 show that for a thickness of 6°, the maximum lift/drag ratio should occur with the upper surfaces streamwise for a Reynolds number of $2{\cdot}65 \times 10^6$. It follows from the arguments of Section 2 that at lower Reynolds numbers the $(L/D)_{max}$ will occur at higher incidences, i.e. with the upper surfaces developing suction. Higher Reynolds numbers will result in $(L/D)_{max}$ occurring with the upper surfaces developing pressure.

This pattern is closely followed by the experimental results of Figs. 3.11 which have been plotted against top surface ridge line incidence to facilitate the comparison. At the test Reynolds number of $3{\cdot}5 \times 10^6$ which is close to the required value of $2{\cdot}65 \times 10^6$ $(L/D)_{max}$ occurred on the plain wings with the upper surfaces developing a slight amount of pressure while for $R_e = 0{\cdot}9 \times 10^6$ $(L/D)_{max}$ occurred with suction on the upper surfaces. These characteristics are in good agreement with the estimates presented above.

4. Discussion and Conclusions

4.1 The experimental results

4.1.1 Comparison with other results in the literature

The apparently beneficial effect of sweep on transition (Section 3.3.2) is in the opposite sense to the normally accepted effect of sweep as given for example by Deem and Murphy [49]. Examination of their results shows that

transition/

transition started slightly earlier with increasing sweep but also that the rate of development of transition was no quicker and sometimes slower than the corresponding result for an unswept plate. Thus earlier transition need not necessarily result in higher total skin friction and the present results do not necessarily contradict the existing experimental evidence. An additional difference is that the results of Ref. 49 were obtained on a yawed flat plate and the effect of sweep on this configuration is not necessarily the same as on three-dimensional bodies.

Some recent results presented by Weinstein and Neal[47] tend to confirm the results of the present tests. They compare the measured skin friction drags on three diamond-cross-section wings at zero incidence with the estimated laminar values and show the onset of transition with increasing Reynolds number. Their results show the wings of higher aspect ratio (lower sweep) also to have lower transition Reynolds numbers.

The lift coefficient results for the AR = $^3/_2$ plain wing clearly demonstrate the very small loss of lift compared to the 2-D value, predicted by Babaev[37]. With allowance for the loss of lift from upper surface separation, the difference between the theoretical estimates and experimental results is less than the possible consistent experimental error of 3%.

The AR = 1·6 plain wing at 12° incidence shows a lift coefficient which has only 7% less lift relative to the 2-D value than the AR = $^3/_2$ wing despite leading edge shock detachment which would start at an incidence of about 4° for the AR = 1 wing. This shows the relatively small loss of lift due to shock detachment also found in pressure surveys such as those by Squire [20] and Peckham [34].

The agreement with theory in general has been good and within the expected order of accuracy of the experimental results. The departures from theory can all be explained in terms of known phenomena, i.e. boundary layer transition and viscous effects in the streamwise corner on the lower surface of the caret wings[48].

The comparison with other experimental data in the literature is reasonable. The only direct comparison is with the results of Penland [30] for the case of the 10° plain wing of AR = 1. The comparable figures for maximum lift/drag ratio are - Penland's results first - 3·6 and 4·1 for $R_e = 0{\cdot}9 \times 10^6$ and 4·3 and 4·5 for $R_e = 3{\cdot}5 \times 10^6$. Penland's results are stated as having been corrected to free stream static pressure on the base. The differences in $(L/D)_{max}$ are within the possible margin of error, but taken together with comparisons with results on similar, but not identical, wings such as Penland's 5° wings and the 11° wings of Blackstock and Ladson [31] the present results would appear a little high. Since the abovementioned results were obtained in continuous facilities with model surface temperatures nearer to the equilibrium values than are obtained in a gun tunnel, it is probable that transition occurred at correspondingly lower values of Reynolds number. These remarks also apply to the results recently obtained by Weinstein and Neal [47] on a 6° plain wing which was tested at a Reynolds number of $1{\cdot}4 \times 10^6$.

4.1.2 Effect of variations of shape

The overriding impression obtained from the results is that there is very little to choose between the three cross-sectional shapes and that each had advantages and disadvantages which tended to cancel. As would be expected, the caret wings, with near two-dimensional flow over the lower surfaces, gave results

which/

which were generally closest to the theoretical estimates. There was some evidence of viscous effects at low incidence and at the lower Reynolds number on these wings and, on average, the higher skin friction drag of the larger wetted area (as compared with the flat wings) could be noticed. The lower aspect ratio wing showed distinct advantages in skin friction over the higher aspect ratio wing, though this effect is probably a result of the particular conditions of these tests. At very least, the lower aspect ratio showed no disadvantages and hence, for the highest value of the volume parameter $\overline{V}$, it is desirable to go to the slenderest shape found possible from other considerations.

Comparisons with the twisted wing are more difficult as there is no satisfactory inviscid theory with which to compare the results. Surprisingly, the results for the twisted wing followed those for the caret wing to a very large extent and there does not appear to be any loss due to the cross-sectional shape. The close identity of behaviour of two such dissimilar shaped wings as a caret and a twisted wing, supports the other evidence that such changes have comparatively little effect.

One aspect, which only arises incidentally in the present investigation, is that of upper surface shape. The separation that occurred as a result of the presence of the comparatively slender balance indicates the extreme sensitivity of suction surfaces to outside influences. However, the proportion of lift developed by the upper surfaces is comparatively small (e.g. about 8% at 12° incidence for the 6° wing). From the theoretical point of view, in conditions where the upper surfaces are producing pressure, caret wings and especially thick caret wings of low aspect ratio, show an advantage because of the angling of the upper surfaces relative to the flow. It is evident that it will be possible to influence the lift/drag ratio by varying the contours of the upper surface, but in general gains are only achieved at the expense of volume.

4.1.3 Significance for cruise vehicles

Many of the variations in the results have arisen from viscous effects and as such are peculiar to the conditions and especially the Reynolds numbers of the tests. Even quite small practical vehicles in the atmosphere will be operating at Reynolds numbers at least an order of magnitude larger and even though large areas of laminar flow could still exist, the very peculiar variations of the present tests are unlikely to be directly applicable. The significance of the results must lie rather in substantiating the theory, where this is possible, and in indicating caution in the use of results obtained under similar tunnel conditions.

For cruise vehicles of optimum thickness θ' (see Section 2) viscous effects will, by definition, be important. However, even here the characteristics are likely to be different at full scale Reynolds numbers and it has been shown in Section 2 that practical vehicles will in any case be well away from this optimum condition and into regions where the viscous drag is only a small proportion of the total drag.

Thus 'inviscid' conclusions are likely to have most significance.

Though there might well be other reasons for preferring caret wings (e.g. engine intakes, external burning, stability) they do not, in general, have any advantages in maximum lift/drag ratio except where leading edge shock detachment or upper surface pressure is important.

A/

A most interesting result was that for the twisted wing. This showed no losses relative to the other wings and even occasional gains. On the other hand, it gave centre of pressure positions forward of the other wings and it has a more useful cross-sectional area distribution. Because the generation of sufficient lift is a problem in the atmosphere a significant comparison between the wings, with respect to cruise vehicles, is the comparison of lift/drag ratio at given lift. In Figs. 4.1 the achieved lift/drag ratios are shown plotted against lift coefficient for the Reynolds numbers of $0{\cdot}9 \times 10^6$ and $3{\cdot}5 \times 10^6$ respectively. For the conditions of these tests the caret and twisted wings show a slight advantage in that they achieve their maximum L/D at a higher lift coefficient. At lift coefficients of 0·12 and greater there was little to choose between any of the wings, indicating the overriding importance of lower surface pressure over all other effects.

This is, in fact, the way in which the greater lifting efficiency of the caret wing shows itself (providing the gain is not lost in viscous drag on the greater wetted area, i.e., at reasonably high Reynolds numbers and lift coefficients). Although the lift/drag ratio is a similar proportion of cot.α for plain and caret wings, the caret wing produces more lift at the same incidence and hence at about the same lift/drag ratio. Hence in appropriate conditions, the same lift coefficient occurs at a slightly lower incidence, resulting in a higher lift/drag ratio for the same lift. Although the maximum lift/drag ratios are little different, the above advantage could be significant when base drag is considered since a caret wing would produce the same lift as a plain wing of equal thickness but at a higher altitude and hence at a lower value of base drag.

Many of the estimates of range performance[1,2,3,6] have used values of L/D of 4 to 6. The experimental results, taken together with the theoretical considerations of Section 2, give additional evidence that these values should be easily attainable, perhaps with a little extra in hand to allow for trim, stability and control requirements.

4.2 Optimum cruise vehicle operating conditions

Because, as has been shown, viscous effects are small for a practical cruise vehicle in the atmosphere, the lift/drag ratio is virtually determined by the thickness while the required wing loading can be achieved by selecting the appropriate altitude. The resultant change of viscous drag due to a change of altitude has only a secondary effect on the lift/drag ratio for the reason given above. It also follows, incidentally, that advantages of performance derived from lower viscous drag and obtained in tunnel tests would show little benefit in full scale, even if the advantages were maintained at full scale Reynolds numbers. Thus the effect of transition on L/D will also be small. This is confirmed in a recent independent analysis by Collingbourne and Peckham [22], who calculate the performance of caret delta wings including the effect of altitude, wing loading, laminar and turbulent flow and the position of transition. Parasite drags such as base drag, are also included.

If base drag is important, i.e. if no provision is made to eliminate it (as in some proposed vehicles with external or integrated propulsion), then the effect of changing altitude can in fact be reversed since the base drag is reduced by an increase in altitude. Increasing Mach number enables the same wing loading to be achieved at a higher altitude and is therefore beneficial.

The above conclusions represent a considerable simplification of the situation and they were only possible because, for the 200 ft vehicle considered, it was possible to show that viscous effects would be small in all conditions.

As the vehicle under consideration becomes smaller, and hence θ' increases, so the pattern will become more complicated in various parts of the flight spectrum.

Collingbourne and Peckham[22] also carry out an analysis, similar in part to that of Section 2 to arrive at expressions for maximum lift/drag ratio with upper surface streamwise, and corresponding lower surface incidence, hence thickness. They also, in an appendix, consider the relationship of the upper surface streamwise condition to the incidence for maximum lift/drag ratio for fixed thickness and arrive at the same conclusion, that for thicknesses of about 5° in the atmosphere, the two conditions are coincident.

The essential difference between Collingbourne's and Peckham's analysis and that of Section 2 is in the assumption made with respect to the variation of skin friction with thickness and incidence. In Section 2 it was assumed that the skin friction was invarient with wing incidence for a wing of constant thickness and this assumption was justified theoretically and can be seen to be reasonable from the experimental results, (in the absence of transition). It follows that there is a change of friction drag with thickness.

This variation and the variation with changing Reynolds number and surface heat transfer, were included in the analysis, enabling the variation of optimum conditions with Mach number and Reynolds number to be explicitly determined.

In Ref. 22 the assumption was made that the skin friction drag is independent of flow deflection, i.e. does not vary with incidence or thickness, and a fixed value of friction drag was obtained from other estimates for the particular atmospheric conditions considered. (This limitation does not apply to the numerical results including boundary layer transition).

4.3 Optimum configurations

There have been many investigations, both theoretical and experimental, into the problem of the optimum configurations for a hypersonic cruise vehicle. In the present author's opinion, several fallacies, which have been consistently repeated, have served to thoroughly confuse the situation. They are discussed below.

Penland, in Appendix A of Ref. 30 writes: "The relatively widespread use of the non-dimensional ratio of volume $^{2}/_{3}$ to the planform areas as an efficiency correlating parameter, further complicates the issue and makes separation of the effects of shape variables difficult." Unlike Mach number, Reynolds number etc. which can be derived from dimensional analysis and can be demonstrated to have significance in particular circumstances, the volume parameter has no such specific and definable significance and contains many shape variables having widely differing effects with changing Mach number, R_e and incidence. Although no better alternative exists, its use does more harm than good. The factors involved are too complicated to be correlated by a single simple parameter.

An assumption often implicitly made is that a flat wing and underslung body configuration, when tested in the inverted body position, corresponds to a normal flat-bottomed wing. Although this arrangement has been proposed in order to shield the body from high heating rates in low lift atmospheric re-entries, it has little merit in the present application and is unlikely to give the optimum upper surface configuration. The assumption is that the exact upper surface shape is irrelevant, an assumption which is demonstrably wrong.

A/

A contributory factor in the effect of the shape of the upper surface is the incidence under consideration and this also determines the available lift to a large extent. Many results are presented in the form of $(L/D)_{max}$ vs volume parameter but the lift coefficient corresponding to the quoted maximum lift/drag ratio is not taken into consideration. In many cases the actual lift coefficient developed is impractically small and the relative merit of different shapes totally different at realistic lift coefficients. An example of this is the caret wing which has similar maximum lift coefficients to plain wings but shows to advantage when compared on a C_L basis at high C_L's. Similarly, rectangular wings which, on a volume parameter basis, are better than triangular wings at low C_L's due to their higher average Reynolds number, lose this advantage at high C_L's due to increasing tip losses. Interference designs show a similar loss of $(L/D)_{max}$ with increasing lift coefficient. Becker[32] dismisses the caret wing with precisely the reasoning given above and draws conclusions regarding the relative merit of a wide range of shapes in terms of the volume parameter and without considering the likely effect of a large increase in Reynolds number.

The problem of Reynolds number affects almost all the published results as most of the variations found were caused or largely influenced by viscous effects and test Reynolds numbers were generally in the $0{\cdot}7 \times 10^6$ to $4{\cdot}5 \times 10^6$ range, mostly about $1{\cdot}5 \times 10^6$. The result is that little of the experimental evidence available can be used directly for estimating the optimum configuration of a full scale hypersonic cruise vehicle.

The conclusion to be drawn from the remarks of this Section is that experimental determination of the effect of variations in shape and of the optimum configuration for a hypersonic cruise vehicle can only be achieved together with theoretical consideration at least until tests are carried out at substantially higher Reynolds numbers. At present, the most realistic answers are probably those derived from theoretical analyses such as that of Collingbourne and Peckham [22] and of Section 2, supported, where possible, by experimental evidence.

4.4 Conclusions

Three-component force measurements have been made on six thin delta wings thought to be suitable for hypersonic cruise vehicles and a theoretical and numerical investigation made into the factors affecting cruise vehicle performance in the atmosphere.

Apart from the direct results of the theoretical study, it showed that viscous forces would be proportionately less important in full scale than at the test Reynolds numbers and hence many of the experimental results would not be directly applicable. The main use of the experimental results would be to substantiate the theoretical methods used in estimating full scale characteristics. Alternatively, by isolating the discreet factors producing the measured results, these could be translated to full scale.

The results confirmed theoretical predictions that the mean pressure over flat delta surfaces with attached leading edge shocks is around 5% less than the value obtained by assuming complete two-dimensional flow. The initial loss with shock detachment was also small. The lift of the caret wings was closely predicted by two-dimensional oblique shock theory except at the lower test Reynolds number of $0{\cdot}9 \times 10^6$ where there was some evidence of an increase of lift due to viscous effects on the lower surfaces.

Analysis of the skin friction drag gave good agreement with theory within the margin of unknowns arising from experimental error and base drag. Those variations outside of this margin indicated the onset of transition on the high aspect ratio plain wing which was not present on the corresponding low aspect ratio wing; an apparent delaying of transition with reducing aspect ratio. There were also significant increases in friction drag on the caret and twisted wings indicating viscous effects on the concave lower surfaces.

The viscous effects, evident on the caret and twisted wings relative to the plain wings at a Reynolds number of $0{\cdot}9 \times 10^6$ were no longer present or reduced at a Reynolds number of $3{\cdot}5 \times 10^6$. This highlights the problem of translating tests at these Reynolds numbers to full scale.

At the test Reynolds numbers there was little difference between the maximum lift/drag ratios achieved on the flat-bottomed, caret or twisted wings of similar aspect ratio. The caret wing showed an advantage in that it achieved its maximum lift/drag ratio at a higher value of lift coefficient and this advantage would be expected to remain or be enlarged at full scale. The twisted wing showed a similar advantage and in addition had a centre of pressure position some 2% further forward than the other wings and a more useful cross-sectional area distribution.

The results also confirmed predictions for the incidence for maximum lift/drag ratio and the Reynolds number at which this would coincide with the condition of upper surface streamwise obtained from the theoretical analysis.

This analysis gave simple expressions for the variation of optimum thickness with Mach number, Reynolds number and surface heat transfer for the case of upper surfaces streamwise. The upper surface streamwise condition was shown to be near to the condition for maximum L/D for vehicles with realistic wing loadings and lift/drag ratios in the atmosphere. In these conditions skin friction drag would be a small proportion of the total drag.

Theoretical estimates indicated that lift/drag ratios from 5 - 10 should be obtainable on wings of thickness angles of 5° to 10° in the altitude range 80,000 to 150,000 ft. Plain, caret or twisted wings would be satisfactory from the lift/drag ratio point of view, with the caret and twisted wings having slight advantages for different reasons.

5. Acknowledgements

This report is an edited extract from a thesis presented at London University for the degree of Ph.D.[50]. Fuller acknowledgements can be found in the thesis but my greatest thanks by far go to Mr. J. L. Stollery of Imperial College who supervised the research and helped with advice and encouragement at every stage of the work.

The work was sponsored by the NPL and Dr. L. Pennelegion and other members of the staff were ever interested and helpful.

Appendix A/

Appendix A

Incidence for maximum lift/drag ratio

Let α = wing centre-line incidence

$$\beta = \frac{\theta}{2} \quad .$$

and remaining notation as on pages 8 to 10.

The pressure coefficient will be assumed to be given to sufficient accuracy by a second order expression, i.e. for $M >> 1$.

$$C_p = \frac{2\delta}{M} + A\delta^2 \qquad \cdots (A.1)$$

then

$$C_D = C_{D_U} + C_{D_L} + C_{D_F}$$

$$= \frac{4}{M}(\beta^2 + \alpha^2) + 2A\beta(\beta^2 + 3\alpha^2) + C_{D_F} \qquad \cdots (A.2)$$

Similarly

$$C_L = \frac{4\alpha}{M} + 4A\beta\alpha \qquad \cdots (A.3)$$

Considering the drag/lift ratio and differentiating with respect to α ,

$$C_L^2 \frac{\partial\left(\frac{C_D}{C_L}\right)}{\partial\alpha} = \left(\frac{4\alpha}{M} + 4A\beta\alpha\right)\left(\frac{8\alpha}{M} + 12A\beta\alpha\right)$$

$$- \left[\frac{4}{M}(\beta^2 + \alpha^2) + 2A\beta(\beta^2 + 3\alpha^2) + C_{D_F}\right]\left[\frac{4}{M} + 4A\beta\right] \qquad \cdots (A.4)$$

$$= 0 \quad \text{for maximum or minimum}$$

At $\left(\frac{C_D}{C_L}\right)_{\min}$ $\alpha \equiv \alpha'$

Hence

$$\alpha^2\left(\frac{4}{M} + 6A\beta\right) - \left(\frac{4}{M}\beta^2 + 2A\beta^3 + C_{D_F}\right) = 0 \qquad \cdots (A.5)$$

and

$$\alpha' = \sqrt{\frac{\beta^2(1 + 0{\cdot}5MA\beta) + 0{\cdot}25MC_{D_F}}{(1 + 1{\cdot}5\,MA\beta)}} \qquad \cdots (A.6)$$

Thus/

Thus it can be seen that for linear theory ($A = 0$) and inviscid flow ($C_{D_F} = 0$), the optimum incidence is achieved with the upper surface streamwise ($\alpha' = \beta$). The Mach number term in the numerator is one-third of that in the denomenator and so the effect of the non-linear pressure term is to decrease α' while the skin friction term will increase it. Taking the Newtonian limit of $C_p = 2\delta^2$, i.e. letting $M \to \infty$, gives $\frac{1}{\sqrt{3}}\beta$ and this is the other limit as compared to the linear result in the absence of skin friction. Numerical calculation for the range of wing loadings and altitudes considered in Section 2 show that the upper surface streamwise condition is optimum for wings of about 5° thickness angle.

[A similar analysis, using different methods and assumptions, is carried out by Collingbourne and Peckham in Ref. 22 with the same result.]

Appendix B

Detailed development of theory of Section 2.2

B.1 Lift

Ref. 74 gives the derivation of a new approximation to pressure versus flow deflection at hypersonic speeds which is used in the theoretical development of this Appendix. In the approximation the pressure is given by:-

$$\left(\frac{p}{p_\infty} - 1 \right) \simeq \gamma M\delta + 1{\cdot}1 (M\delta)^{2{\cdot}15} \qquad \cdots (B.1)$$

For slender bodies with upper surfaces streamwise,

$$C_L \simeq C_{p_L} \qquad \cdots (B.3)$$

and hence from (B.1) above,

$$C_L = \frac{2\theta}{M} + 1{\cdot}5 M^{0{\cdot}15} \theta^{2{\cdot}15} \qquad \cdots (B.4)$$

for $\gamma = 1{\cdot}4$.

B.2 Skin friction drag

The Blasius solution for the laminar boundary layer on a flat plate with zero pressure gradient is,

$$C_f = \frac{\tau_0}{0{\cdot}5\rho U^2} = \frac{0{\cdot}664}{\sqrt{R_{e_x}}} \qquad \cdots (B.5)$$

In high speed flow, the reference temperatures method (see, for example, Ref. 71) gives the same expression except that conditions are evaluated at a reference temperature T^*, (where $T^* = T_3 + 0{\cdot}5(T_W - T_3) + 0{\cdot}22 (T_{W_0} - T_3)$ see page 36) giving:-

$$C_F = 0{\cdot}664 \sqrt{\frac{C^*_\infty}{R_{e_x}}} \qquad \cdots (B.6)$$

where C^*_∞ is the constant of proportionality in the viscosity/temperature relationship,

$$\frac{\mu^*}{\mu_\infty} = C^*_\infty \frac{T^*}{T_\infty} \qquad \cdots (B.7)$$

and/

and

$$C^*_\infty = \frac{T_\infty + 110}{T^* + 110} \left(\frac{T^*}{T_\infty} \right) \qquad \cdots (B.8)$$

from Sutherland's law (e.g. Ref. 53) and with temperature in °K.

If the less accurate but more amenable relationship

$$\frac{u^*}{u_\infty} = \left(\frac{T^*}{T_\infty} \right)^n \qquad \cdots (B.9)$$

is used then

$$\bar{C}^*_\infty = \left(\frac{T^*}{T_\infty} \right)^{n-1} \qquad \cdots (B.10)$$

where the bar distinguishes this value from that obtained using the previous formula.

For a triangular surface with conditions on its surface shown by suffix ' , the skin friction drag is given (obtained by integrating over the surface, e.g. Ref. 19) by,

$$C_{D_{F_1}} = 1{\cdot}77\, Q_1 \sqrt{\frac{C_f}{R_{e_{1_L}}}} \qquad \cdots (B.11)$$

where

$$Q_1 = \frac{\rho_1 U_1^2}{\rho_\infty . U_\infty^2} \qquad \cdots (B.12)$$

and $R_{e_{1_L}}$ is the Reynolds number based on conditions ' and the wing length L.

It can be seen from equation (B.26a) that the skin friction coefficient on any surface varies as $\left(\frac{p}{p_\infty} \right)^{1/2}$. Thus $C_{D_F} \sim \delta^n$ with n increasing with M. For slender wings near zero incidence the two surfaces have nearly equal and opposite variation of skin friction drag with flow deflection. Thus the skin friction can be taken as approximately independent of incidence (but not of thickness) and can be determined at any convenient incidence.

If the small change due to the angled vee roof is ignored, the upper and lower surfaces are at equal incidence when each is at half the thickness angle to the flow. With suffix ³ designating conditions on the surfaces in this case, the total skin friction drag is given approximately by:-

C_{D_F}/

$$C_{D_F} \simeq 1{\cdot}77\, Q_3\, (E_L + E_U) \sqrt{\frac{\bar{C}_3}{R_{e_{3_L}}}} \qquad \cdots (B.13)$$

where

$$E_L = \frac{\text{Lower surface area}}{\text{plan area}}$$

$$E_U = \frac{\text{Upper surface area}}{\text{plan area}}$$

Other terms are as previously defined but for conditions 3 ,

and

$$\bar{C}_3 \equiv \left(\frac{T^*}{T_3}\right)^{1-n} \qquad \cdots (B.14)$$

where,

$$T^* = T_3 + 0{\cdot}5(T_W - T_3) + 0{\cdot}22(T_{W_0} - T_3) \qquad \cdots (B.15)$$

(Ref. 71)

where

T_W = wall temperature

T_{W_0} = adiabatic wall temperature

and

$$T_{W_0} = T_3 \left(1 + \sigma_p^{1/2}\, \frac{\gamma - 1}{2}\, M_3^2\right)$$

Hence

$$T_{W_0} - T_3 \simeq \frac{\gamma - 1}{2} M_3^2\, T_3 \qquad \cdots (B.16)$$

for

$$\sigma_p \simeq 1 .$$

The practical extremes of wall temperatures T_W in (B.15) above can be taken as,

$T_W = T_3$ for '100%' cooling,

and

$T_W = T_{W_0}$ for zero cooling.

Thus, substituting (B.16) into (B.15) for $M \gg 1$,

T*/

$$T^* \simeq T_3 + H(T_{W_O} - T_3)$$

$$\simeq T_3 \left(\frac{H(\gamma - 1)}{2} M_3^2 \right)$$

$$T^* \simeq \frac{H(\gamma - 1)}{2} \cdot M_3^2 \cdot T_3 \qquad \cdots \text{(B.17a)}$$

where H varies from 0·22 to 0·72 as cooling varies from 100% to zero.

For hypersonic flow and slender bodies,

$$\frac{U_3}{U_\infty} \simeq \frac{U_3^2}{U_\infty^2} \simeq 1 \qquad \cdots \text{(B.18)}$$

Hence,

$$M_\infty = \frac{U_\infty}{a_\infty} \simeq \frac{U_3}{a_3} \simeq \frac{U_3}{a_{(3)}} \cdot \frac{a_3}{a_\infty} \simeq M_3 \frac{a_3}{a_\infty}$$

but

$$\left(\frac{a_3}{a_\infty} \right)^2 = \frac{T_3}{T_\infty}$$

$$\therefore \quad M_3^2 T_3 = M_\infty^2 T_\infty \qquad \cdots \text{(B.19)}$$

and hence

$$T^* \simeq \frac{H.(\gamma - 1)}{2} \cdot M_\infty^2 T_\infty \qquad \cdots \text{(B.17b)}$$

$$\therefore \quad Q_3 \sqrt{\frac{\bar{C}_3}{R_{e_3}}_L} = \frac{\rho_3}{\rho_\infty} \sqrt{\left(\frac{T^*}{T_3} \right)^{n-1} \cdot \frac{\mu_3}{\rho_3 U_3 L}}$$

$$= \sqrt{\left[\frac{H(\gamma - 1)}{2} \right]^{n-1} \left(\frac{M_\infty^2 T_\infty}{T_3} \right)^{n-1} \frac{u_\infty}{\rho_\infty U_\infty L} \frac{\rho_3}{\rho_\infty} \left(\frac{T_3}{T_\infty} \right)^n}$$

$$= \frac{1}{\bar{H} M^{1-n}} \cdot \left(\frac{p_3}{p_\infty} \right)^{1/2} \cdot \sqrt{\frac{1}{R_{e_\infty}}_L} \qquad \cdots \text{(B.20a)}$$

where

$$\bar{H} = \left[\frac{H.(\gamma - 1)}{2} \right]^{\frac{1-n}{2}} \qquad \cdots \text{(B.21)}$$

$\bar{H}$ varies from 0·7 to 0·8 as the wall cooling varies from 100% to zero for $n = 0·76$, the usual value. ($n = 0·84$ for tunnel).

For/

For conditions in the atmosphere, the effect of altitude can be more clearly seen by writing the Reynolds number in terms of a standard Reynolds number taken at some defined standard conditions. With suffix s to define standard values,

$$R_{e_{\infty_L}} = \sigma_s \, R_{e_s} \left(\frac{T_s}{T_\infty} \right)^{1-n} M_\infty \qquad \cdots \text{(B.22)}$$

where $$\sigma_s = \frac{\rho_\infty}{\rho_s} \quad \text{the relative density} \qquad \cdots \text{(B.23)}$$

and $$R_{e_s} = \frac{\rho_s \, a_{s_L}}{\mu_s} \qquad \cdots \text{(B.24)}$$

In the atmosphere, the temperature range 216°K to 266°K covers the range 13,000 ft to 200,000 ft [73] and using 242°K constant in this range introduces only ±2·5% error. The appropriate standard conditions are those at 125,000 ft. In terms of standard conditions,

$$Q_3 \sqrt{\frac{C_3}{R_{e_3}}}_L = \frac{1}{\sigma_s^{1/2} \, \bar{H} \, M^{1\cdot5-n}} \sqrt{\frac{1}{R_{e_s}}} \left(\frac{p_3}{p_\infty} \right)^{1/2} \qquad \cdots \text{(B.20b)}$$

The term $\left(\frac{p_3}{p_\infty} \right)^{1/2}$ has been treated in the same way as $\left(\frac{p}{p_\infty} - 1 \right)$ in Ref. 74 to arrive at the approximation,

$$\left(\frac{p_3}{p_\infty} \right)^{1/2} = 1 + 0\cdot25\gamma M\theta + 0\cdot0485 \, (M\theta)^{1\cdot77} \qquad \cdots \text{(B.25)}$$

which is valid to 5% for $M\theta \leq 4$, sufficient for the present purpose.

Then, substituting (B.20a) into (B.13),

$$C_{D_F} = \frac{1\cdot77(E_L + E_U)}{\bar{H} \, M_\infty^{1-n} \, R_{e_{\infty_L}}} \cdot \left(\frac{p_3}{p_\infty} \right)^{1/2} \qquad \cdots \text{(B.26a)}$$

or in terms of conditions at a standard altitude,

$$C_{D_F} = \frac{1\cdot77 \, (E_L + E_U)}{\bar{H} \, M_\infty^{1\cdot5-n} \sigma_s^{1/2} \, R_{e_s}^{1/2}} \cdot \left(\frac{p_3}{p_\infty} \right)^{1/2} \qquad \cdots \text{(B.26b)}$$

B.3 Lift/drag ratio

It is more convenient to treat the reciprocal,

$$\frac{C_D}{C_L} = \theta + \frac{C_{D_F}}{C_L} + \frac{C_{D_B}}{C_L} \qquad \cdots (B.27)$$

for upper surfaces streamwise and where

C_{D_B} = base drag coefficient based on plan area.

Let $p_B \equiv$ base pressure $\equiv (1-b)p_\infty$ $\cdots$ (B.28a)

then $$C_{D_B} = \frac{2.bp_\infty}{\gamma M^2 p_\infty} \cdot \frac{\theta Ls}{sL}$$

$$C_{D_B} = \frac{2b\theta}{\gamma M^2} \qquad \cdots (B.28b)$$

Hence from equations (B.4), (B.25), (B.26a), (B.28b) and (B.27)

$$\frac{C_D}{C_L} = \theta \frac{1{\cdot}77(E_L + E_U)\, M^{(1+n)} \left[1 + 0{\cdot}35(M\theta) + 0{\cdot}0485(M\theta)^{1{\cdot}77}\right]}{\bar{H}\, R_{e_{\infty_L}}^{1/2} \left[2\theta M + 1{\cdot}5(M\theta)^{2{\cdot}15}\right]} + \frac{b\theta}{1{\cdot}4M\theta + 1{\cdot}05(M\theta)^{2{\cdot}15}} \qquad \cdots (B.29a)$$

Or, for flight in the atmosphere,

$$\frac{C_D}{C_L} = \theta + \frac{1{\cdot}77(E_L + E_U)\, M^{(0{\cdot}5+n)} \left[1 + 0{\cdot}35\, M\theta + 0{\cdot}048(M\theta)^{1{\cdot}77}\right]}{\bar{H}\, \sigma_s^{1/2}\, R_{e_s}^{1/2} \left[2\theta M + 1{\cdot}5(M\theta)^{2{\cdot}15}\right]} + \frac{b\theta}{1{\cdot}4M\theta + 1{\cdot}05(M\theta)^{2{\cdot}15}} \qquad \cdots (B.29b)$$

B.4 Thickness for $(L/D)_{max}$ with upper surfaces streamwise

For a maximum or minimum

$$\frac{\partial\left(\frac{D}{L}\right)}{\partial\theta} = 0$$

$$\frac{\partial}{\partial\theta}\left[\frac{C_L\,\theta + C_{D_F} + C_{D_B}}{C_L}\right] = 0$$

It/

It will be assumed that the base drag has little effect on the thickness for maximum lift/drag ratio, an assumption confirmed by the numerical results, and hence,

$$\frac{\partial\left(\frac{D}{L}\right)}{\partial\theta} = C_L \frac{\partial(C_L\,\theta)}{\partial\,\theta} - C_L \frac{\partial C_L}{\partial\theta} + C_L \frac{\partial C_{D_F}}{\partial\theta} - C_{D_F} \frac{\partial C_L}{\partial\theta}$$

$$= C_L^2 + C_L \frac{\partial C_{D_F}}{\partial\theta} - C_{D_F} \frac{\partial C_L}{\partial\theta}$$

$$= 0$$

With the expressions for C_{D_F} and C_L obtained from equations (B.26) and (B.4), the following expression can be obtained,

$$\left[2(M\theta') + 1{\cdot}5(M\theta')^{2{\cdot}15}\right]^2 = K\left[2 + 3{\cdot}23(M\theta')^{1{\cdot}15} - 0{\cdot}075(M\theta')^{1{\cdot}77}\right.$$

$$\left. + 0{\cdot}604(M\theta')^{2{\cdot}15} + 0{\cdot}028(M\theta')^{2{\cdot}92}\right] \qquad \cdots \text{(B.30)}$$

where θ' is the thickness angle for maximum lift/drag ratio with upper surfaces streamwise and K is given by

$$K = \frac{1{\cdot}77(E_L + E_U)\,M^{(2+n)}}{\bar{H}\,R_{e_{\infty_L}}^{1/2}} \qquad \cdots \text{(B.31a)}$$

$$= \frac{1{\cdot}77(E_L + E_U)\,M^{(1{\cdot}5+n)}}{\bar{H}\,\sigma_s^{1/2}\,R_{e_s}^{1/2}} \qquad \cdots \text{(B.31b)}$$

Equation (B.30) has been solved(graphically)* to give:-

$$M\theta' = 0{\cdot}688K^{0{\cdot}477} \qquad \cdots \text{(B.32a)}$$

or

$$\theta' = \frac{0{\cdot}688K^{0{\cdot}477}}{M} \qquad \cdots \text{(B.32b)}$$

Then, substituting equations (B.32a) and (B.32b) into equation (B.29) gives:-

$$M'\left(\frac{D}{L}\right)_{\theta'}\Big/$$

---

*Plotting the L.H.S. and R.H.S. of equation (B.30) against $(M\theta)$ for various values of K produces a series of solutions which when plotted against K on log paper, produce a straight line.

$$M\left(\frac{D}{L}\right)_{\theta'} = \left[0{\cdot}688K^{0{\cdot}477} + \frac{K(1 + 0{\cdot}241K^{0\,477} + 0{\cdot}025K^{0{\cdot}845})}{1{\cdot}376K^{0{\cdot}477} + 0{\cdot}672K^{1{\cdot}03}} + \frac{0{\cdot}688bK^{0{\cdot}477}}{(0{\cdot}95K^{0{\cdot}477} + 0{\cdot}47K^{1{\cdot}03})}\right] \quad \cdots \text{(B.33)}$$

Equation (B.33) has been approximated (graphically) to give:-

$$M\left(\frac{D}{L}\right)_{\theta'} = 1{\cdot}28K^{0{\cdot}466} + \frac{b}{1{\cdot}38 + 0{\cdot}684K^{0{\cdot}553}} \quad \cdots \text{(B.34b)}$$

or, for zero base drag,

$$M\left(\frac{D}{L}\right)_{\theta'} = 1{\cdot}28K^{0{\cdot}466} \quad \cdots \text{(B.34a)}$$

Finally, it is possible to show the effect of Mach number explicitly by combining that part included in the parameter K with that outside to give,

$$\theta' = 0{\cdot}688\left[\frac{1{\cdot}77(E_L + E_U)\,M^{n-0{\cdot}6}}{\bar{H}\,\sigma_s^{1/2}\,R_{e_s}^{1/2}}\right]^{0{\cdot}477} \quad \cdots \text{(B.35a)}$$

and

$$\left(\frac{D}{L}\right)_{\theta'} = 1{\cdot}28\left[\frac{1{\cdot}77(E_L + E_U)\,M^{n-0{\cdot}66}}{H\,\sigma^{1/2}\,R_{e_s}^{1/2}}\right]^{0{\cdot}466} \quad \cdots \text{(B.36a)}$$

for zero base drag.

Taking the usual value of $n = 0{\cdot}76$, this gives,

$$\theta' \sim M^{0\,076} \quad \cdots \text{(B.35b)}$$

and

$$\left(\frac{L}{D}\right)_{\theta'} \sim M^{-0{\cdot}047} \quad \cdots \text{(B.36b)}$$

which confirms the insensitivity of maximum lift/drag ratio to Mach number at hypersonic speeds, shown by experimental results.

The wing loading, ω, corresponding to optimum conditions can be obtained from,

$$C_L \simeq Cp \simeq \frac{\omega}{0{\cdot}5\gamma M^2 p_\infty} \quad \cdots \text{(B.37)}$$

hence,/

hence,

$$\omega = p_{\infty} \left(\gamma M\theta + 1{\cdot}1 (M\theta)^{2{\cdot}15} \right) \qquad \cdots \quad (B.38)$$

The various approximations used in deriving the expressions of this appendix have been accurate to within 5% in the required range of variables. Hence it is estimated that the results obtained from these expressions would be accurate to about ± 20% (including possible inaccuracies in the theoretical assumptions) while the trends would be accurate to ±5%.

Appendix C/

Appendix C

Derivation of expressions for the twisted wing

It is desired to find the dimensions of a twisted delta wing of given twist that will have the same volume as a plain delta wing of equal plan area and aspect ratio. With system of axis, origin at the rear, on the centre-line of lower surface, x forwards, z upwards +ve, and y sideways let the body dimensions be length ℓ, span $\pm S$ and trailing edge thickness Z as shown below.

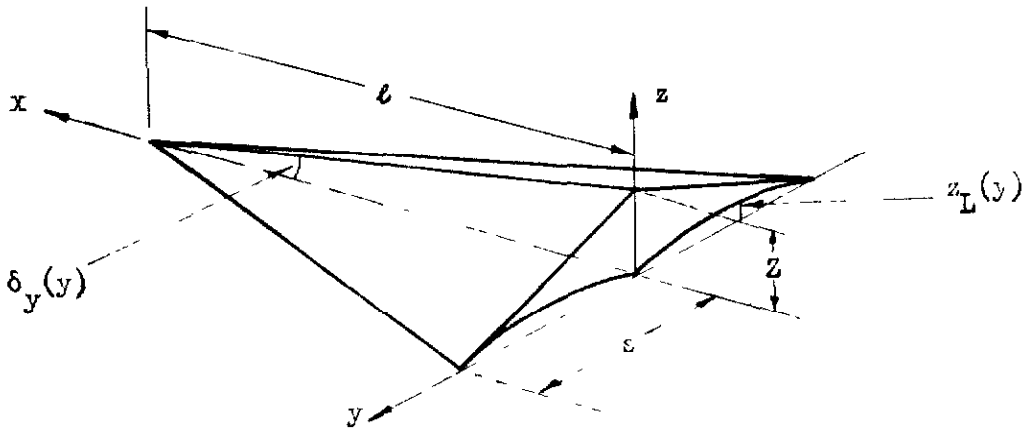

Let the thickness angle taken along y = constant be $\delta y(y)$ and the height of the lower surface at the trailing edge be $z_L(y)$, and upper surface $z_U(y)$.

Then
$$x = \ell\left(1 - \frac{y}{S}\right) \qquad \ldots (C.1)$$

and for linear twist
$$\delta y = \delta_o\left(1 - \frac{ay}{S}\right) \qquad \ldots (C.2)$$

where δ_o is root thickness angle

and
$$a = \left(1 - \frac{\delta t}{\delta_o}\right) \qquad \ldots (C.3)$$

where δt is tip thickness angle.

Also let $z_U(y) - z_L(y) = z_y$ the local trailing edge thickness, then the elemental volume at any plane y = constant is,

$$\delta V = 0{\cdot}5 x_y z_y \delta_y \qquad \ldots (C.4)$$

$$dV = 0{\cdot}5\ell^2 \delta_o \left(1 - \frac{y}{S}\right)^2 \left(1 - \frac{ay}{S}\right) dy \qquad \ldots (C.5)$$

Transforming the variable to $Y = \frac{y}{S}$, $dy = SdY$, and

dV/

$$dV = 0{\cdot}5S\ell^2\,\delta_o(1-Y)^2\,(1-aY)\,dY$$

$$V = 0{\cdot}5S\ell^2\,\delta_o(1-Y)^2\,(1-aY)\,dY \qquad \cdots (C.6)$$

$$= \frac{S\ell^2\delta_o}{12}\left[4-a\right]$$

$$= \frac{(25)\mathscr{A}}{b}\left(1-\frac{a}{4}\right) \qquad \cdots (C.7)$$

where $\frac{a}{4}$ represents the change of volume due to twist and a, the twist ratio is given by (C.3).

For equal length and aspect ratio, with suffix 1 for plain wing and suffix 2 for the twisted wing of equal volume,

$$\delta_{o_1} = \delta_{o_2}\left(1-\frac{a}{4}\right) \qquad \cdots (C.8)$$

and for the twisted wing of the present tests where the tip thickness was half the root thickness,

$$a = 0{\cdot}5$$

and $\therefore$

$$\delta_{o_2} = 1{\cdot}143\,\delta_{o_1} \qquad \cdots (C.9)$$

The trailing edge contour z_L is given by,

$$z_L = Z\left(1-\frac{y}{S}\right) - zy = Z\left[\left(1-\frac{y}{S}\right) - 1 + (1+a)\frac{y}{S} - a\left(\frac{y}{S}\right)^2\right]$$

$$z_L = aZ\left[\frac{y}{S}\left(1-\frac{y}{S}\right)\right] \qquad \cdots (C.10)$$

BMG

References/

References

No.	Author(s)	Title, etc.
1	Küchemann, D.	Hypersonic Aircraft and their Aerodynamic Problems. Progress in Aeronautical Sciences, Vol.6., Pergamon Press 1965.
2	Peckham, D. H. and Crabtree, L. F.	The range performance of hypersonic aircraft. A.R.C. C.P.932, 1966.
3	Küchemann, D. and Weber, J.	An analysis of some performance aspects of various types of aircraft designed to fly over different ranges at different speeds. RAE Tech Report No.66188. June, 1966. A.R.C.28 369.
4	Eggers, Jn., A. Allen, H. J. and Neice, S. E.	A comparative analysis of the performance of long-range hypervelocity vehicles. NACA Report 1382. 1958.
5	Crabtree, L. F.	Boundary-layer effects on hypersonic aircraft. Unpublished RAE Memo.
6	Nonweiler, T.	Delta wings of shapes amenable to exact shock-wave theory. A.R.C.22 644, March, 1961.
7	Townsend, L. H.	On lifting bodies which contain two-dimensional supersonic flows. A.R.C. R & M 3383, 1963.
8	Flower, J. W.	Configurations for high supersonic speeds derived from simple shock waves and expansion. Communicated by Prof. A. R. Collar. A.R.C.24 750, April, 1963. and Jn. of Royal Aero.Soc.Vol.67. May, 1963.
9	Jones, J. G.	A method for designing lifting configurations for high supersonic speeds using the flow field of non-lifting cones. RAE Report Aero.2674. A.R.C.24 846, March, 1963.
10	Molder, S.	Lifting configurations for high supersonic speeds derived from internal axisymmetric conical flow fields. McGill University Report 1965.
11	Woods, B. A.	The construction of a compression surface based on an axisymmetric conical flow field. RAE T.N. Aero 2900. June, 1963. A.R.C.25 087.
12	Moore, K. C.	The application of known flow fields to the design of wings with lifting upper surfaces at hypersonic speeds. RAE Tech. Report No.65034. February, 1965.

13/

No.	Author(s)	Title, etc.
13	Pike, J.	The analytical performance of lifting surfaces supporting plane shock waves. RAE Tech. Report No.66127. April, 1966. A.R.C.28 452.
14	Pike, J.	Minimum drag surfaces of given lift which support two-dimensional supersonic flow fields. RAE Tech. Report 66305. September, 1966. A.R.C.28 825.
15	Bartlett, R. S.	High lift-drag ratio double wedges of given volume which support two-dimensional supersonic flow fields. RAE Tech. Report 66306. October, 1966. A.R.C.28 826.
16	Peckham D. H.	On three-dimensional bodies of delta planform which can support plane attached shock wave. A.R.C. C.P.640. 1962.
17	Catherall, D.	Boundary-layer characteristics of caret wings. A.R.C. C.P.694. 1963.
18	Cooke, J. C.	Leading-edge effects on caret wings. A.R.C. C.P.978. 1964.
19	Catherall, D.	Boundary-layer effects on caret wings. RAE Tech. Note Aero.2972. August, 1964. A.R.C.26 391.
20	Squire, L. C.	Pressure distributions and flow patterns at M = 4.0 on some delta wings. Part I. Wings of inverted 'V' cross-section Part II. Flat wings A.R.C. R & M 3373. 1963.
21	Pennelegion, L. and Cash, R. F.	Preliminary measurements in a shock tunnel of shock angle and undersurface pressure related to a Nonweiler wing. A.R.C. C.P.684. 1962.
22	Collingbourne, J. R. and Peckham, D. H.	The lift and drag characteristics of caret wings at Mach numbers between 5 and 10. A.R.C. C.P.930. 1966.
23	Trimpi, R. L. et al.	Aerodynamic and heating problems of advanced re-entry vehicles. NASA SP-23. December, 1962.
24	Roe, P. L.	Some exact calculations of the lift and drag produced by a wedge in supersonic flow either directly or by interference. A.R.C. R & M 3478. 1964.

25/

No.	Author(s)	Title, etc.
25	McLellan, C. H. and Ladson, C. L.	A summary of the aerodynamic performance of hypersonic gliders. NASA. TM.X-237. March, 1960.
26	Fetterman, D.	Favorable interference effects on the maximum lift-drag ratios of half-cone delta-wing configurations at Mach 6.86. NASA. TN.D-2942. August, 1965.
27	Fetterman, D. et al.	Studies relating to the attainment of high lift-drag ratios at hypersonic speeds. NASA TN.D-2956. August, 1965.
28	Baines, D.	Estimates of leading-edge bluntness for a swept-wing hypersonic aircraft. RAE Tech. Memo Aero.795. A.R.C.24 972, May, 1963.
29	Capey, E. C.	Alleviation of leading-edge heating by conduction and radiation. RAE Tech. Report No.66311. October, 1966. A.R.C.28 924.
30	Penland, J. A.	Maximum lift-drag ratio characteristics of rectangular and delta wings at Mach 6.9. NASA TN.D-2925. August, 1965.
31	Blackstock, T. A. and Ladson, C. L.	Comparison of the hypersonic aerodynamic characteristics of some simple winged shapes in air and helium. NASA TN D-2328. June, 1964.
32	Becker, J. V.	Studies of high lift/drag configurations. AIAA paper 64-551. 1964. also ICAS. Congress (4th) Paris 1964. Spartan and MacMillan & Co. Ltd., 1965.
33	Eggers, Jn., A. and Syvertson, C.	Aircraft configurations developing high lift-drag ratios at high supersonic speeds. NACA RM A55L05. 1956.
34	Peckham, D. H.	Pressure distribution measurements on a series of slender delta body shapes at Mach number of 6.85 and 8.60. A.R.C. C.P.791. 1964.
35	Bertram, M. H. et al.	The aerodynamics of hypersonic cruising and boost vehicles. NASA SP.23. December, 1962.
36	Ames Staff	Equations, tables and charts for compressible flow. NACA Report 1135. 1953.

37/

No.	Author(s)	Title, etc.
37	Babaev, D. A.	Numerical solution of the problem of supersonic flow past the lower surface of a delta wing. AIAA Jn.,Vol.1., No.9. September, 1963.
38	Opatowski, T.	Lift drag and pitching moment measurements on a 70° cone, a flat delta and a caret delta wing at a Mach number of 8.3. ARC CP908. 1965.
39	Monagham, R. J.	Formulae and approximations for aerodynamic heating rates in high speed flight. ARC CP360. 1956.
40	Monagham, R. J.	An approximate solution of the compressible laminar boundary layer on a flat plate. R & M 2760. 1949.
41	-	US Standard Atmosphere 1962.
42	Opatowski, T.	A new approximation for pressure versus flow deflection at hypersonic speeds. Jn. R.Ae.S. May, 1967.
43	Picken, J. and Greenwood, G.	Free-flight measurements of heat transfer and observations of transition on a caret wing at Mach numbers up to 5.6. RAE TR.65237. October, 1965. A.R.C.27 820.
44	Needham, D. A.	Progress report on the Imperial College Hypersonic Gun Tunnel. Imperial College of Science and Technology, Aeronautics Dept. Tech. Note No.118. 1963.
45	King, H. H.	A tabulation of base flow properties for cones and wedges. Electro-optical Systems Inc. Rep. RN-17.
46	Hama, F. R.	Experimental studies on the lip shock. AIAA paper No.67-29. 5th Aerospace Sciences Meeting, New York. January, 1967.
47	Weinstein, L. and Neal, Jn., L.	Hypersonic performance of several basic and modified diamond-cross-section delta wing configurations. NASA TN.D-3894. 1967.
48	McLellan, C. H. Bertram, M. H. and Moore, J. A.	An investigation of four wings of square planform at a Mach number of 6.9 in the Langley 11 inch hypersonic tunnel. NACA Report 1310. 1957.

49/

No.	Author(s)	Title, etc.
49	Deem, R. E. and Murphy, J. S.	Flat plate boundary-layer transition at hypersonic speeds. AIAA Paper No.65-128. January, 1965.
50	Opatowski, T.	An experimental study of the flow around and the forces developed by hypersonic lifting vehicles. Thesis submitted for degree of Ph.D. to University of London. September, 1967.
51	Opatowski, T.	A three-component gun tunnel balance designed for testing thin delta wings. To be published as A.R.C. R & M 3664

BMG
PFC

FIG. 2.1

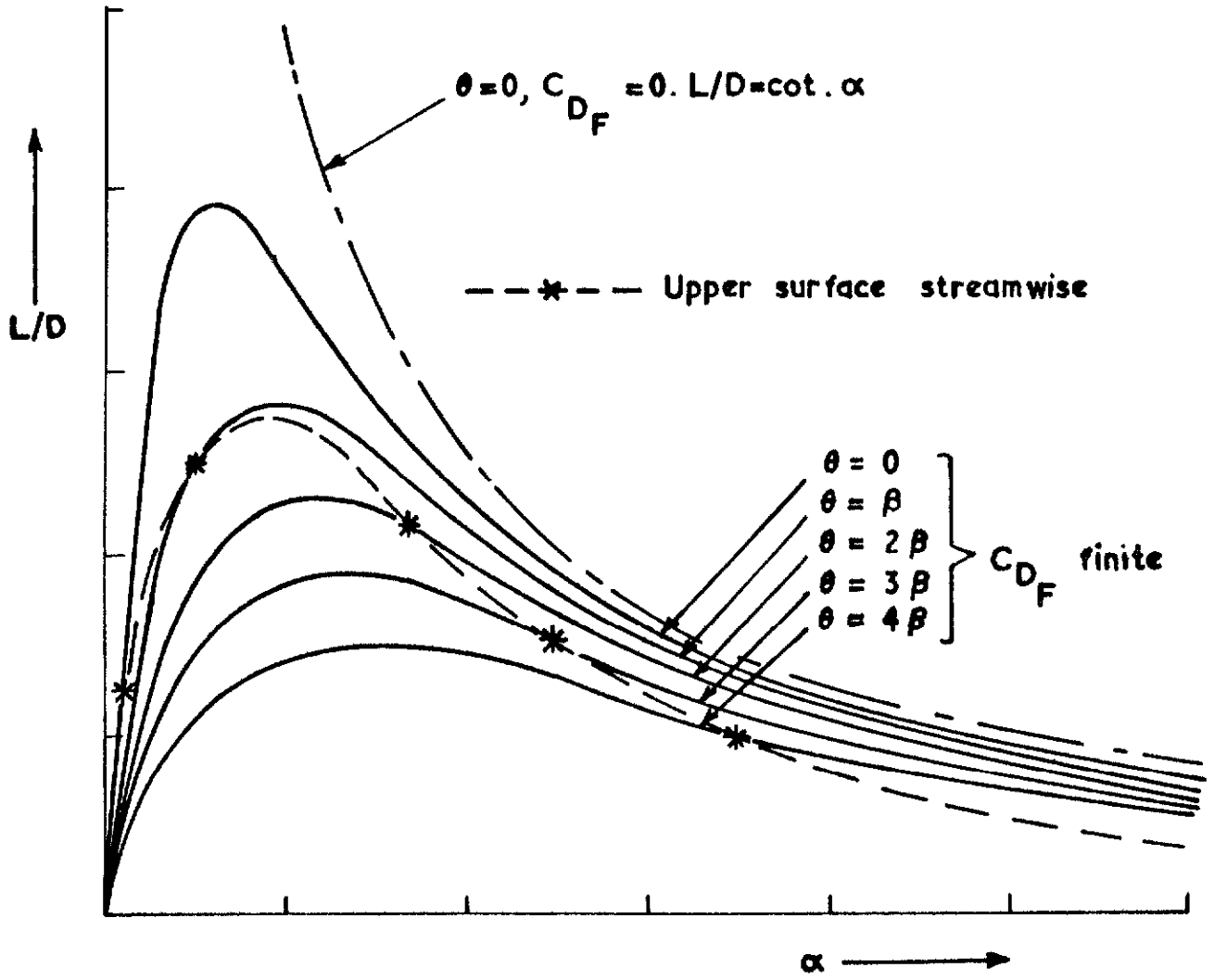

Sketch showing the variation of L/D with incidence for various thickness angles

FIG. 2.2.

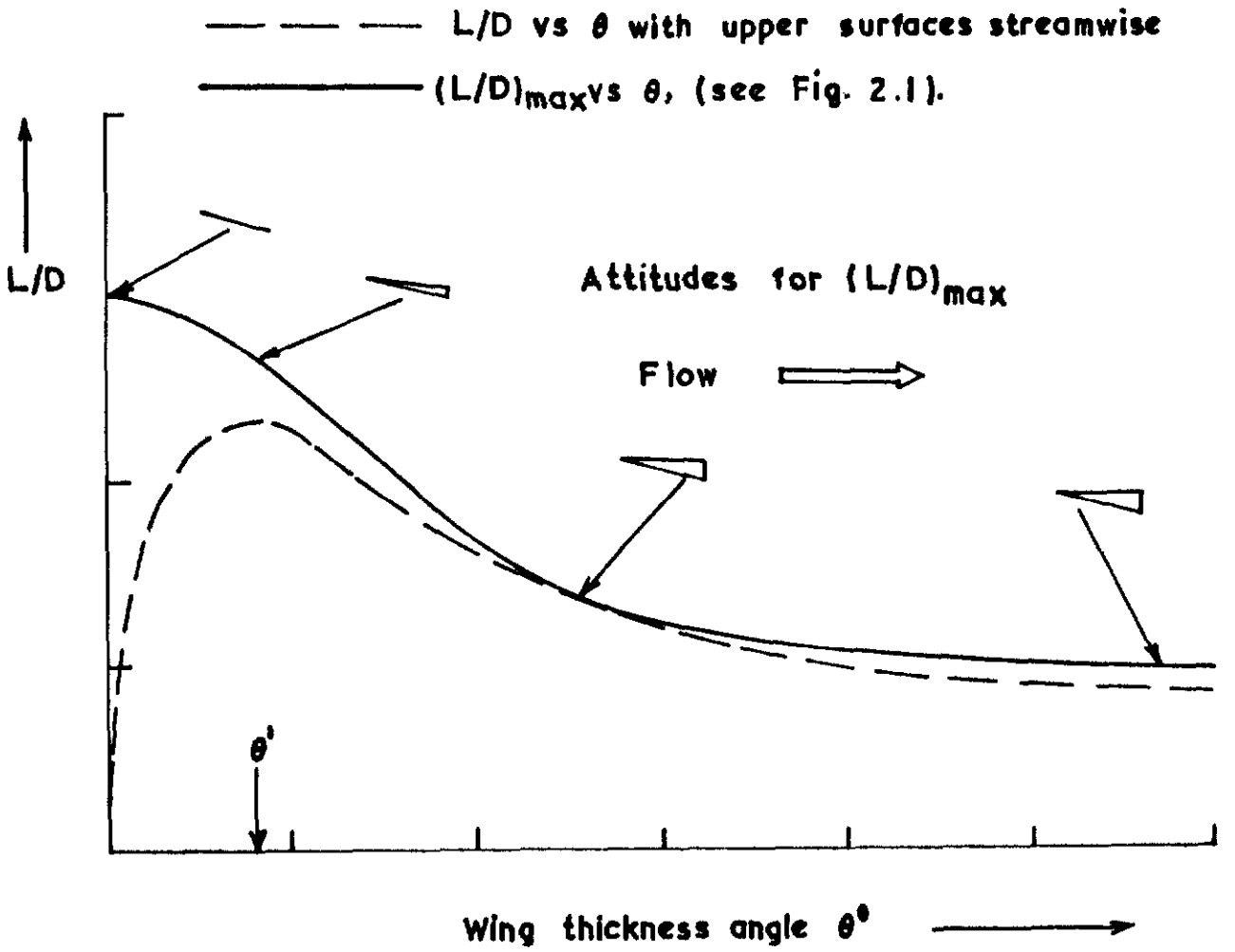

Sketch showing relationship between $(L/D)_{max}$ and the L/D with upper surfaces streamwise

FIG. 2 3

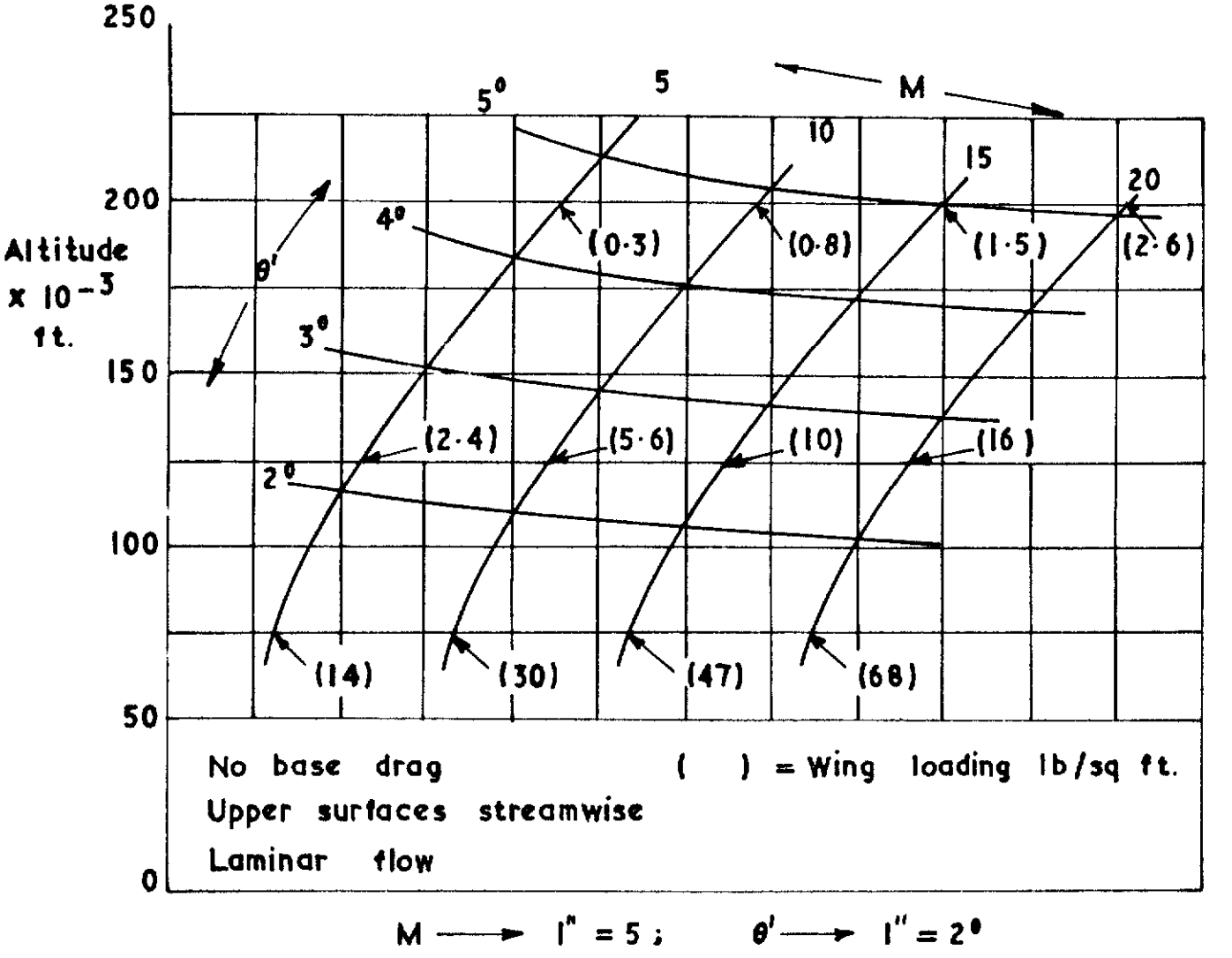

Optimum thickness angle θ' for a delta wing of 200 ft length in the atmosphere

FIG. 2.4

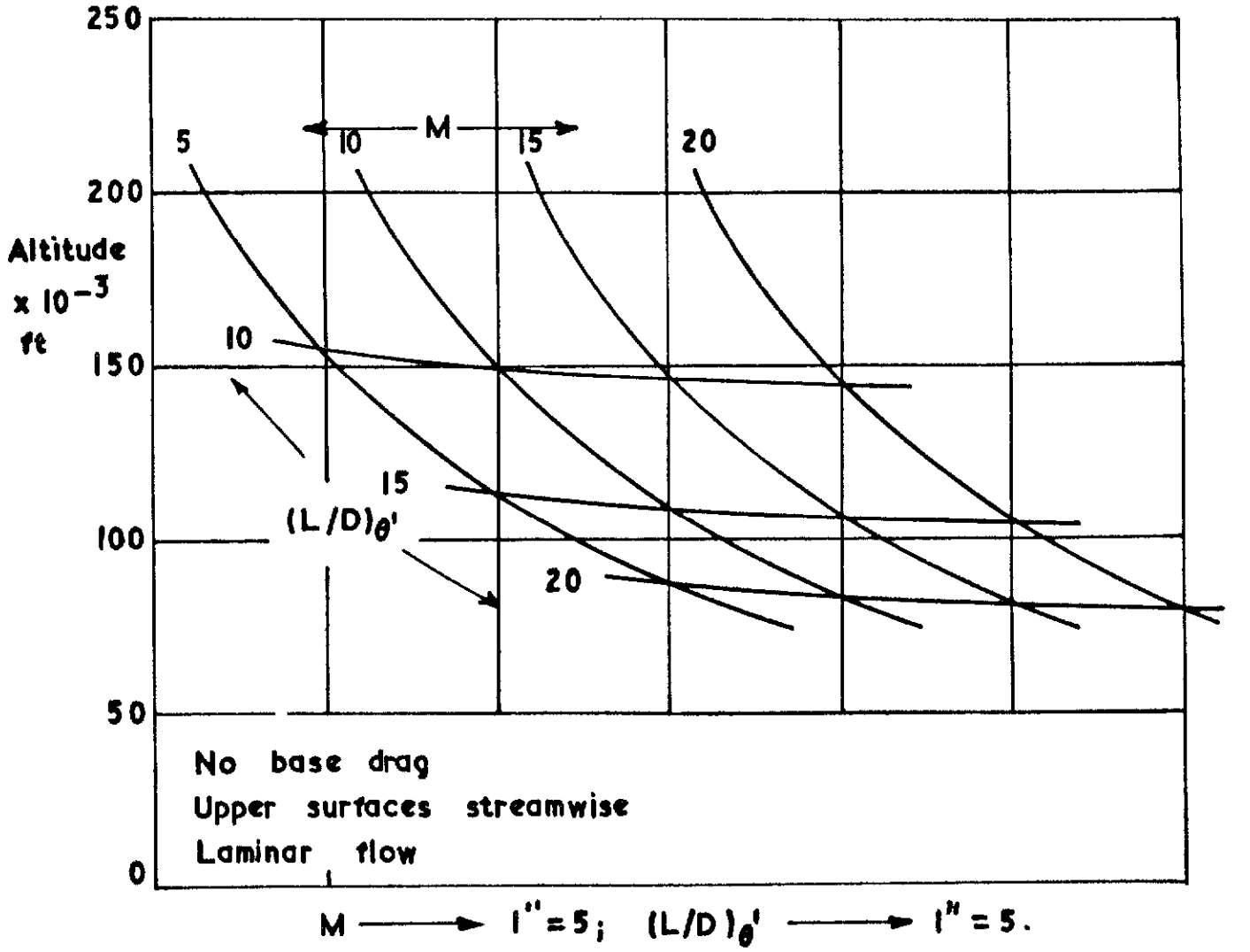

$(L/D)_{\theta}'$ for a delta wing of 200 ft length in the atmosphere

FIG. 2.5(a)

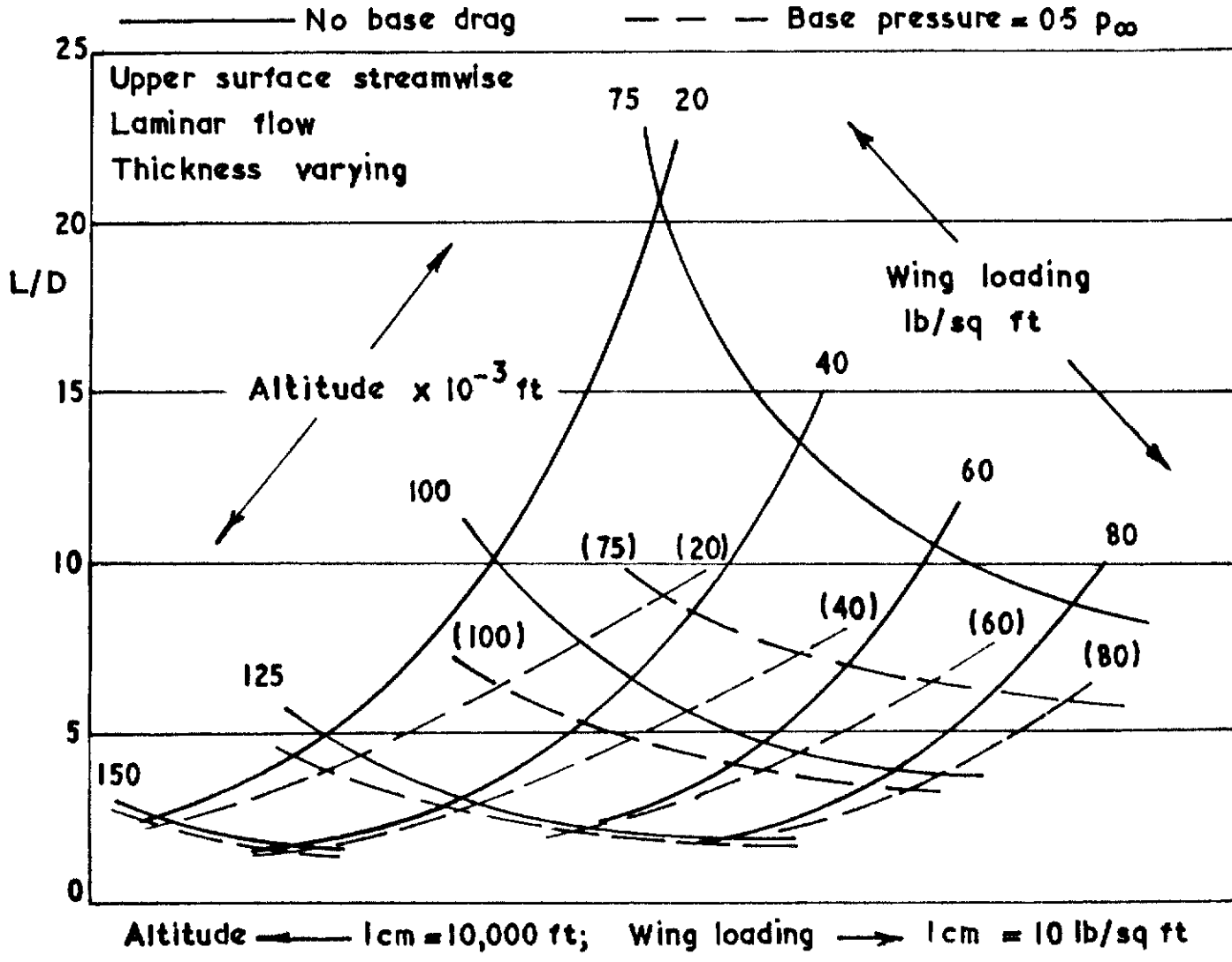

(a) L/D vs wing loading and altitude for a delta wing of 200 ft length at M = 5

FIG. 2.5 (b)

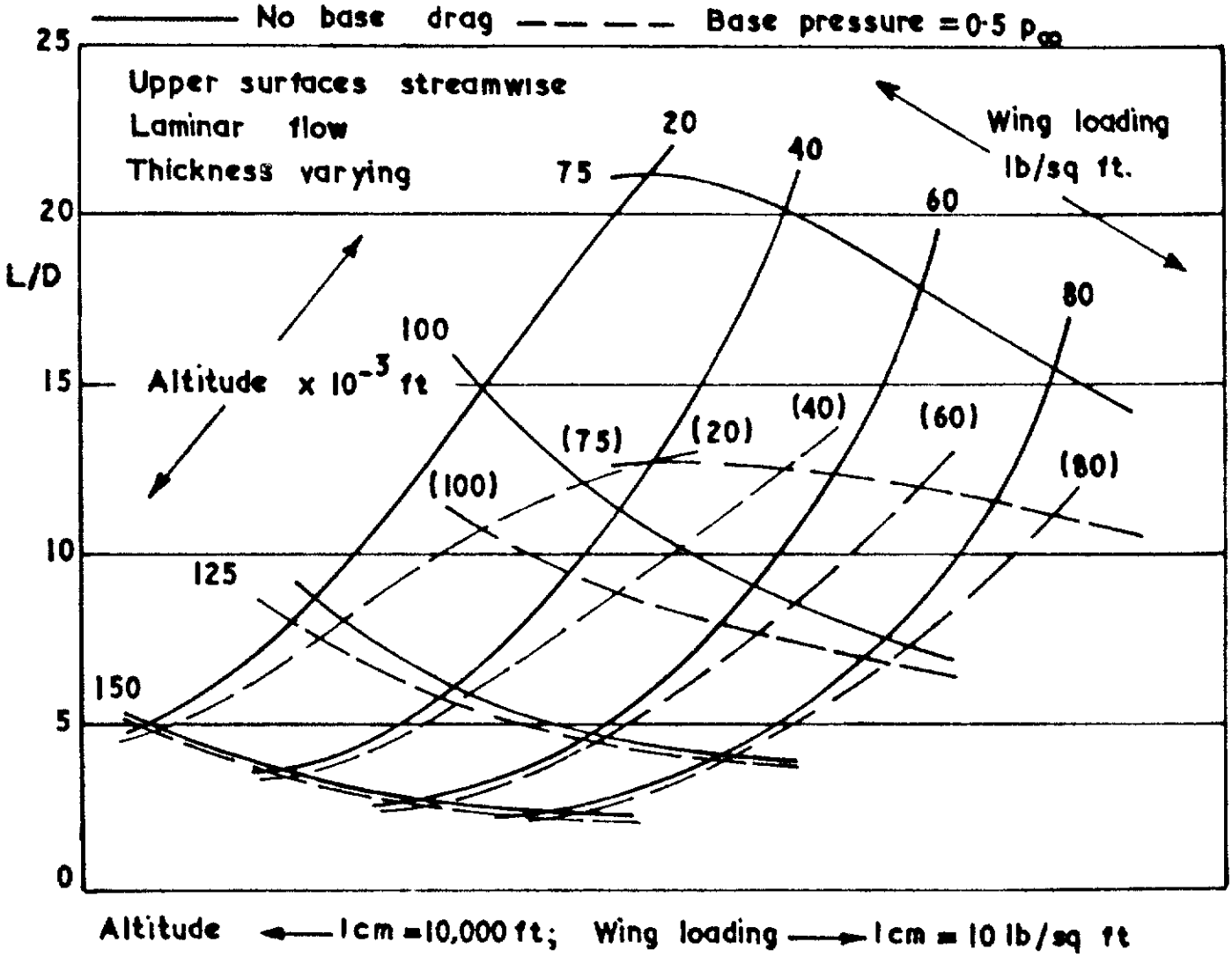

(b) L/D vs wing loading and altitude for a delta wing of 200 ft length at M = 10

FIG. 2.5 (c)

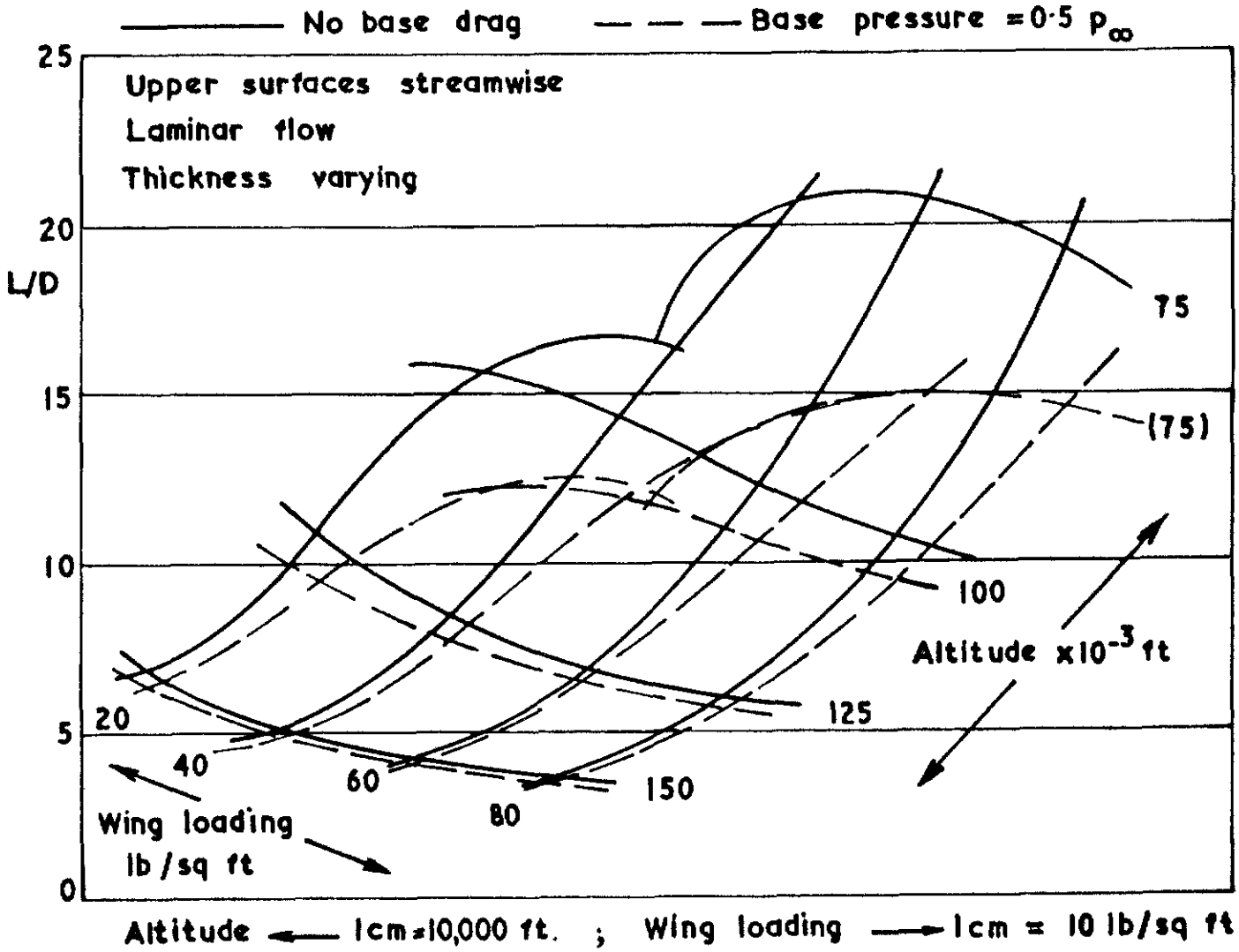

L/D vs wing loading and altitude for a delta wing of 200 ft length at M = 15

FIG. 2.6 (a)

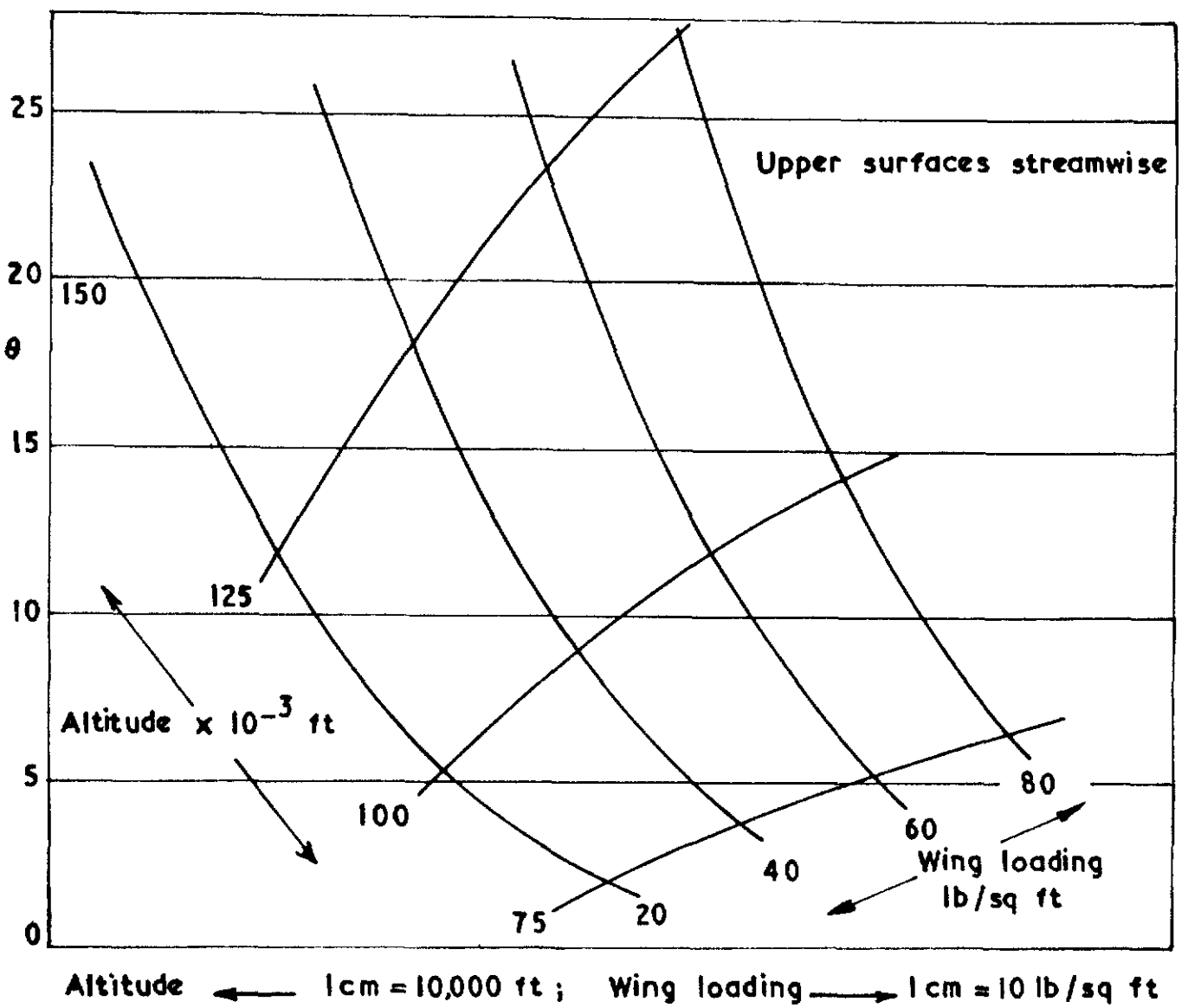

Wing thickness angle θ vs wing loading and altitude for a delta wing at M = 5

FIG. 2.6 (b)

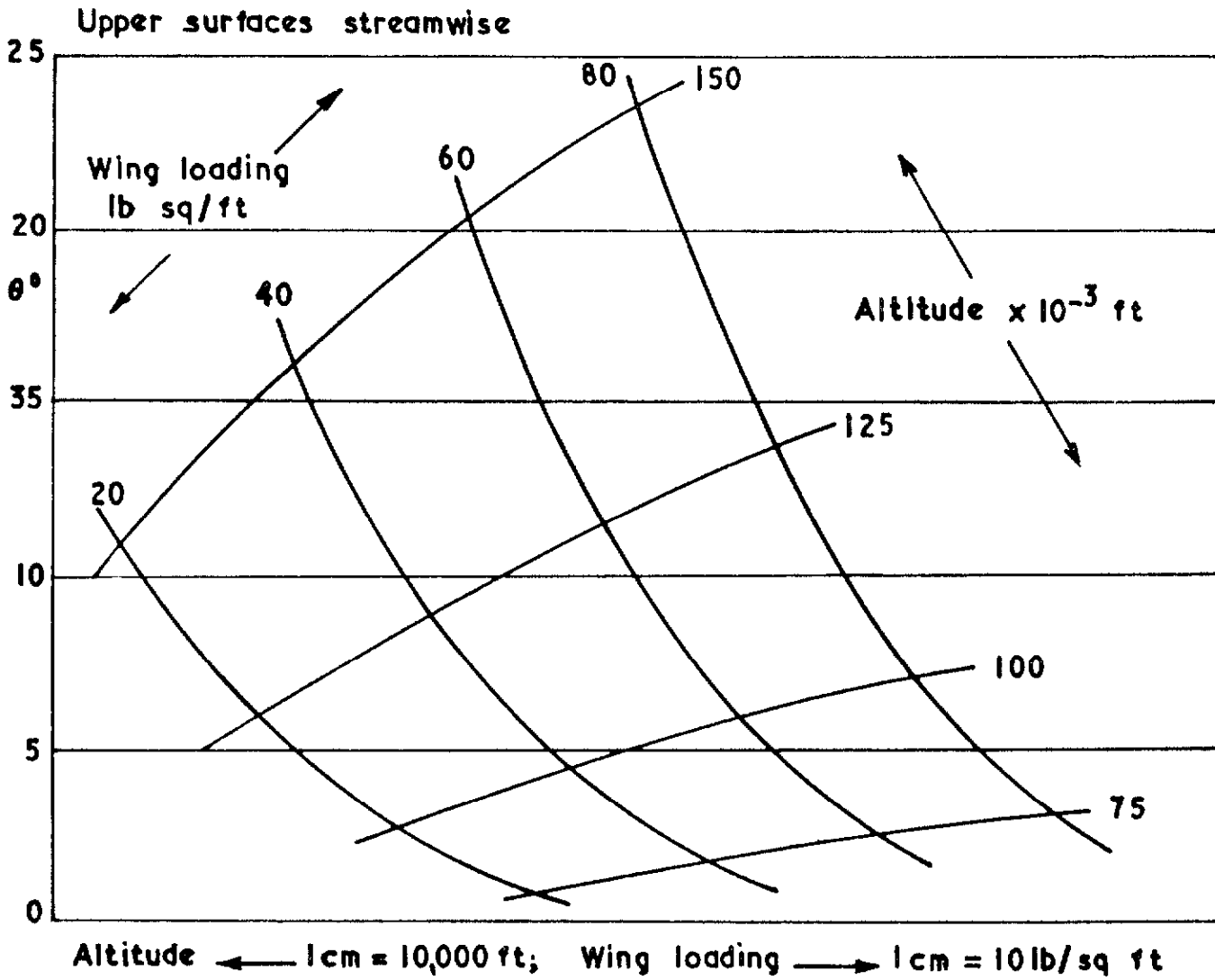

Wing thickness θ vs wing loading and altitude for a delta wing at M = 10

FIG. 2.6(c)

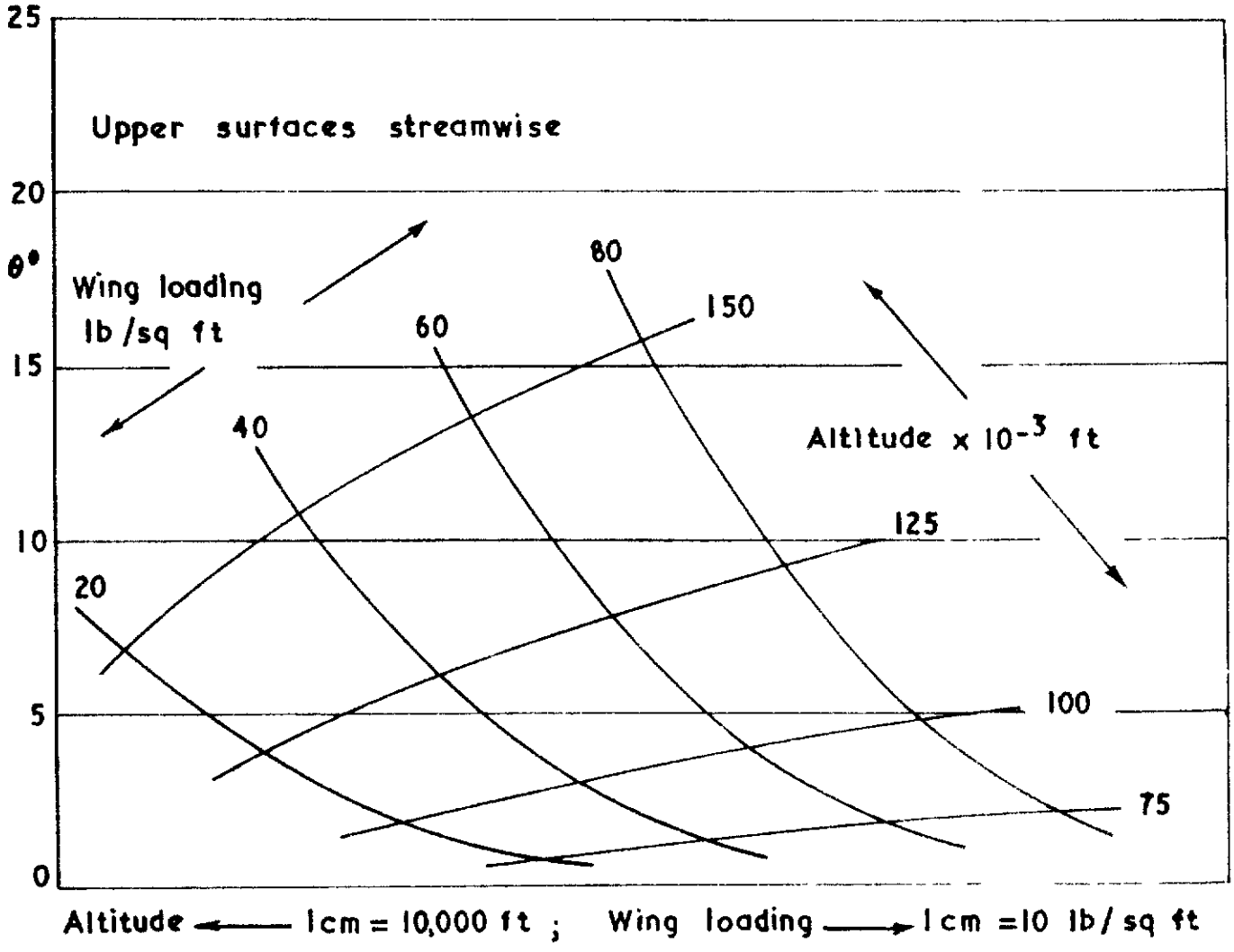

Wing thickness θ vs wing loading and altitude for a delta wing at M = 15

FIG. 2.7(a)

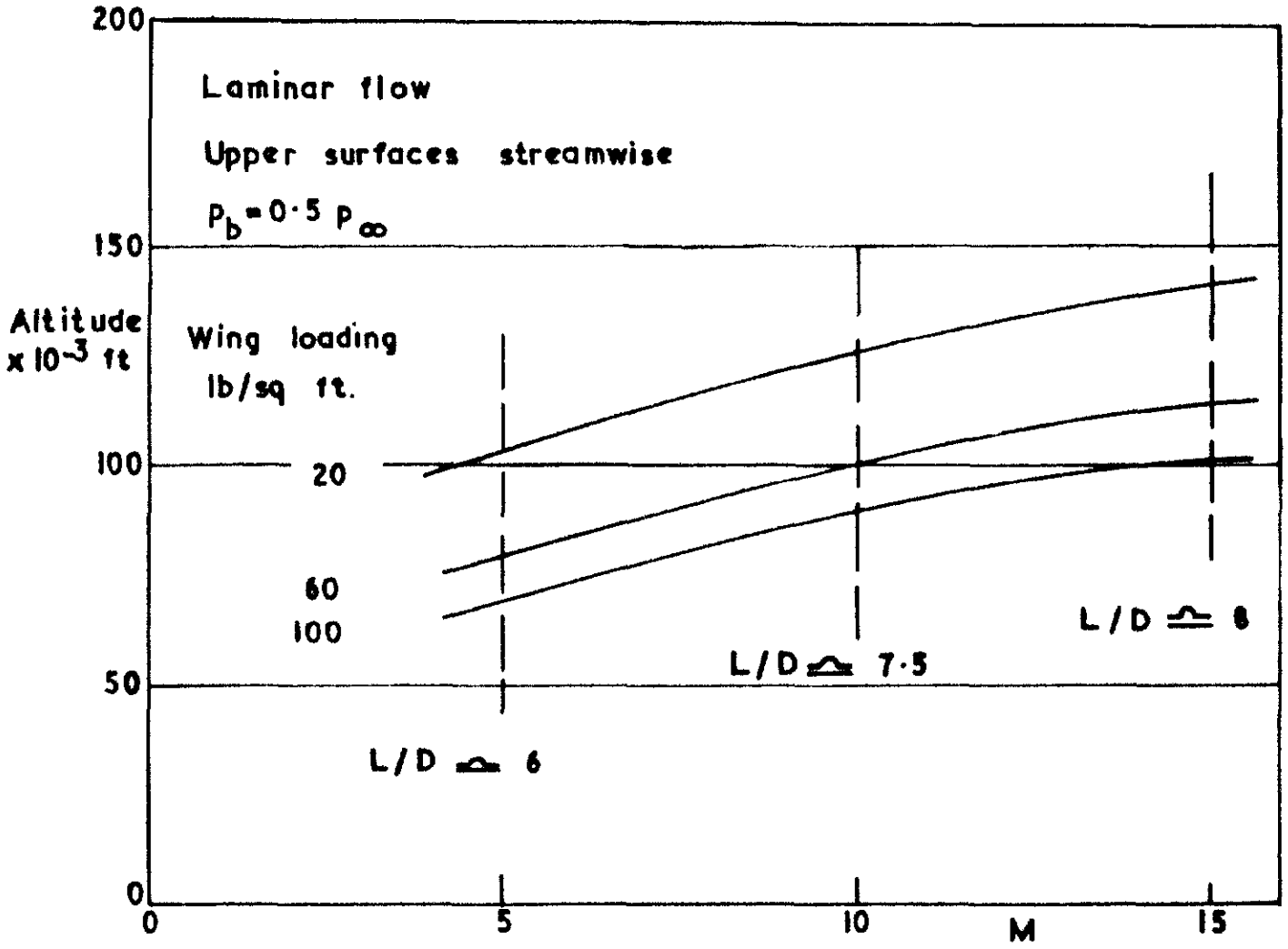

Performance of a 200 ft delta wing of constant thickness angle in the atmosphere, $\theta = 6^\circ$

FIG. 2.7 (b)

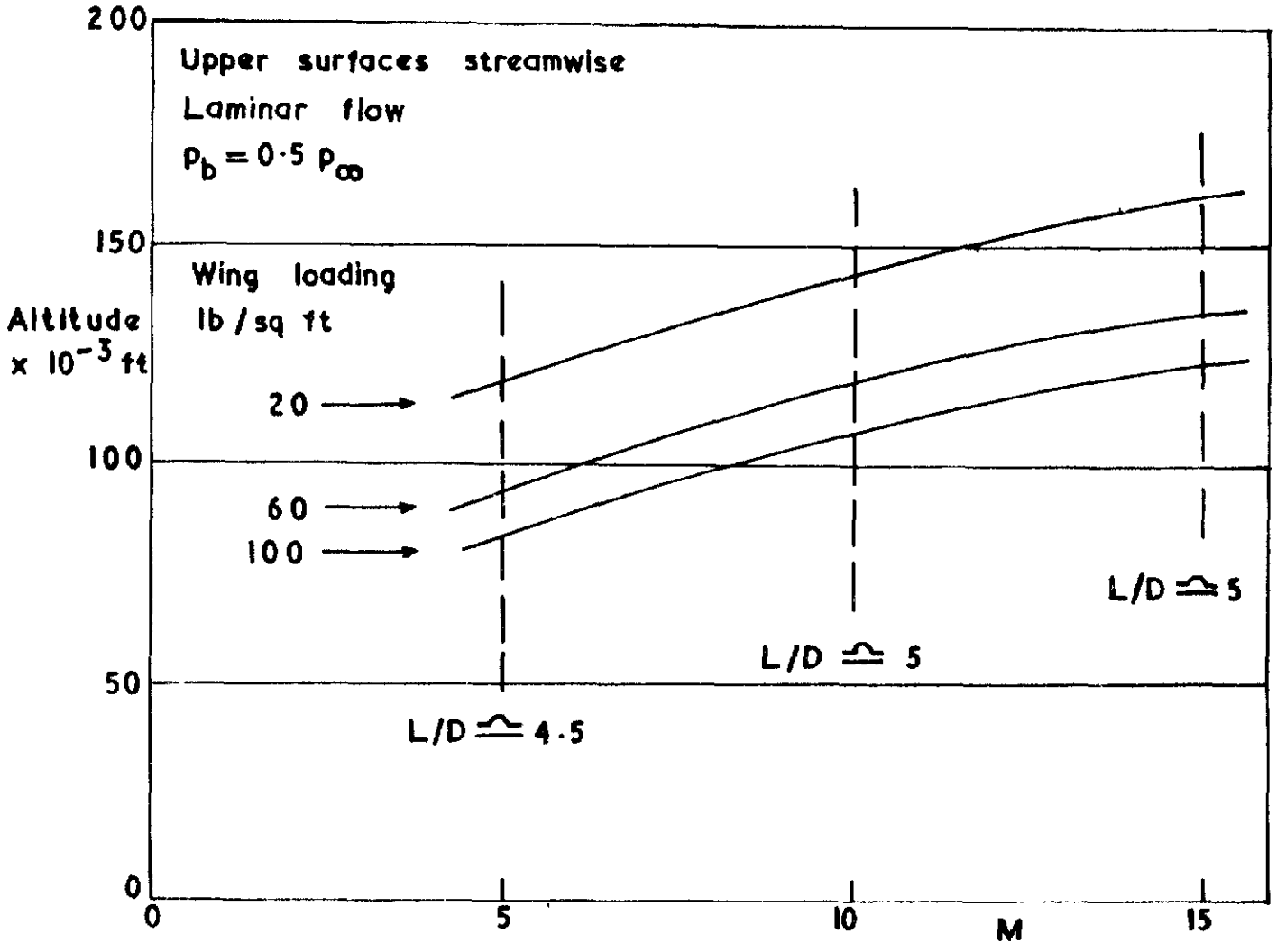

Performance of a 200 ft delta wing of constant thickness angle in the atmosphere, $\theta = 10^0$

FIG. 3.1

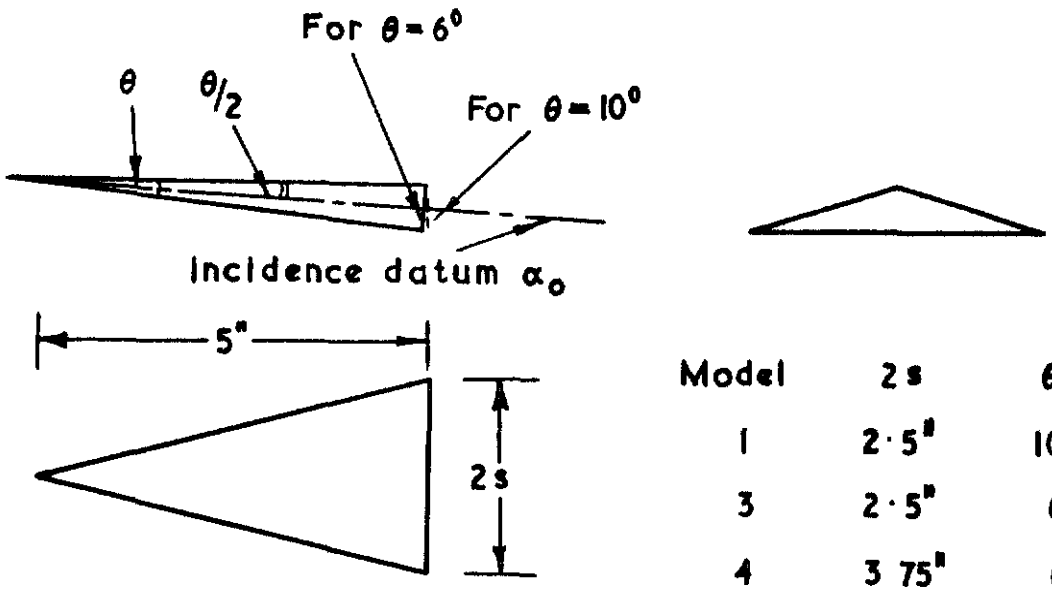

Model	2s	θ
1	2·5"	10°
3	2·5"	6°
4	3·75"	6°

(a) Plain wings.

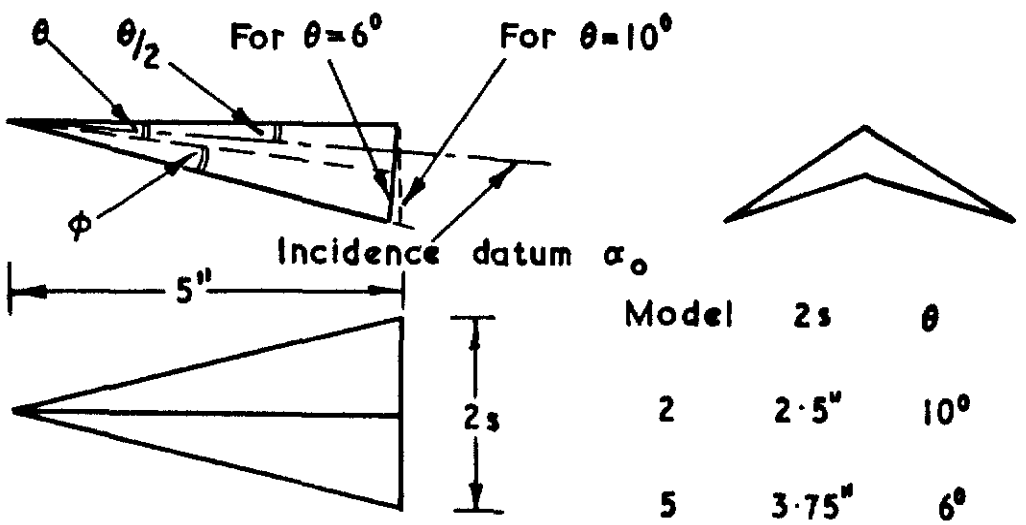

Model	2s	θ	φ
2	2·5"	10°	6°
5	3·75"	6°	6°

(b) Caret wings.

Model dimensions and details

FIG. 3 1 (Concld)

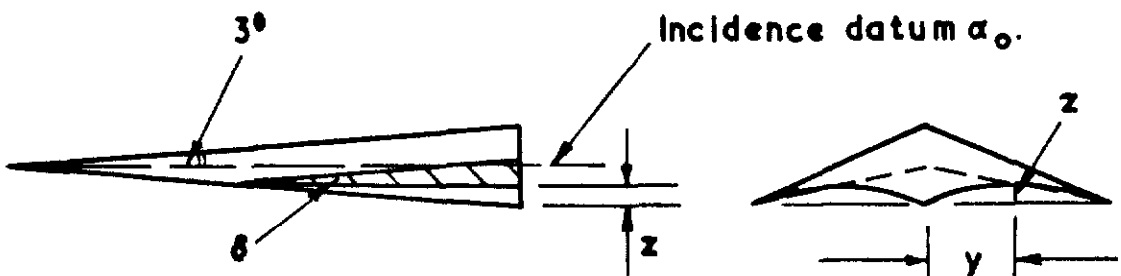

View on AA.

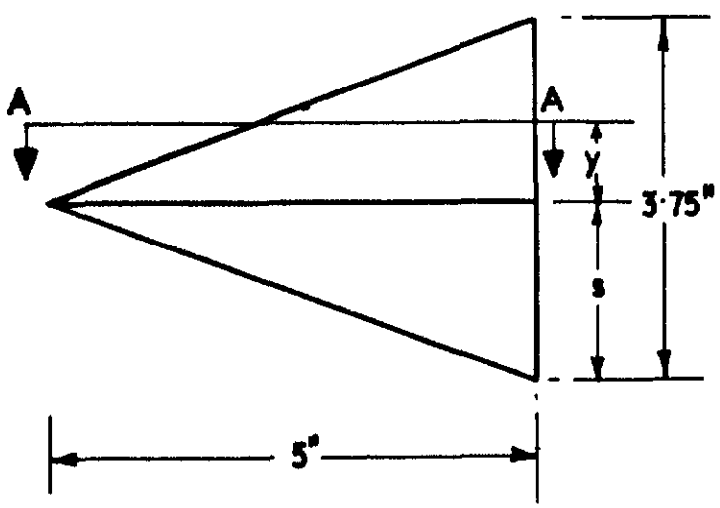

Model 6, having same volume as other 6° wings. δ varies linearly from root to tip. Upper surfaces are flat.

y/s	0	0·1	0·2	0·3	0·4	0·5	0·6	0·7	0·8	0·9	1·0
z"	0	·027	·048	·063	·072	·075	·072	·063	·048	·027	0
δ°	6·85	6·51	6·17	5·82	5·48	5·14	4·80	4·45	4·11	3·77	3·43

(c) Twisted wing.

FIG. 3 2

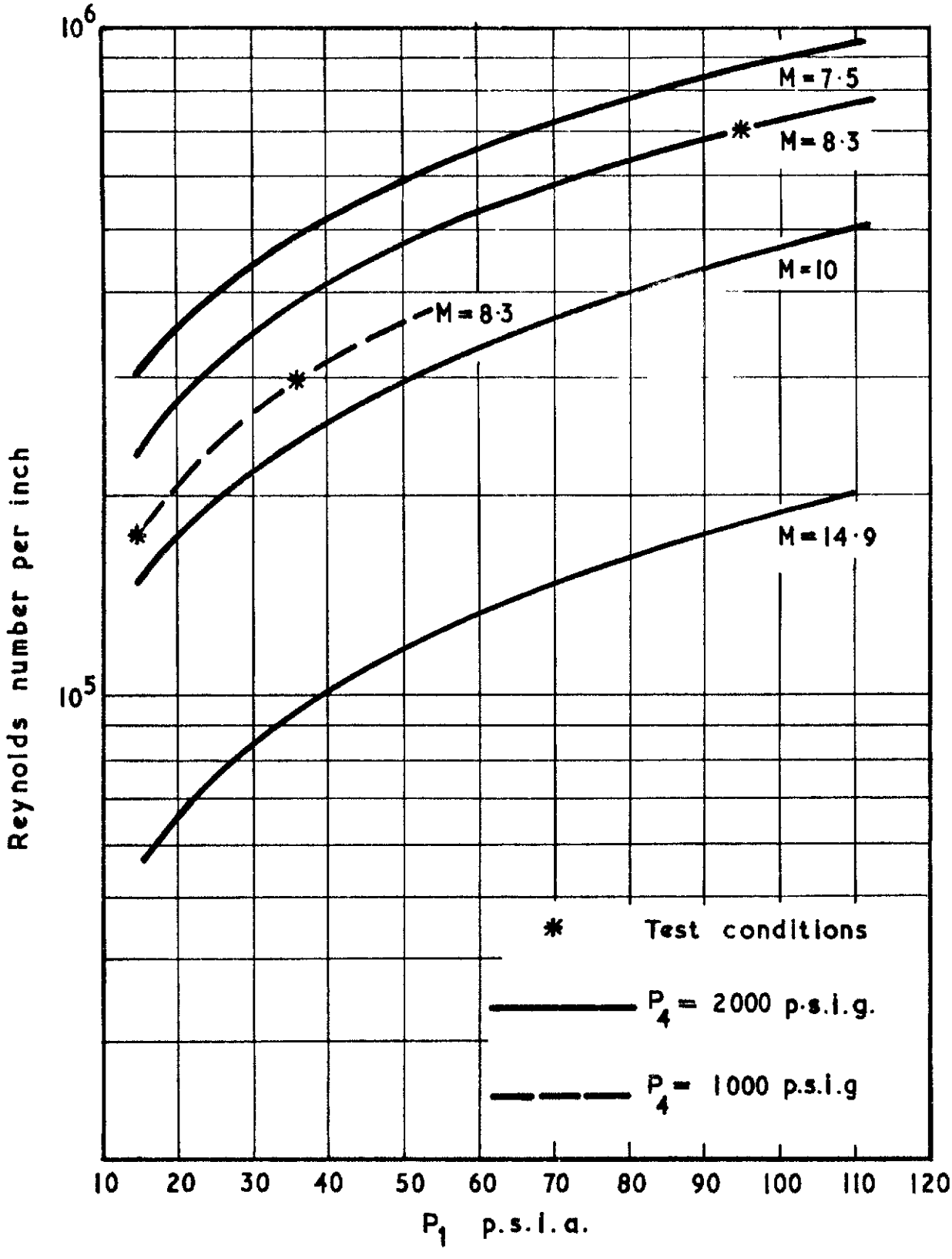

Tunnel Reynolds number vs driver conditions

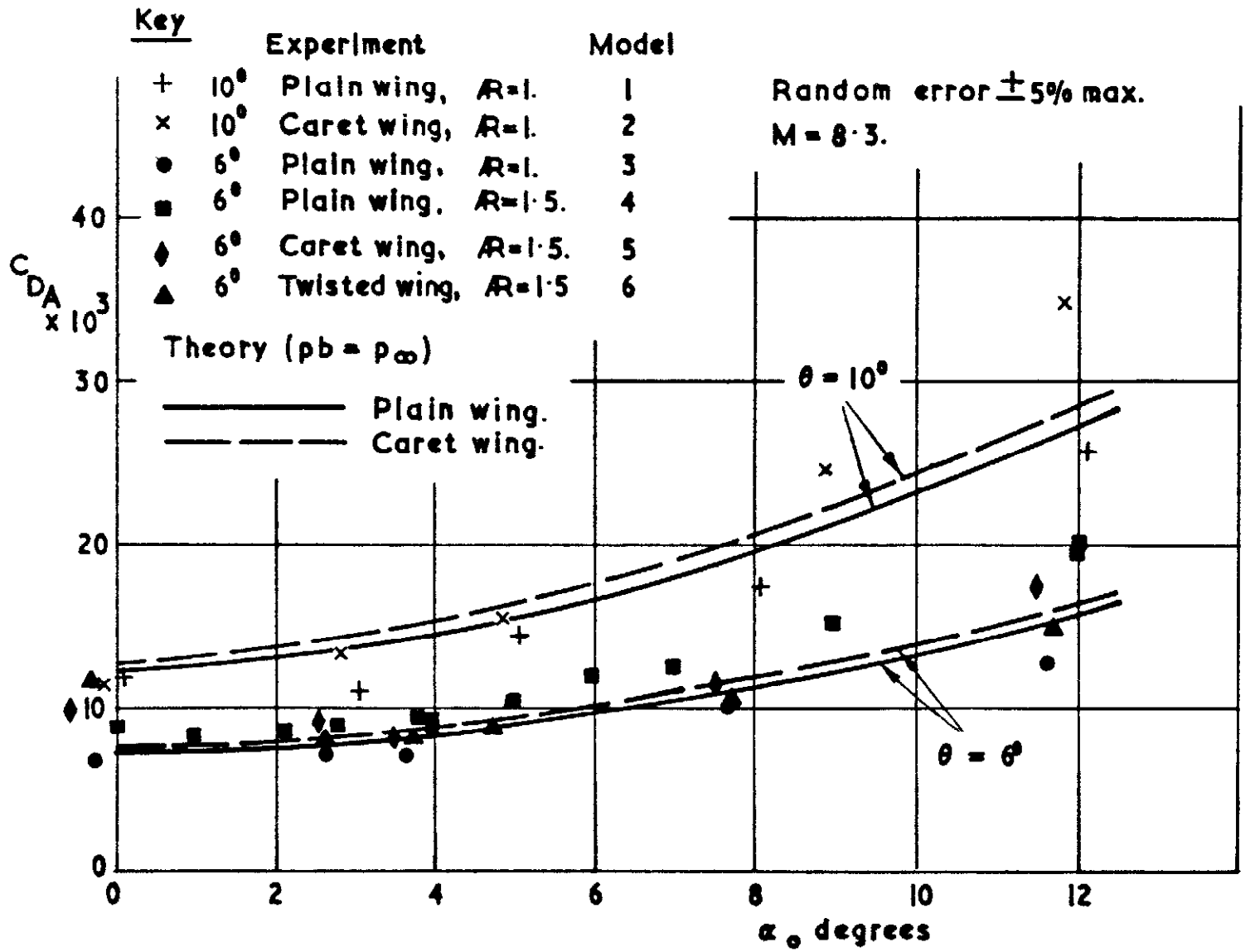

(a) Axial force coefficient, C_{D_A}, vs incidence for $Re = 0{\cdot}9 \times 10^6$

FIG.3.3. (a)

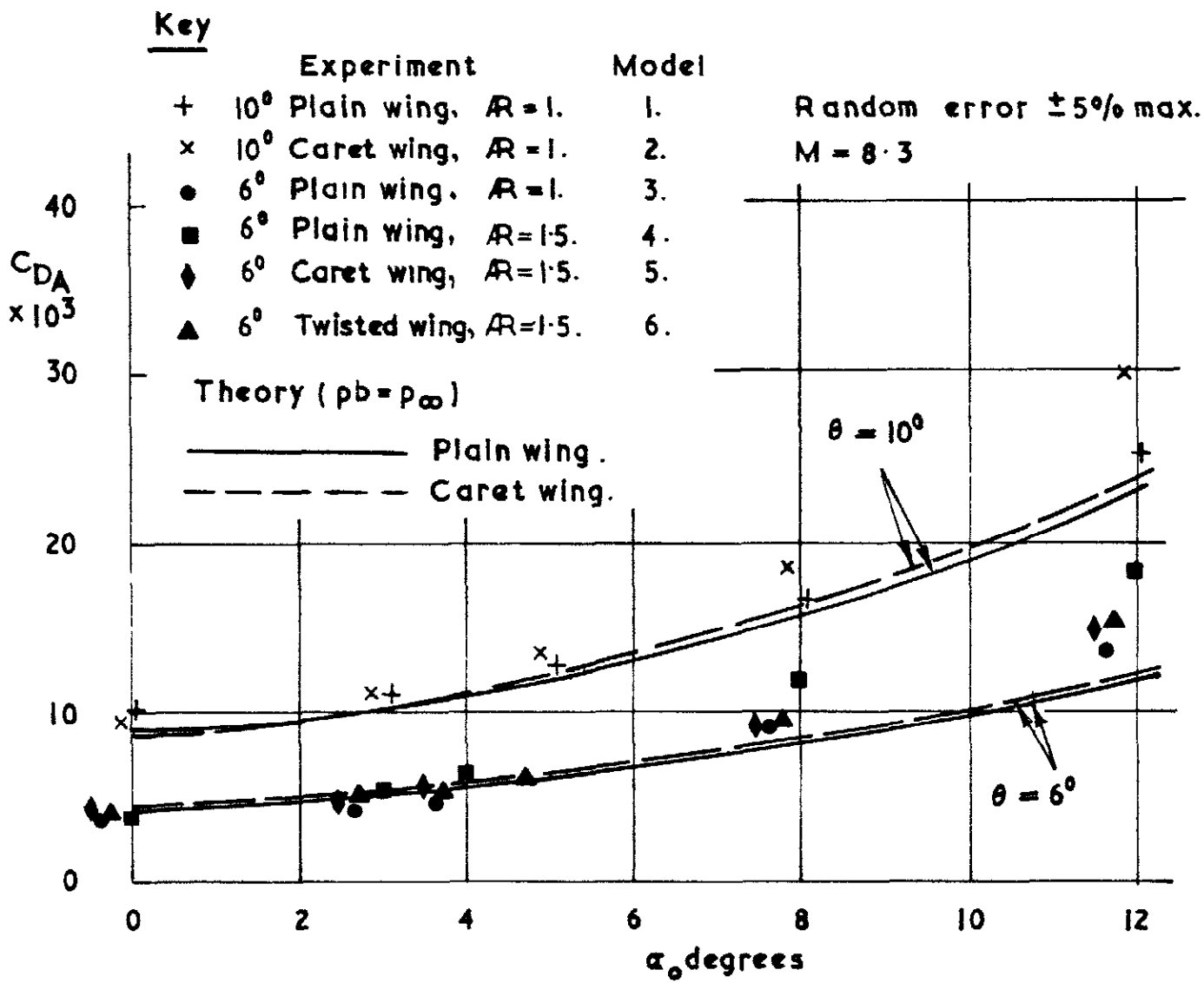

(b) Axial force coefficient, C_{D_A}, vs incidence for $R_e = 3 \cdot 5 \times 10^6$

FIG. 3.3 (b)

FIG. 3.4 (a)&(b).

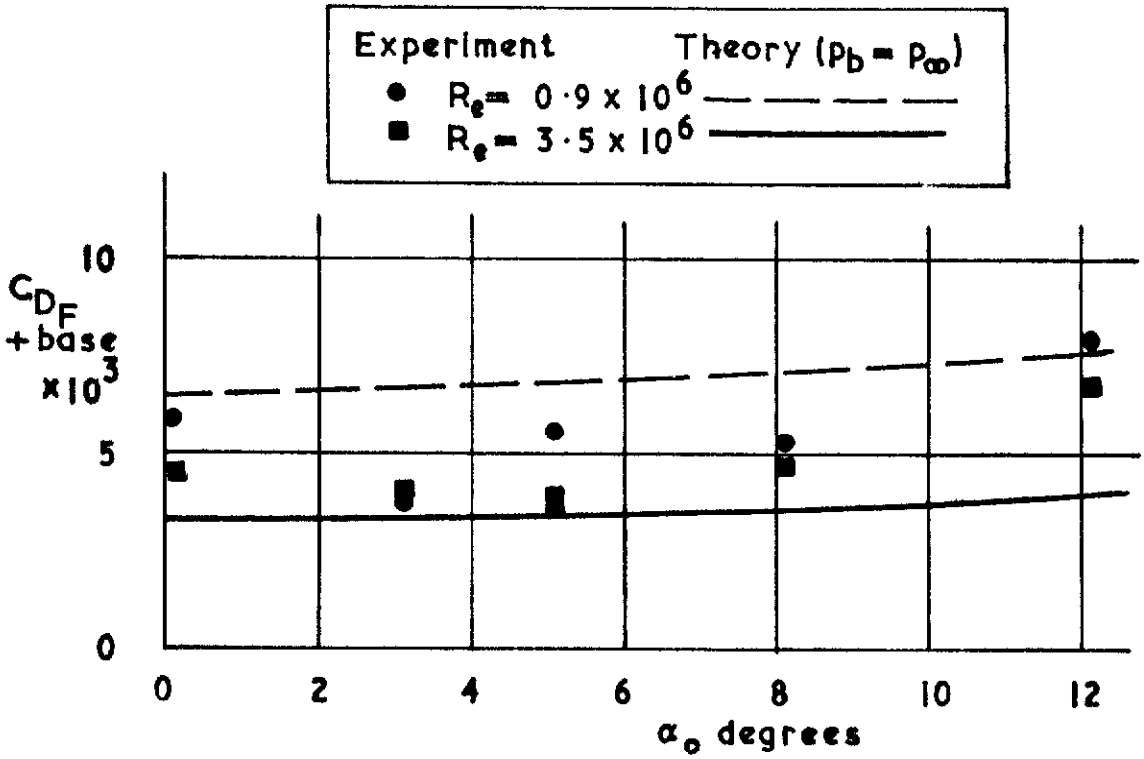

(a) Model 1, 10°, Plain wing AR = 1.

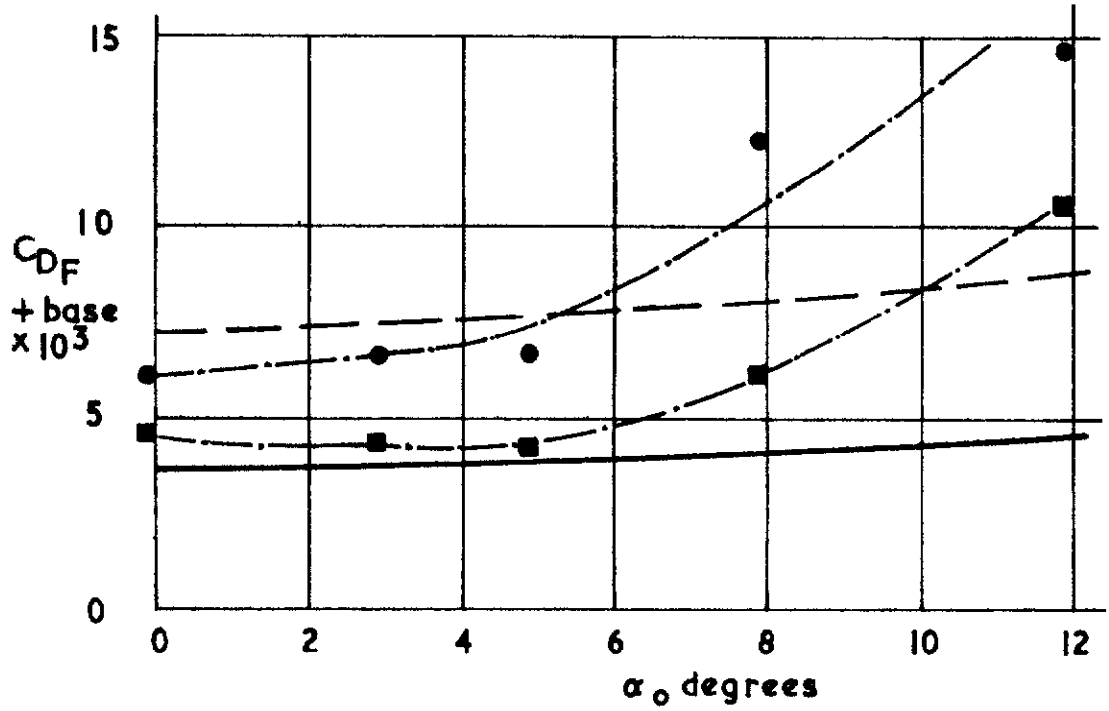

(b) Model 2, 10° Caret wing AR = 1.

Skin friction plus base drag vs Incidence for $R_e = 0{\cdot}9 \times 10^6$ and $R_e = 3{\cdot}5 \times 10^6$

FIG 3.4 (c) & (d)

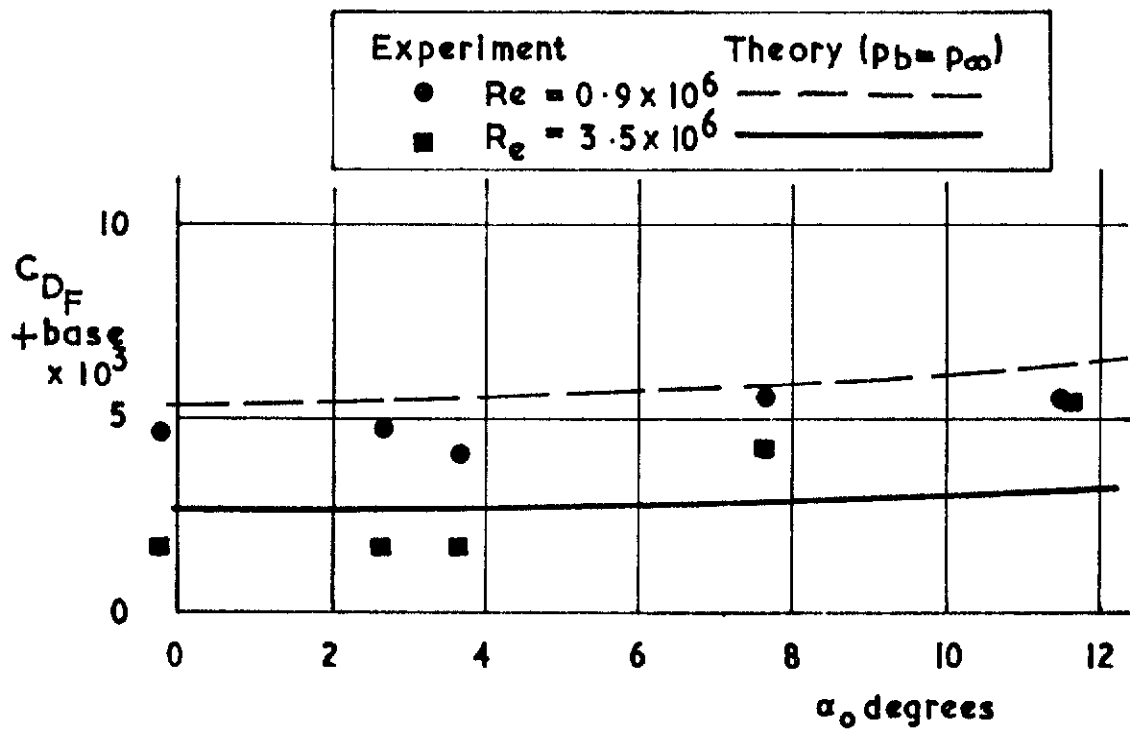

(c) Model 3, 6° Plain wing AR = 1.

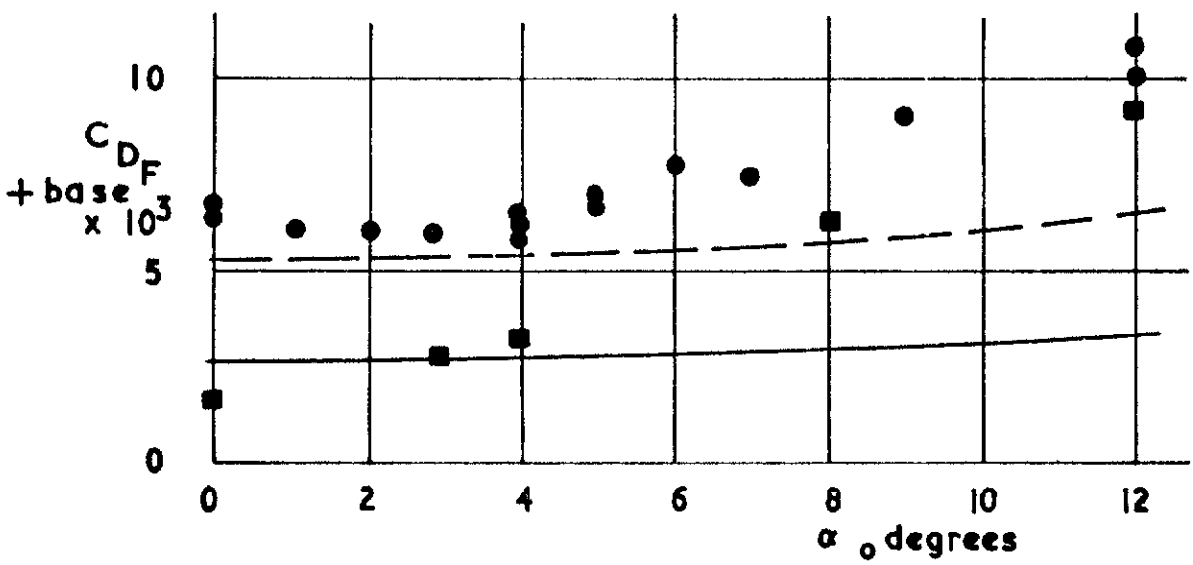

(d) Model 4, 6° Plain wing AR = 1·5

FIG. 3.4 (e)

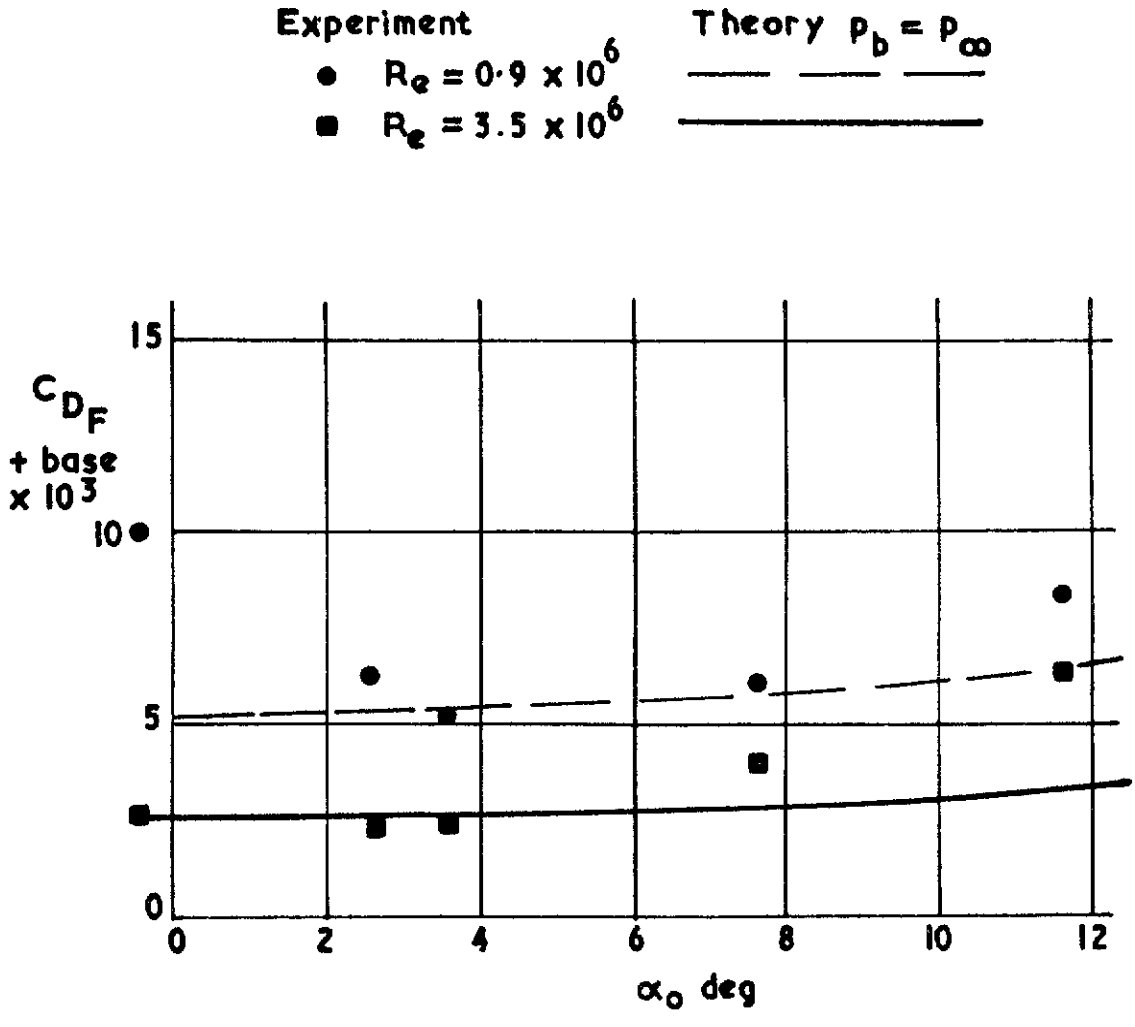

Mode 5, 6° caret wing, AR = 1·5

FIG. 3.5 (a & b)

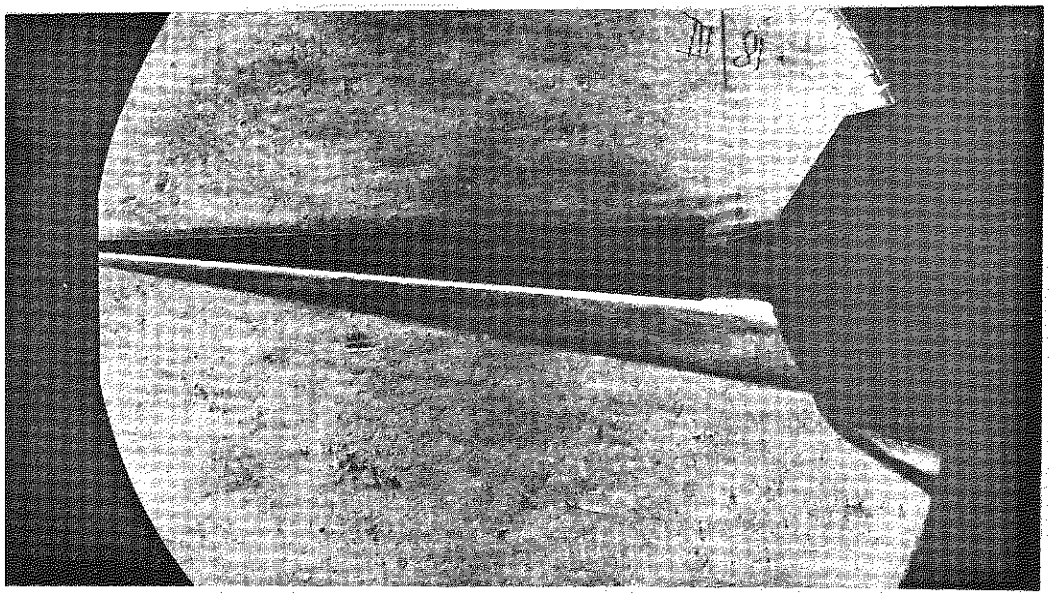

(a) $\alpha_o = 3^0$

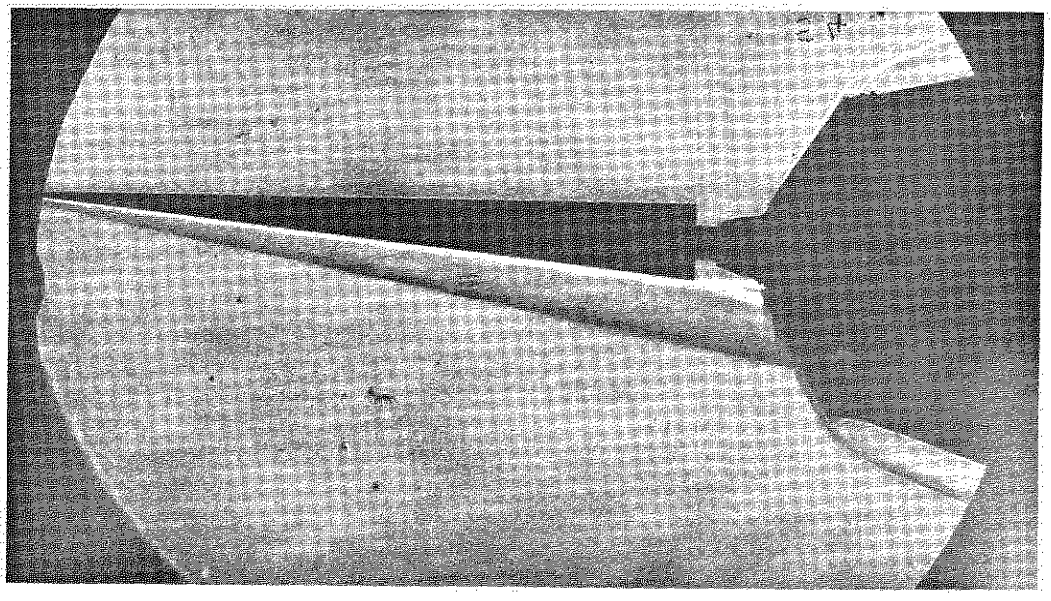

(b) $\alpha_o = 5^0$

Schlieren photographs of flow separation on 6^0 models

FIG. 3.5 (c & d)

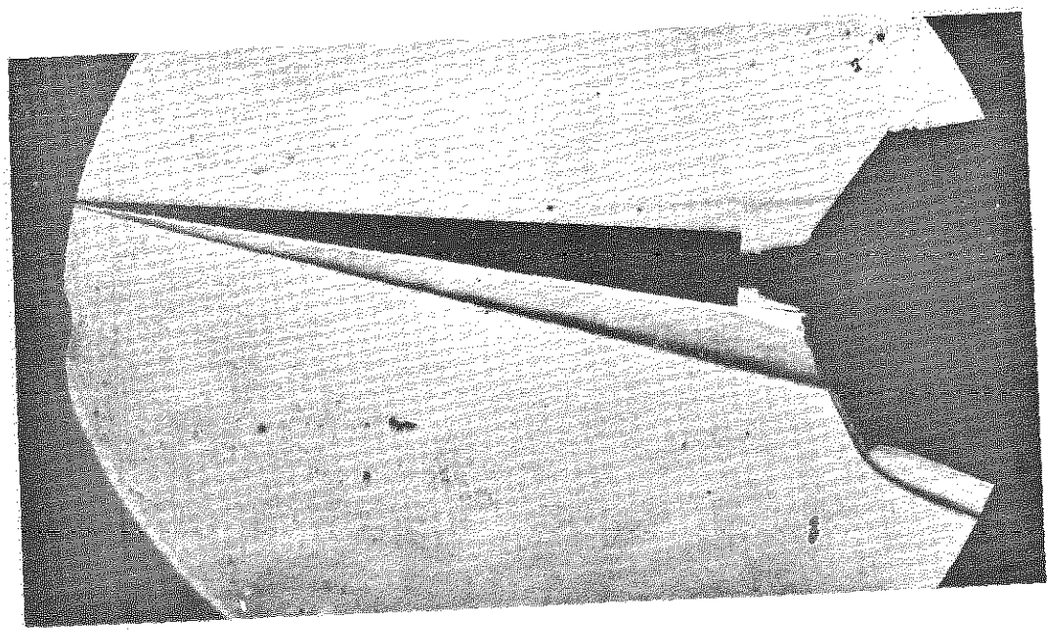

(c) $\alpha_o = 8^0$

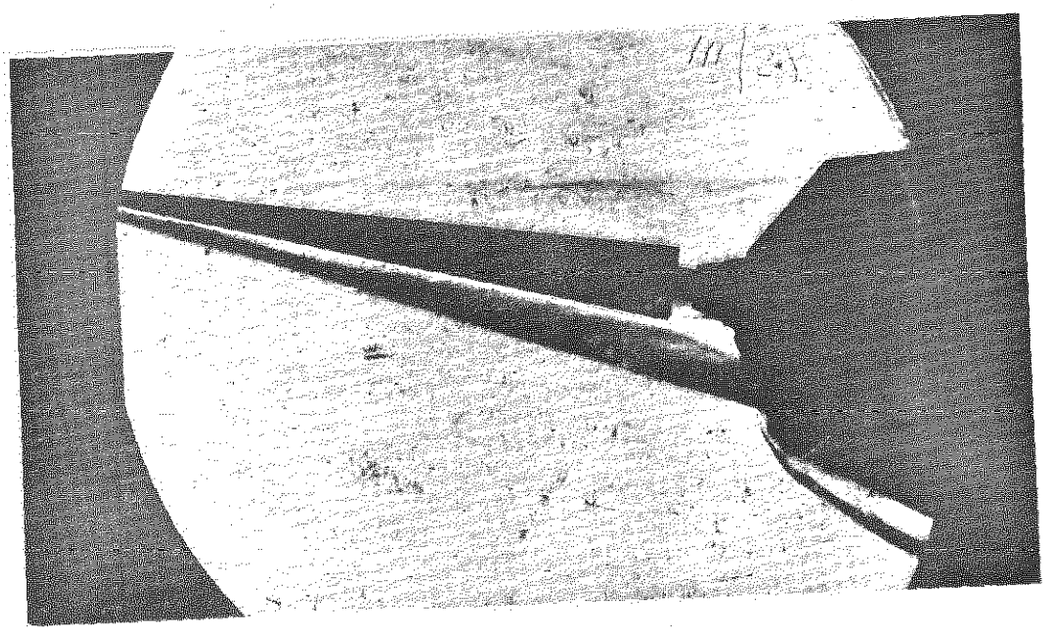

(d) $\alpha_o = 12^0$

Schlieren photographs of flow separation on 6^0 models

FIG 3.6 (a)

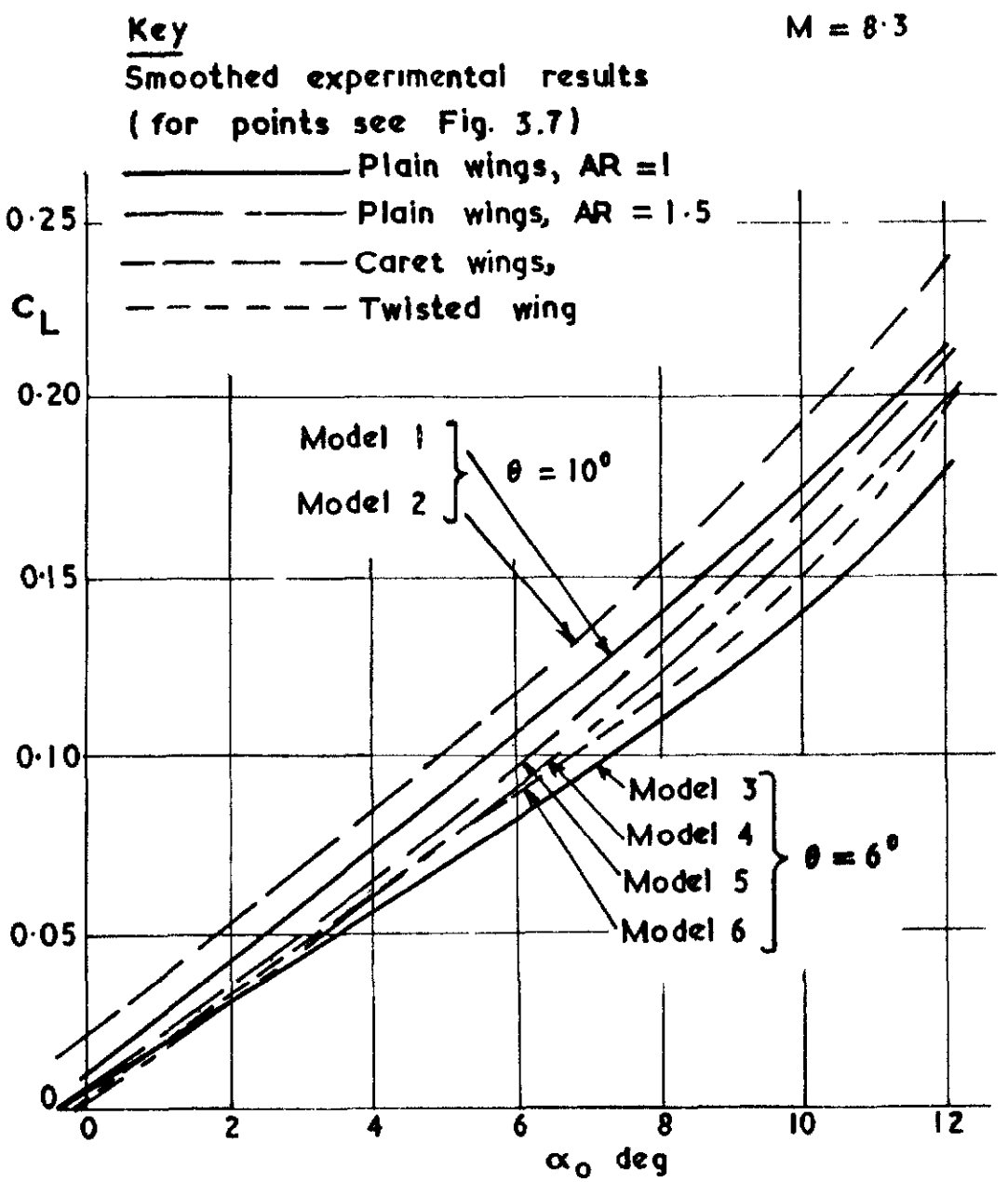

Lift coefficient vs incidence for all models at $R_e = 0{\cdot}9 \times 10^6$

FIG. 3 6 (b)

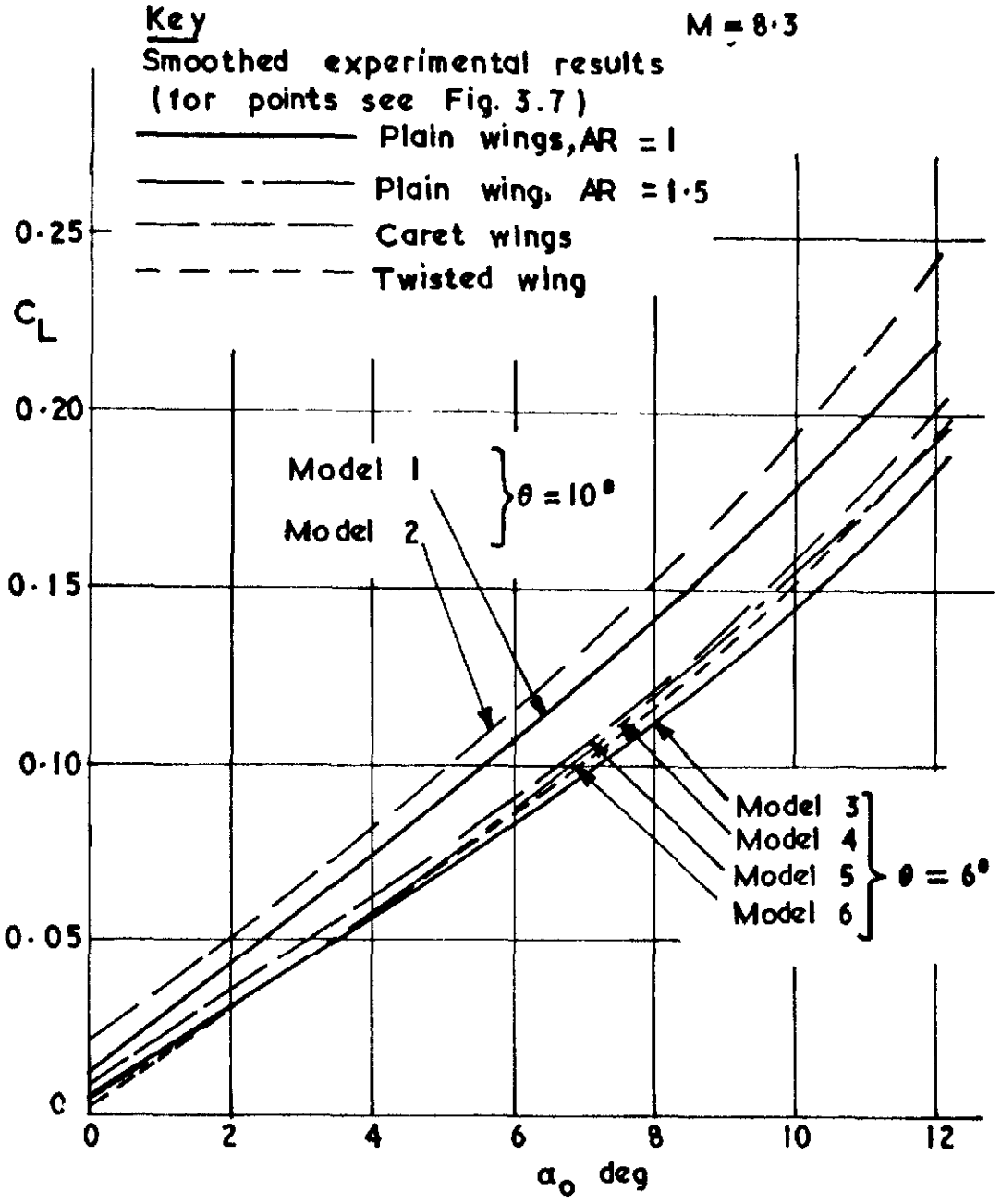

Lift coefficient vs incidence for all wings at $R_e = 3·5 \times 10^6$

FIG. 3 7 (a)&(b)

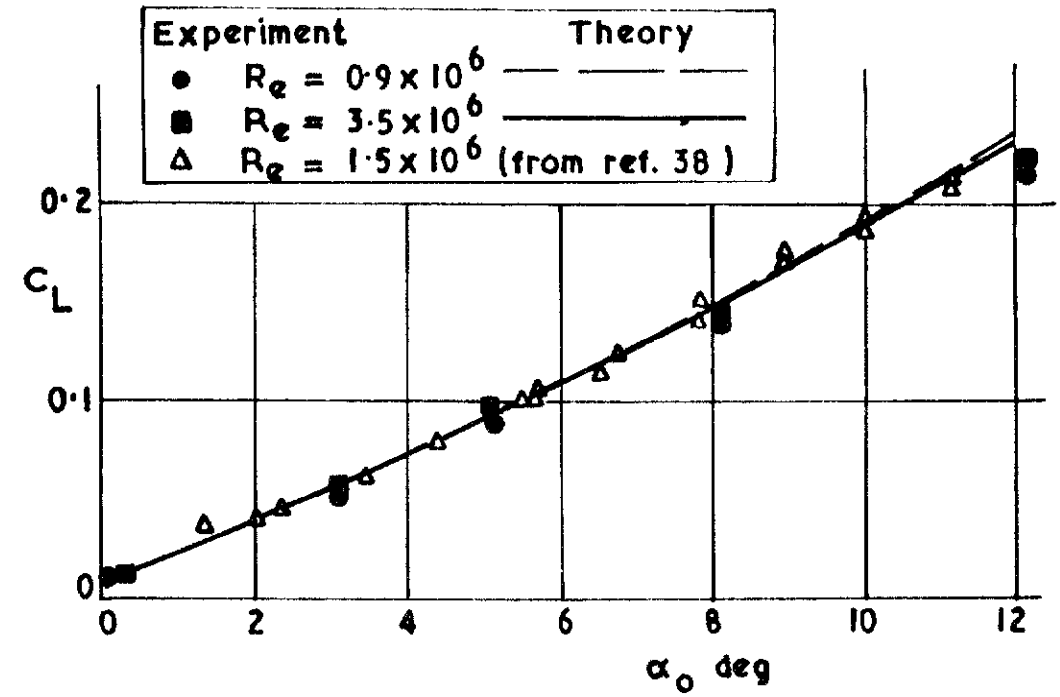

(a) Model 1, 10° plain wing AR = 1

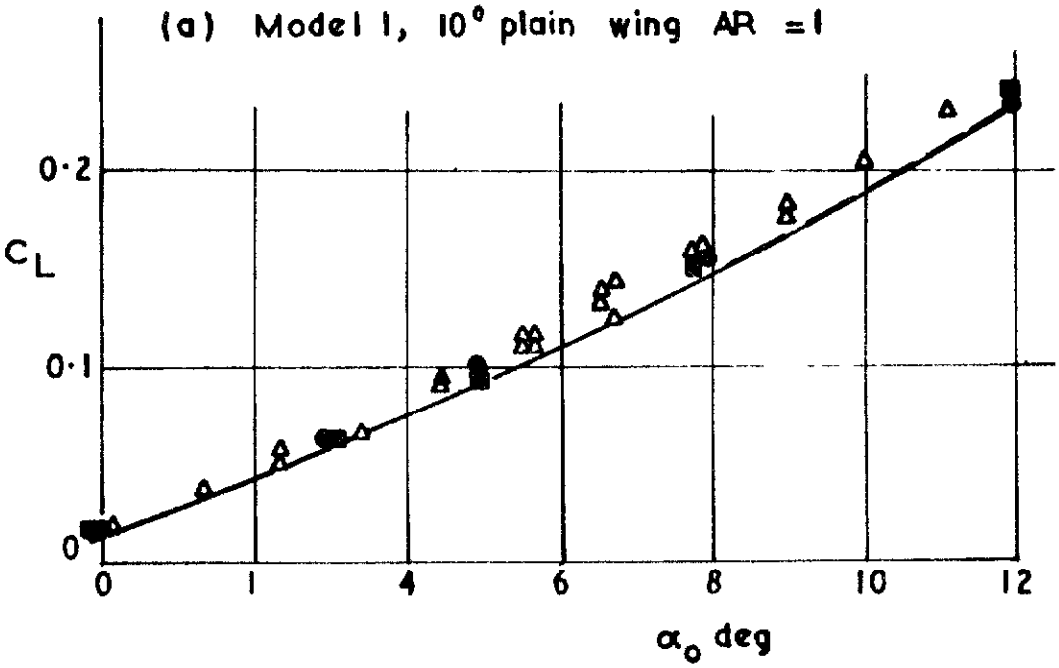

Model 2, 10° caret wing, AR = 1

(b) Lift coefficient vs incidence and Reynolds number with theoretical estimates

FIG. 3.7 (c) & (d)

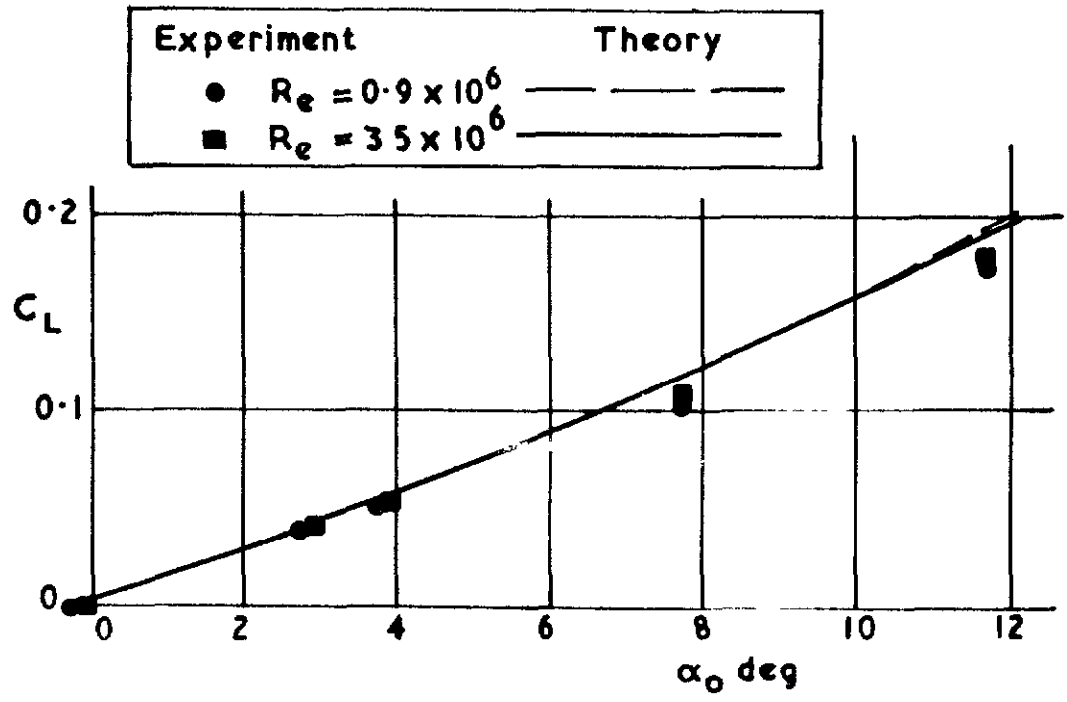

(c) Model 3, 6° plain wing, AR = 1

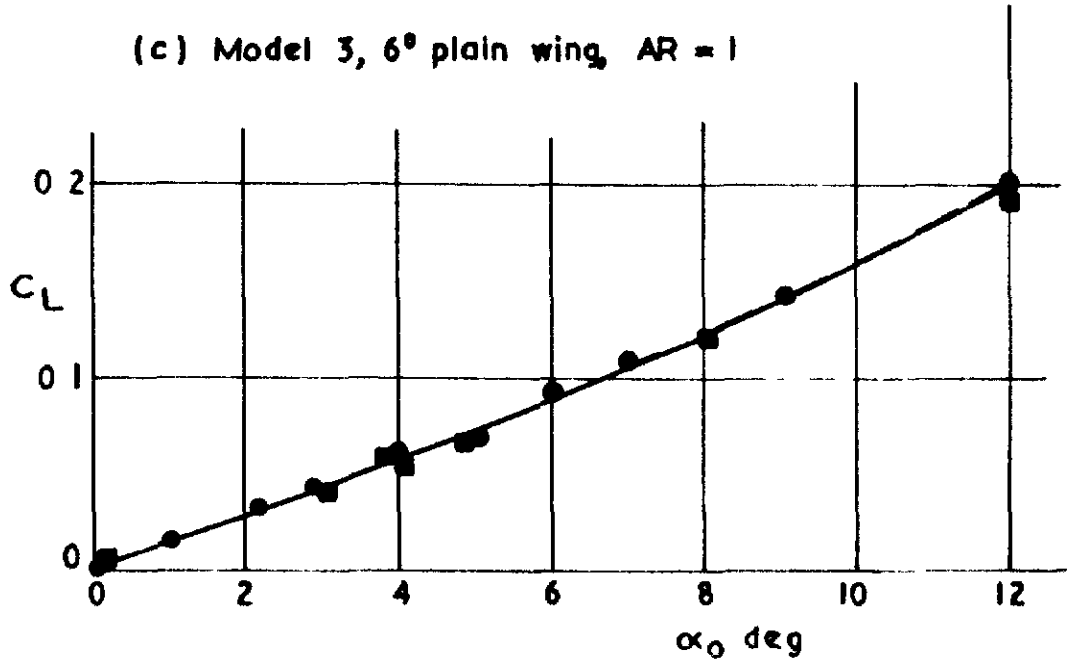

(d) Model 4, 6° plain wing, AR = 1·5

FIG. 3.7 (e) & (f)

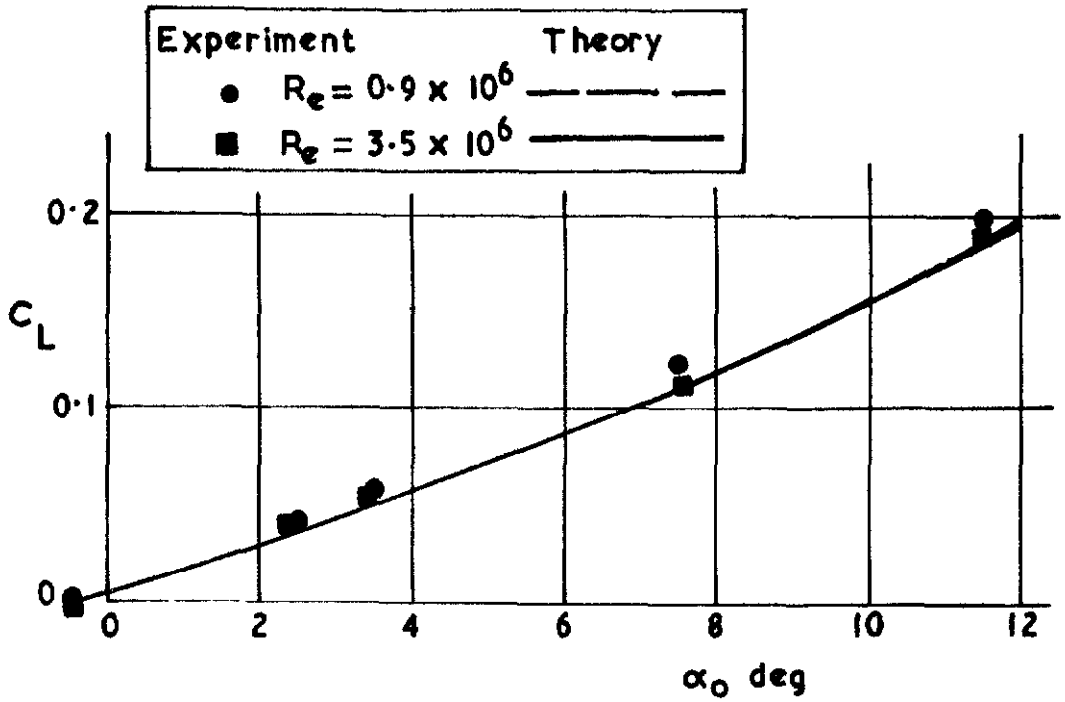

(e) Model 5, 6° caret wing, AR = 1·5

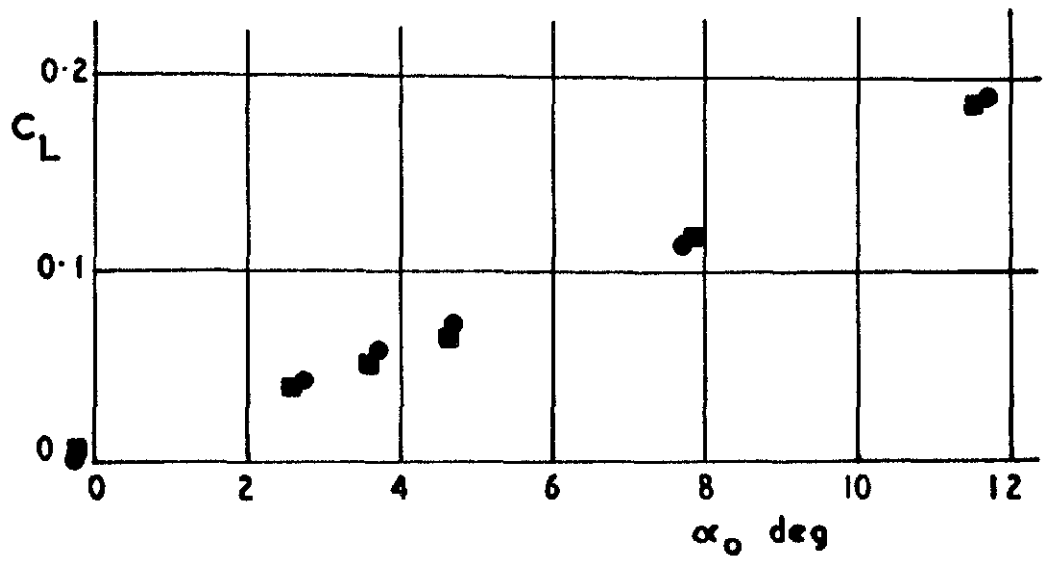

(f) Model 6, 6° twisted wing, AR = 1·5

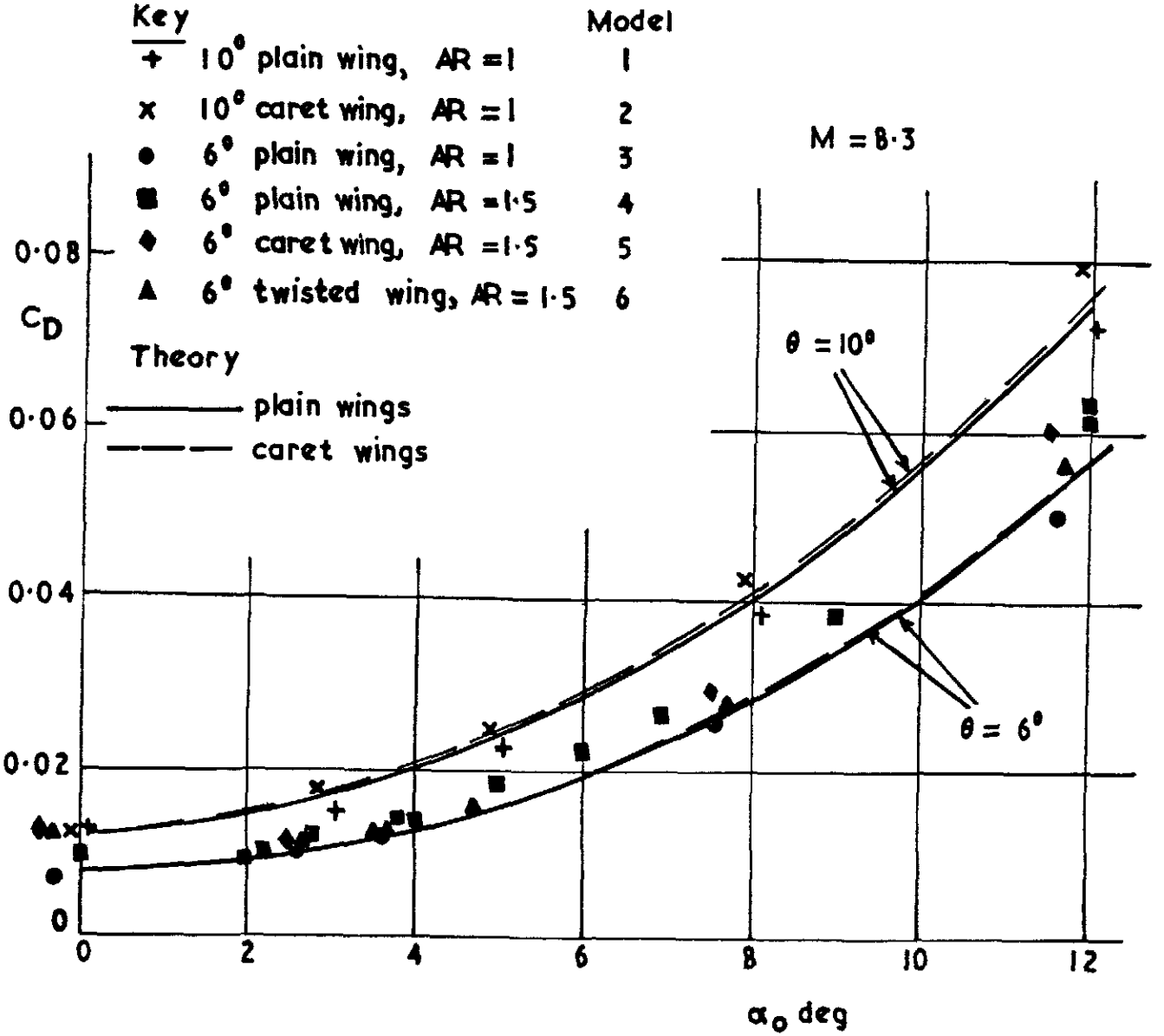

Drag coefficient vs incidence for $R_e = 0{\cdot}9 \times 10^6$

FIG. 3.8 (a)

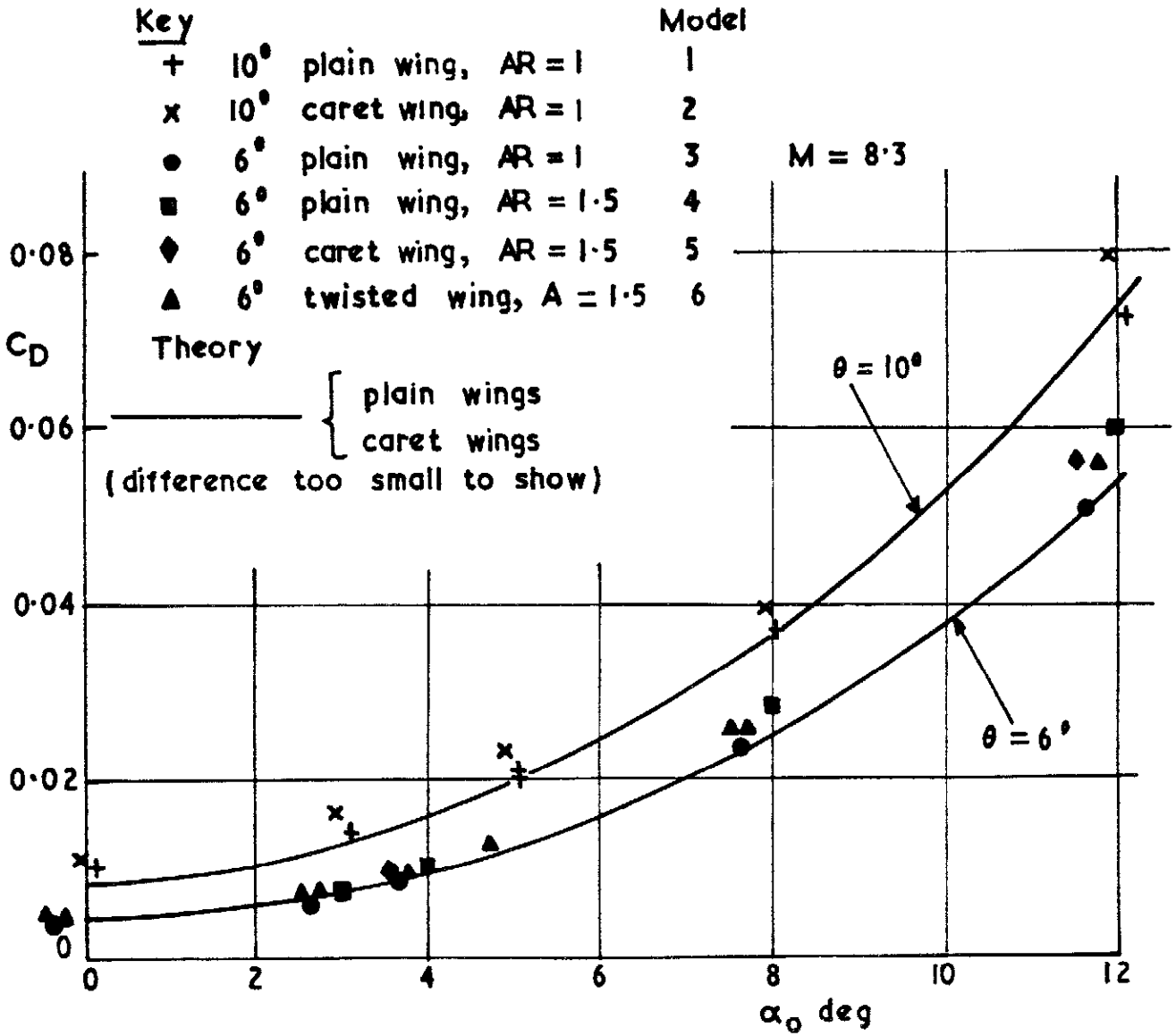

Drag coefficient vs incidence for $R_e = 3{\cdot}5 \times 10^6$

FIG. 3·8 (b)

FIG.3.9 (a)&(b)

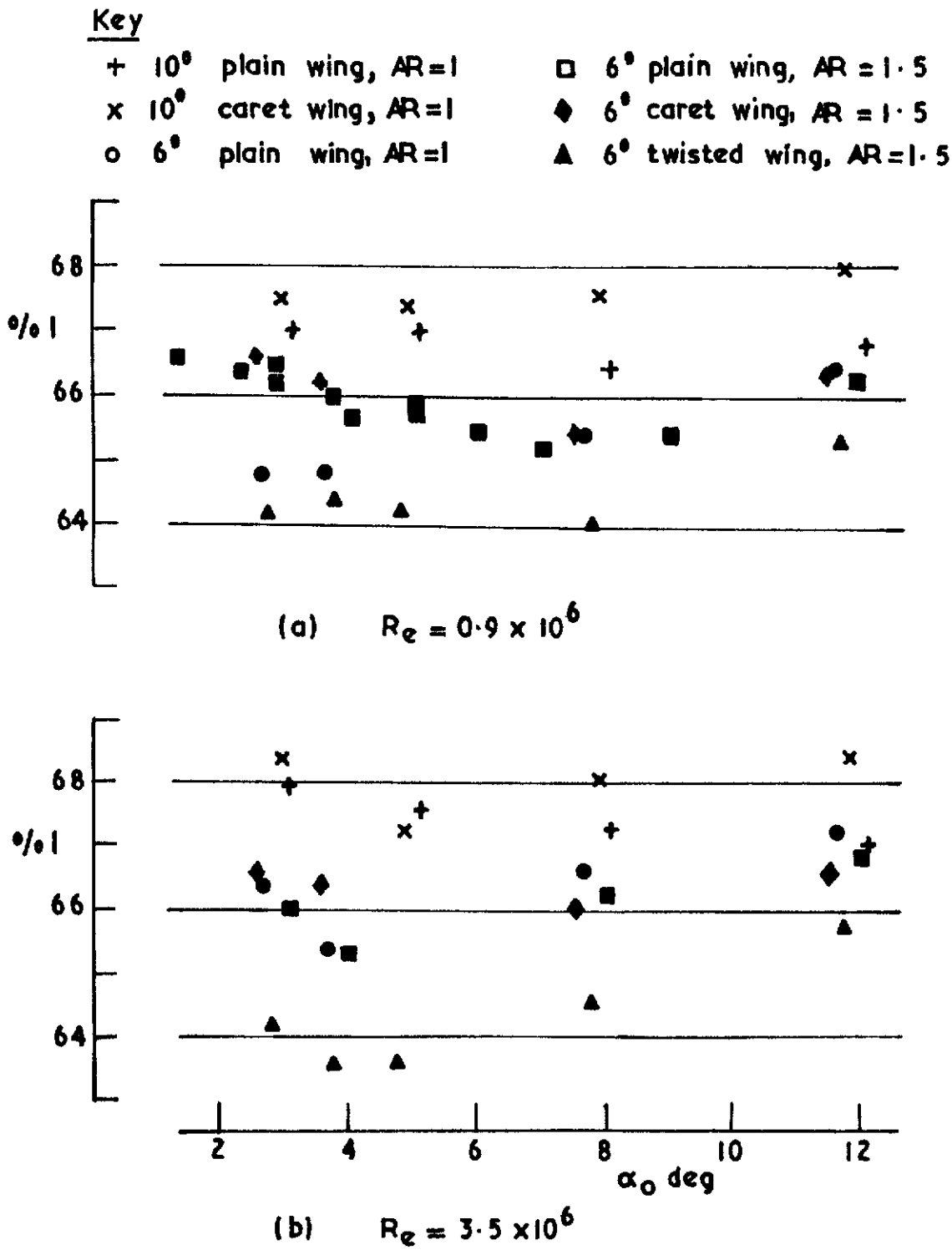

Centre of pressure position vs incidence

FIG. 3.10(a)

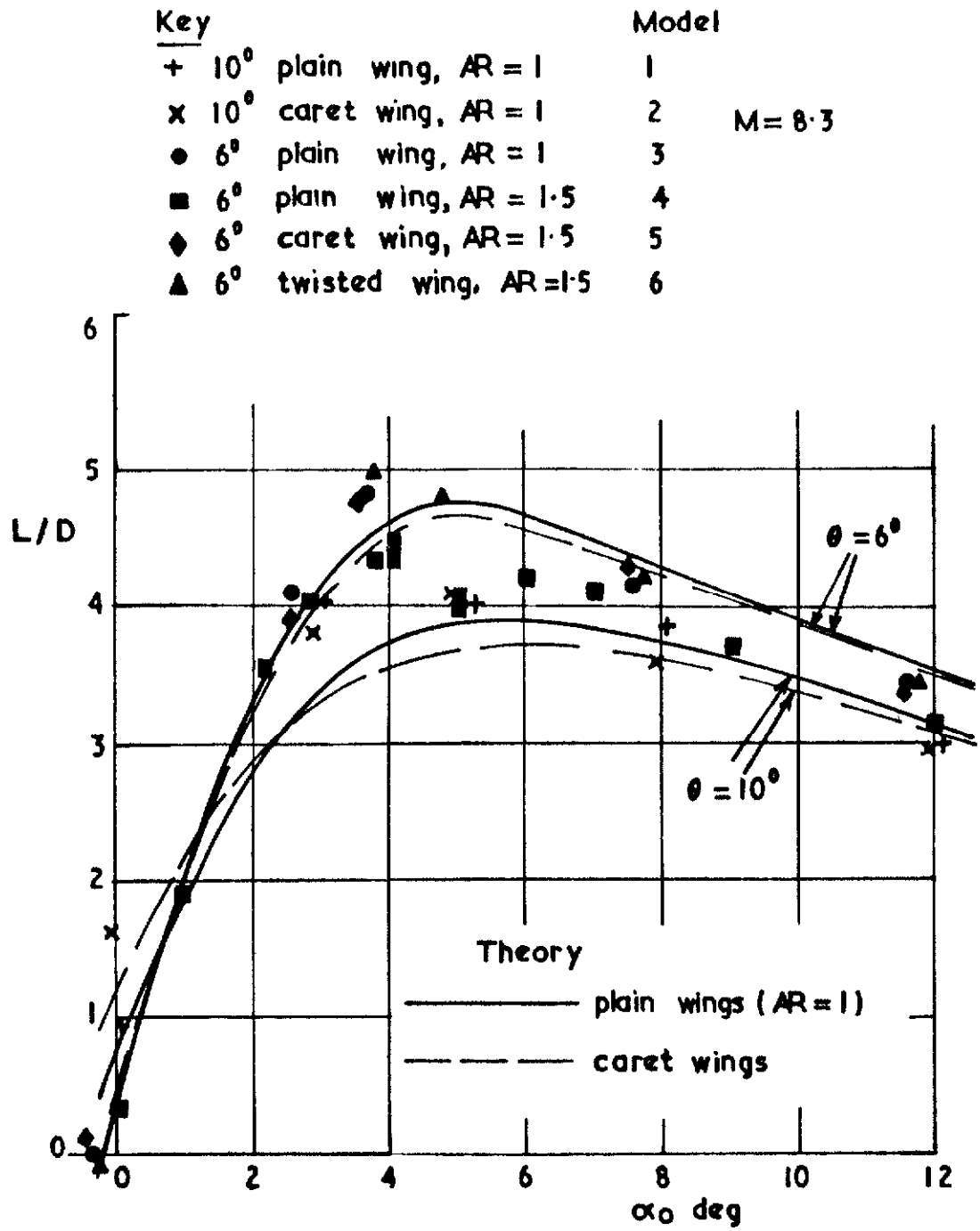

Lift / drag ratio vs incidence for $R_e = 0{\cdot}9 \times 10^6$

FIG 3.10 (b)

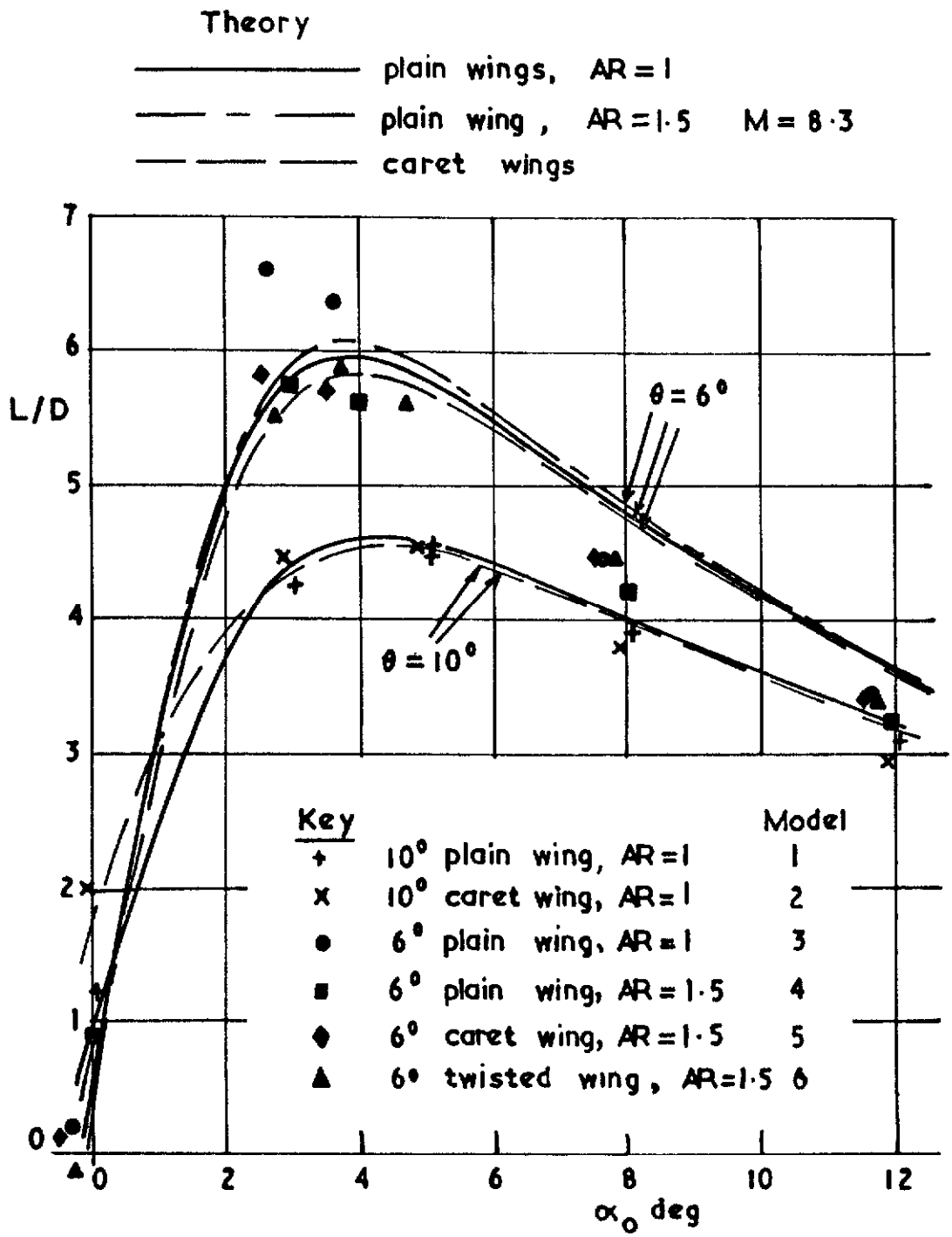

Lift / drag ratio vs incidence for $R_e = 3{\cdot}5 \times 10^6$

FIG.3.11(a)

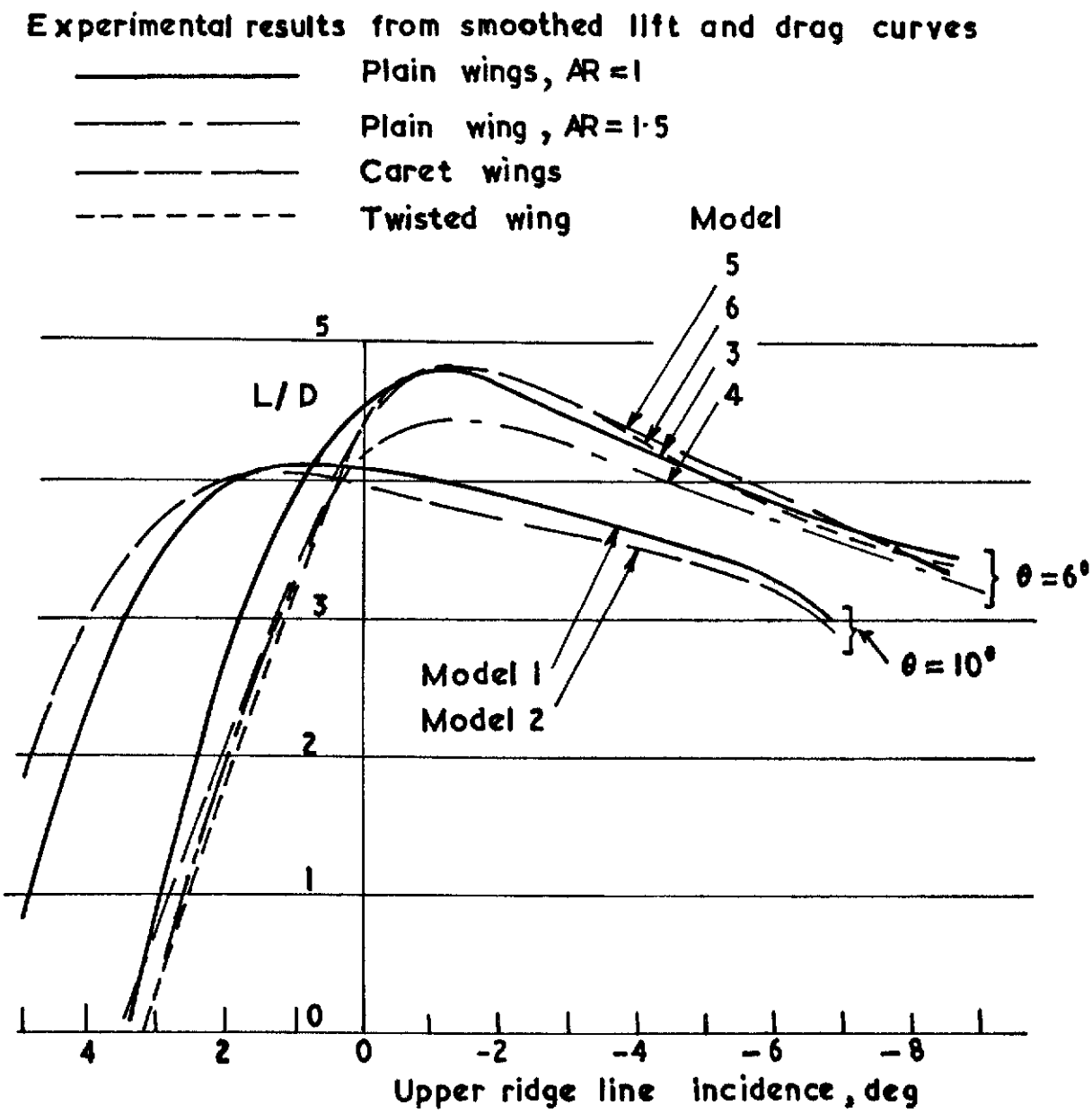

$R_e = 0{\cdot}9 \times 10^6$

Smoothed curves of lift/drag ratio vs upper ridge line incidence

FIG. 3. 11 (b)

Experimental results from smoothed lift and drag curves

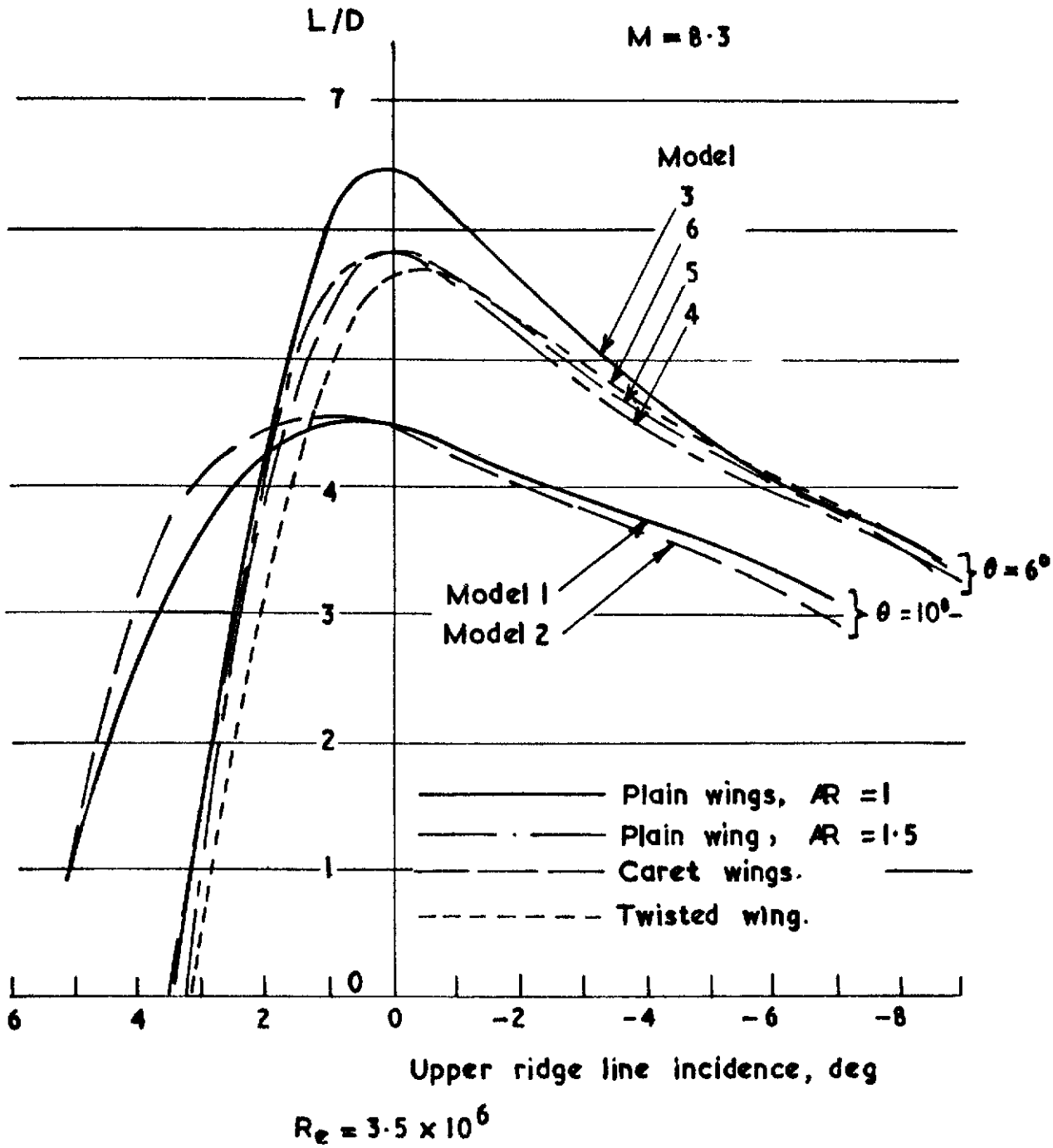

Smoothed curves of lift /drag ratio vs upper ridge line incidence

FIG. 4.1 (a)

Experimental results from smoothed lift and drag curves

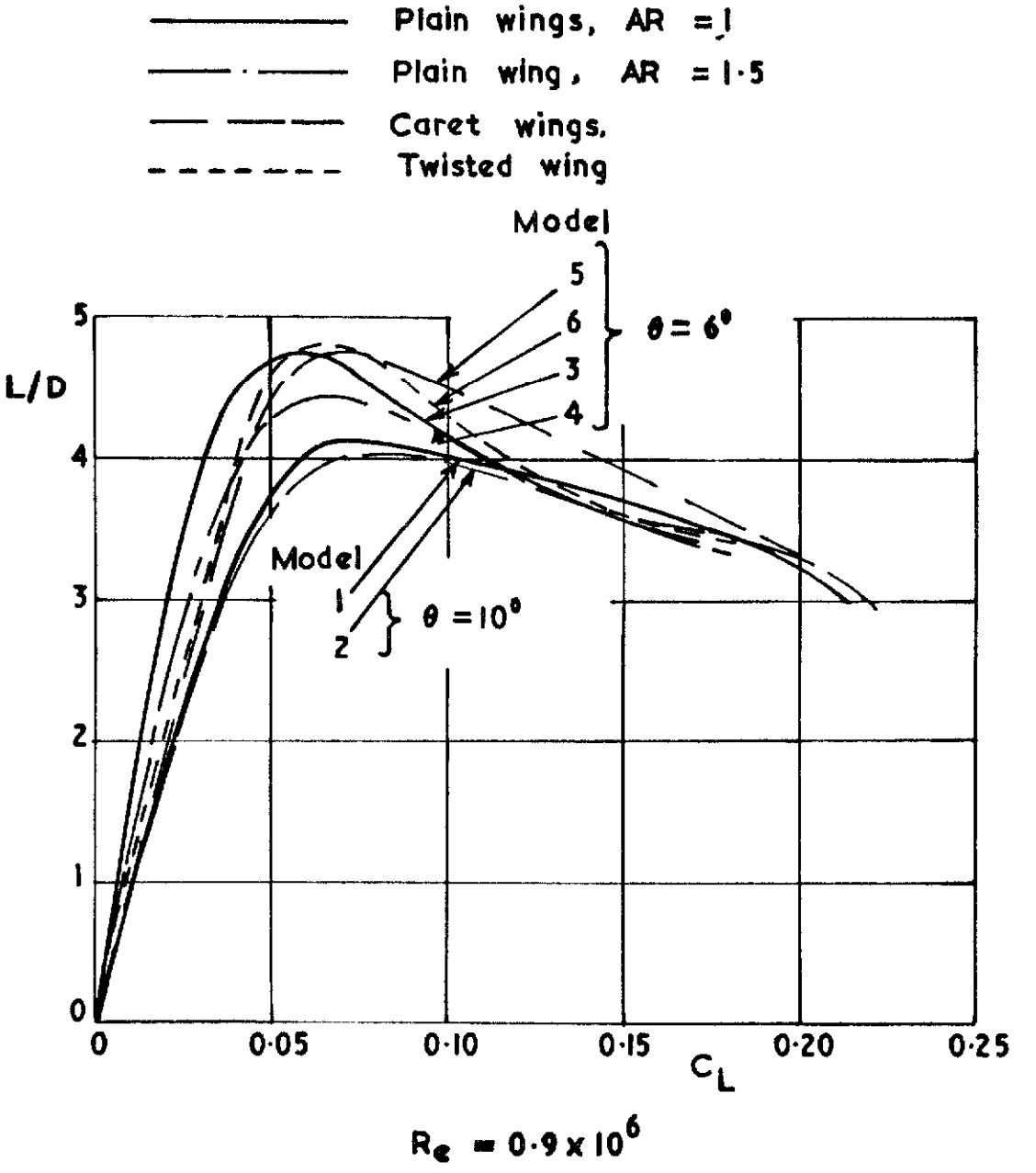

$R_e = 0.9 \times 10^6$

Lift / drag ratio vs lift coefficient

FIG. 4.1 (b)

Experimental results from smoothed lift and drag curves

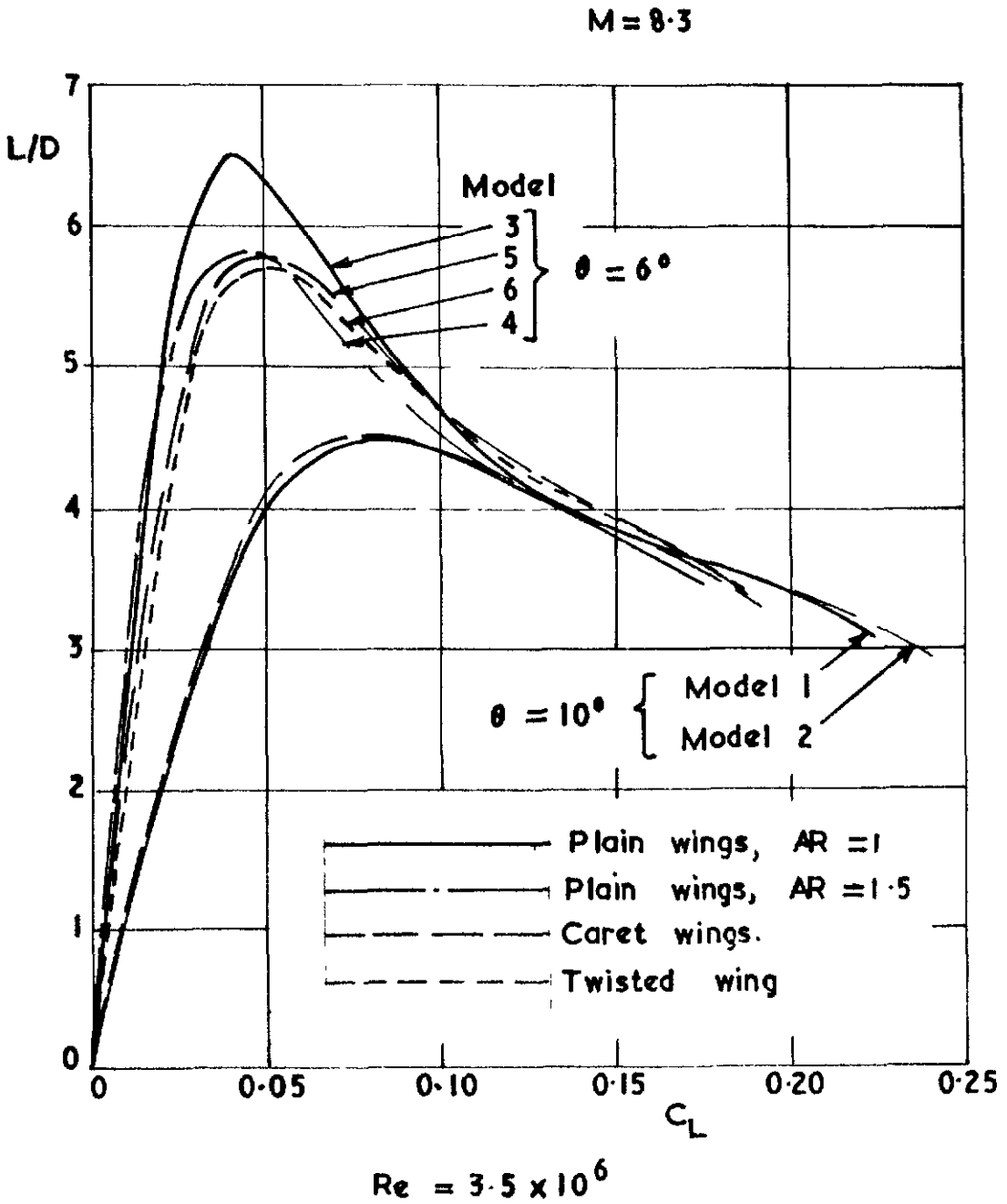

R594/1/501371 K4 3/71 P

A.R.C. C.P. No.1148
February, 1969
T. Opatowski

GUN TUNNEL FORCE MEASUREMENTS ON SOME THIN DELTA WINGS SUITABLE FOR HYPERSONIC CRUISING FLIGHT

Lift, drag and pitching moment measurements are presented for six thin delta wings at a Mach number of 8.3 and compared with theoretical estimates. Consideration is given to hypersonic cruise vehicles in the atmosphere and the relevance of tunnel tests to full scale. An optimum thickness is derived and compared to the tunnel results.

A.R.C. C.P. No.1148
February, 1969
T. Opatowski

GUN TUNNEL FORCE MEASUREMENTS ON SOME THIN DELTA WINGS SUITABLE FOR HYPERSONIC CRUISING FLIGHT

Lift, drag and pitching moment measurements are presented for six thin delta wings at a Mach number of 8.3 and compared with theoretical estimates. Consideration is given to hypersonic cruise vehicles in the atmosphere and the relevance of tunnel tests to full scale. An optimum thickness is derived and compared to the tunnel results.

A.R.C. C.P. No.1148
February, 1969
T. Opatowski

GUN TUNNEL FORCE MEASUREMENTS ON SOME THIN DELTA WINGS SUITABLE FOR HYPERSONIC CRUISING FLIGHT

Lift, drag and pitching moment measurements are presented for six thin delta wings at a Mach number of 8.3 and compared with theoretical estimates. Consideration is given to hypersonic cruise vehicles in the atmosphere and the relevance of tunnel tests to full scale. An optimum thickness is derived and compared to the tunnel results.

Produced and published by
HER MAJESTY'S STATIONERY OFFICE

To be purchased from
49 High Holborn, London WC1V 6HB
13a Castle Street, Edinburgh EH2 3AR
109 St Mary Street, Cardiff CF1 1JW
Brazennose Street, Manchester M60 8AS
50 Fairfax Street, Bristol BS1 3DE
258 Broad Street, Birmingham B1 2HE
80 Chichester Street, Belfast BT1 4JY
or through booksellers

Printed in England

C.P. No. 1148

SBN 11 470396 5